Hungarian University of Agriculture and Life Sciences

Doctoral School of Environmental Sciences

Analysis of Irrigation Efficiency Based on Remote Sensing

Test Area: New Halfa Scheme, Sudan

Doctoral Dissertation (PhD.)

Taha Ibrahim Mohammed Ahmed Ibrahim

GÖDÖLLŐ, HUNGARY

2023

Hungarian University of Agriculture and Life Sciences, Hungary

Name of Doctoral School: Doctoral School of Environmental Sciences

Discipline: Environmental Sciences / Water Resources Management

Head of Doctoral school: Professor Csákiné Dr Erika Michéli, Institute of Environmental Sciences, Hungarian University of Agriculture and Life Sciences.
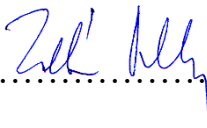

Supervisor(s): Dr Zoltán Vekerdy, Professor, Department of Water Management and Climate Adaptation, Institute of Environmental Sciences, Hungarian University of Agriculture and Life Sciences.

Dr István Waltner, Associate professor, Department of Water Management and Climate Adaptation, Institute of Environmental Sciences, Hungarian University of Agriculture and Life Sciences.
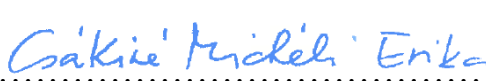
Approval of Supervisor(s)   Approval of Head of Doctoral School

Professor Dr. Zoltán Vekerdy   Professor Csákiné Dr. Erika Michéli

………………………………….   …………………………………..

Dr. István Waltner

…………………………………..

Analysis of Irrigation Efficiency Based on Remote Sensing

Test Area: New Halfa Scheme, Sudan

Table of Contents

List of Figures

List of Tables

LIST OF ABBREVIATIONS AND SYMBOLS

Abbreviation	Description
DEM	Digital Elevation Model
EC	Electric Conductivity
ET	Evapotranspiration
ET_o	Reference Evapotranspiration
ET_a	Actual Evapotranspiration
ETM+	Enhanced Thematic Mapper
FAO	Food and Agriculture Organization of the United Nations
GIS	Geographical Information System
GPS	Global Positioning System
km^2	Square Kilometre
LCLU	Land Cover and Land Use
MODIS	Moderate Resolution Imaging Spectroradiometer
NDVI	Normalized Difference Vegetation Index
OLI	Operational Land Imager
PET	Potential evapotranspiration
RS	Remote Sensing
SEBS	Surface Energy Balance System
SSEBop	Operational Simplified Surface Energy Balance System
SS	Soil Salinity
TIRS	Thermal Infrared Sensor
TM	Thematic Mapper
UTM-WGS84	Universal Transverse Mercator- World Geodetic System
NIWR	Net Irrigation Water Requirement
CWR	Crop Water Requirement
METRIC	Satellite-Based Energy Balance for Mapping Evapotranspiration with Internalized Calibration
SEBAL	Surface Energy Balance Algorithm for Land
dT (K)	Difference Between Land Surface Temperature and Air Temperature
r_a	air aerodynamics resistance
H	sensible heat flux
Etc	crop evapotranspiration

LST	Land Surface Temperature
ET_c adj	crop evapotranspiration below normal conditions
r_s	surface resistance
G	soil heat flux
$(e_s - e_a)$	vapour pressure deficit of the air
P	mean air density at constant pressure
γ	psychrometric constant
R_n	net radiation
Δ	slope of the saturation vapour pressure temperature relationship
LAI	Leave Area Index
U_2	Wind speed at 2 m height
T	Mean daily air temperature at 2 m height
D	Slope vapour pressure
K_c	Single crop coefficient
K_{cb}	basal crop coefficient
K_e	soil evaporation coefficient
i	Thorthwaite Heat Index
I	theoretical sunshine hours for each month
N	number of days for each month the elevation
d	latitude
T_a, T_d	mean and the dew-point temperature
λ	indicates the latent heat of the vaporization of water

Rn	net radiation flux
TR	radiometric surface temperature
λE	latent heat flux
ε	surface emissivity
$L^{\downarrow}$	downwelling long wave radiation
$L^{\uparrow}$	upwelling long wave radiation solar radiation
ρ_a	air density
C_{pa}	air specific heat at constant pressure
Λ	Evaporative fraction
α	Albedo
σ	Stefan-Bolzmann
T_O^4	surface temperature
f_c	fractional canopy coverage
H_{wet}	sensible heat flux at the wet limit
H_{dry}	sensible heat flux at the dry limit
Λ_r	relative evaporation
DisTrad	disaggregation procedure of radiometric surface temperature
TsHARP	Temperature Sharpening
FC	vegetation fractional cover
CV	coefficient of variation
CPMs	Crop productivity maps

WUMs	Water use maps
WPMs	Water productivity maps
θm	water content within the soil root depth
P	total rainfall
I	effective depth of water applied with irrigation.
CR	capillary rise from deep (free) water table
RO	run off
DP	deep percolation
ETi	portion of irrigation water provided.
Ei	irrigation efficiency
W_g	gross supply
Pe	effective precipitation
CWSI	crop water stress index
T_S	LST over the crop
T_{Cold}	temperature for the well-watered plants
T_{Hot}	temperature for the pixels with maximum amount of water stress

1. INTRODUCTION

1.1 Background

Water management for agricultural purposes is a complex task because it depends on several social, environmental, and political factors such as population growth rate, change in water use patterns, climate change, changes in hydraulic systems of rivers and the development of water resources in riparian countries. Its performance can be far below its potential, especially in drought-prone areas, which can make the level of agricultural production and irrigation economically inefficient (K. Raju, 1999). Effective irrigation systems are inevitable in providing adequate food to the world. Agriculture consumes about 60 to 70 % of the world's freshwater resources in the irrigation process, and the irrigation systems have efficiency ranging from 30 to 60 %. Although the available resources are mostly renewable, they have a limit for regeneration that cannot be exceeded (Darshana *et al.*, 2012).

Monitoring of soil and crop during the growing season is essential for agricultural production. Changes of plant characteristics occur according to the plant's phenological stage from the seedling until it reaches full maturity. The optimal crop transpiration, i.e., of the crop water requirements is a function of this process. In the primary stages of growth, most of the evaporation occurs from the surface of the soil. However, as plants grow, the contribution of transpiration as one of the components of the evapotranspiration increases until maturity and gradually decreases afterwards. The collection of information about crop evapotranspiration is very important in the irrigation scheduling process to raise the efficiency of water use (Allen *et al.*, 1998b).

Methods for assessing the performance of irrigation using data from satellites have been developed since the second half of the 1980s. There is a consensus that it is difficult to gather reliable and continuous areal information on it. Initially, the focus was on the relationship between quantifying of water use and cultivated area, but later attention was given to other aspects such as the crop water requirements, water productivity, water stress and salinity of water (Akdim *et al.*, 2014).

With the global population explosion, there is an excessive pressure on the freshwater resources. Irrigated agriculture is the most stressing sector, consuming a high percentage of fresh water, although it is highly competitive with other sectors such as industry and domestic use. With the increase of population and the reduction of the amount of water available for agricultural purposes, the agricultural sector is facing a major challenge as it must increase food

production using less water, i.e., increase the crop water productivity (Zwart and Bastiaanssen, 2004a).

The first step in improving water use efficiency is defining the net irrigation water requirement (NIWR). NIWR is the water that must be supplied by irrigation to satisfy evapotranspiration, leaching and miscellaneous water needs/losses, which are not covered by the water stored in the soil and provided by precipitation. Therefore, the calculation of NIWR requires estimating several closely related elements. These elements are crop water requirement (CWR), soil water balance, and evapotranspiration (ET). In the last decades, an increasing knowledge related to the methods of estimating the NIWR and ET was collected. The papers published by FAO (Doorenboos & Pruitt, 1977 and Doorenboos and Kassam 1979) are among the most widely used references around the world to estimate the NIWR and CWR. They are also connected to the methods that explain the relationship between crop production and water (Calera *et al.*, 2017).

Irrigation performance indicators were first introduced in the 1970s and described the hydraulic behaviour of irrigation systems (Bastiaanssen *et al.*, 2001). Later, crop-oriented indicators were also developed. For example, overall consumed ratio quantifies the degree to which crop irrigation requirements are met by irrigation water in the irrigated area (Bos and Nugteren, 1990). Crop water deficit over a period is defined as the difference between ET_p and ET_a of the cropping pattern within an area (Bastiaanssen *et al.*, 2001).

Remote sensing images captured by sensors on satellites or aeroplanes can be considered, among others, as tools to give spatial information about evapotranspiration. But the lack of availability of these images with sufficiently high temporal resolution and accuracy is one of the obstacles to using this technique. However, with the evolution of communication and computing technology, together with the policy changes of the national aeronautics administrations, like the NASA of the United States of America's government, (i.e., they provided free access to satellite data), an increase was observed in the development of this technology (Calera *et al.*, 2017).

In the past decade, many models have been developed that simulate plant growth and water balance. These models help us understand the process of plant development and are solutions to control the use and distribution of water (Wang *et al.*, 2001). Evapotranspiration is the main component of the water balance that consumes the largest amount of irrigation water and rainfall in cultivated areas. Several models have been developed for the quantification of actual

ET that are based on the surface energy balance such as the Surface Energy Balance Algorithm for Land (SEBAL) (Bastiaanssen *et al.*, 1998), the Simplified Surface Energy Balance Index (S-SEBI) (Roerink, Su and Menenti, 2000), the Surface Energy Balance System (SEBS) (Su, 2002), satellite-based energy balance for Mapping Evapotranspiration with Internalized Calibration (METRIC) (Allen, Tasumi and Trezza, 2007), the Operational Simplified Surface Energy Balance (SSEBop) (Senay *et al.*, 2013).

Estimating evapotranspiration (ET) on a field scale has been accomplished using high spatial resolution but low temporal resolution satellite data from the Landsat TM and ASTER. However, due to the long repeat cycle of these satellites, this method is not well-suited for routine ET estimation. Others have attempted to use daily or more frequent satellite data from AVHRR and GOES, which have a coarser spatial resolutions (1 to 5 km), resulting in ET estimates that represent averages over areas of 1 to 25 km^2 (Senatilleke *et al.*, 2022). Unfortunately, this method cannot distinguish the ET of individual fields. The MODIS offered pixel resolutions (ranging from 250 m to 4 km) have been used to assess land cover changes accurately, showing that a pixel resolution of 500 m or less is necessary. Even at the 1-km pixel resolution, detecting the areal extent of such changes is often unreliable. Land Surface Temperature (LST) is needed to monitor significant changes in surface energy balance and ET with land use and land cover changes. However, higher temporal frequency and coarser resolution thermal-infrared data is required to monitor such changes on a routine basis, which should be at the 50- to 100-m pixel size (Kustas *et al.*, 2003).

It is known that water shortage leads to the reduction of crop productivity and the purpose of irrigation is to reduce plant stress. There are several factors to consider in planning irrigation, such as crop water requirement, costs, water availability and other factors, especially in the arid zones. The response of crop yield to irrigation has been studied extensively. Through proper irrigation management, it should be possible to provide only the water that matches the crop ET (Wang *et al.*, 2001).

1.2 Problem statement

Many parts of the world are suffering from a lack of sufficient amount of irrigation water. In the New Halfa scheme, Sudan, this is the case. Winter wheat is one of the primary irrigated crops in the New Halfa project and one of the most important economic drivers in the area. Continuous cotton, sorghum, and groundnut follow winter wheat as the most common agricultural rotations in the region. Recent water scarcity circumstances, along with increased

intensive agricultural production are raising major worries about the availability and sustainability of water resources in the future. This, as a result of the aforementioned factors, should give farmers with an environmental incentive to match irrigation applications to crop water requirements. Through well-designed irrigation management schemes, accurate estimation of the actual crop evapotranspiration (ETa) may increase water resource usage efficiency. Planning in-season irrigation management, water allocations, water supply, defining water demand, and water usage, as well as the impact of changes in land use and management of water, all depend on accurate estimates of ETa. A necessity for producers to produce crops with less water is being brought on by the water deficit. Utilizing more effective irrigation methods, like sprinkler irrigation and drip irrigation, is a possibility, but it is constrained mostly by their high initial cost and upkeep needs.

Surface irrigation is one of the most common irrigation methods in the world, especially in developing countries, due to its low cost. This type of irrigation has many disadvantages, primarily due to its low efficiency of water use. The New Halfa scheme in Sudan uses this type of irrigation. This project is one of the most important economic and agricultural resources in Sudan, but it was noted that there is a sharp decline in productivity compared to the limited availability of water and declining soil fertility.

The lack of knowledge on the spatial variation of evapotranspiration remains one of the main problems. This makes water management a hard task under conditions of data scarcity in the New Halfa scheme. For this reason, a method to improve water management under conditions of data scarcity is required.

1.3 Objectives

1.3.1 Main objective

Develop a remote sensing-based method that supports improving the efficiency of irrigation water use.

1.3.2 Specific objectives

To achieve the main objective, the following specific objectives are set:

1. Improve the DisTrad method of downscaling LST for large areas with complex land cover.

2. Create high spatial and temporal resolution time series of actual evapotranspiration maps using remote sensing to define the spatial distribution of the actual ET.

3. Propose an optimal integration method of the optical data to overcome the cloud cover problem.

4. Analyse the irrigation efficiency for the New Halfa irrigation scheme to Demonstrate water stress and irrigation efficiency:

   a. Evaluate the irrigation performance in the New Halfa scheme to define the spatial and temporal distribution of the water applied and demanded.

   b. Analyse the spatial distribution of water stress occurring with the existing irrigation practice to improve the irrigation schedule.

   c. Estimate the crop water productivity for wheat crop.

5. Propose a method to optimize the irrigation schedule for wheat.

1.4 Research questions

1. How can we create high spatial and temporal resolution LST time series? (Objective 1)

2. How can we create an optimal ET_a map using the high spatial and temporal resolution LST? (Objective 2)

3. What is the optimal way of integrating the data from different optical sensors to improve the spatial and temporal resolution of ET_a? (Objective 3)

4. How can remote sensing data be optimally used to identify crop development and crop water requirement? (Objective 4)

5. How can remote sensing be a reliable tool to identify the irrigation needs and contribute to improving the irrigation efficiency in case of data scarcity? (Objective 5)

2. LITERATURE REVIEW

2. 1 Overview

Evapotranspiration from agricultural lands is one of the vital issues that scientific studies and researchers are currently paying attention to (Lott and Hunt, 2001). This problem is enhanced by the diminishing quantities of renewable water sources in several regions of the world, especially in the arid and semi-arid regions, characterized by high temperatures that increase potential evapotranspiration.

There are several methods to estimate the rates of evaporation and evapotranspiration. Practical methods include devices, calculations and empirical methods depending on different meteorological parameters based on point-like in situ measurements (Xu and Singh, 2001). Spatial techniques are using remote sensing images captured by sensors on satellites or airplanes are considered as tools to give spatial information about the actual evapotranspiration. Unfortunately, the lack of availability of these images with sufficiently high temporal resolution and accuracy is an obstacle in the operational use of the spatial methods. The purpose of the present chapter is to review the most common and efficient methods of calculating and modelling evaporation from open water bodies and evapotranspiration from agriculture using integrated data acquisition from remote sensing to gain special and temporal resolution for E and ET. ET estimation needs several parameters from meteorological stations and sometime the missing data and uncorrected measurement causes an increase in the error rate (Tabari *et al.*, 2012).

The accuracy and limitation of climatic data procedures for estimating ET ought to be valid at the regional level. this may be done for weather stations with full data sets by comparison ET_o calculated with full and with restricted data sets (Lott and Hunt, 2001). Methods based on point-like data (even when interpolation is made on them) provide ET information with limited accuracy. RS-based data provide the spatial variability of the measured parameters, thus the ET estimates are more representative to the observed region (Jia *et al.*, 2009).

2.1.1 Evapotranspiration Concepts

Distinctions have to be made between reference crop evapotranspiration (ET_0), crop evapotranspiration under standard (no stress) conditions (ET_c) and crop evapotranspiration under non-standard (stress) conditions ($ET_c\ adj$) (Figure 1). ET_o may be considered as a climatic parameter expressing the evaporation power of the atmosphere. ET_c refers to the evapotranspiration from excellently managed, large, well-watered fields that reach full production underneath the given climate. In case of sub-optimal crop management and environmental constraints that have an effect on crop growth and limit evapotranspiration, ET_c below non-standard conditions usually needs a correction (Allen *et al.*, 1998a).
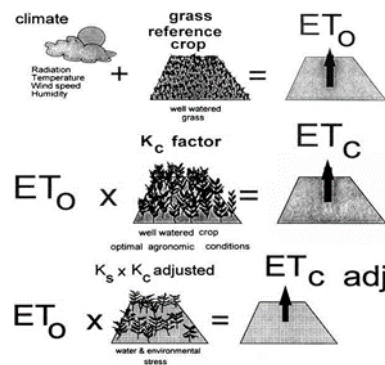
Figure 1. Reference crop evapotranspiration (ET_o), crop evapotranspiration under standard (ET_c), and non-standard conditions (ET_c adj) (Allen et al., 1998a).

2.1.2 Original Penman's Equation

Penman in 1948 combined the energy balance with the mass transfer method and derived an equation to calculate the E from an open water surface from ideal climate records of temperature sunshine, wind speed, and humidity. This called combination method was additionally developed by several researchers and extended to cropped surfaces by introducing resistance factors.

The resistance terminology distinguishes between surface resistance factors and aerodynamic resistance (Figure 2). The surface resistance parameters are usually combined into one parameter, the 'bulk' surface resistance parameter, which operates nonparallel with the aerodynamic resistance.

The surface resistance, r_s, describes the resistance of vapour flow through stomata openings, total leaf space and soil surface. The aerodynamic resistance, r_a, describes the resistance from

the vegetation upward and involves friction from air flowing over vegetative surfaces. Although the exchange method during a vegetation layer is just too complicated to be totally delineated by the 2 resistance factors, smart correlations may be obtained between measured and calculated evapotranspiration rates, particularly for the same grass reference surface (Allen *et al.*, 1998a) (Doorenbos and Pruitt, 1977).
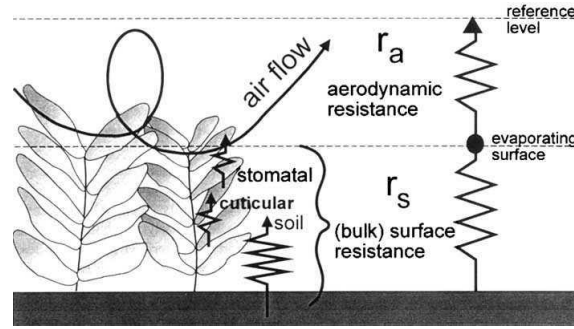
Figure 2. Simplified representation of the (bulk) surface and aerodynamic resistances for water vapour flow (Allen *et al.*, 1998a)

The Penman-Monteith form of the combination equation is

$$\lambda ET = \frac{\Delta(R_n - G) + p_a c_p \dfrac{(e_s - e_a)}{r_a}}{\Delta + \gamma \left(1 + \dfrac{r_s}{r_a}\right)} \tag{1}$$

where: G is the soil heat flux; cp is the specific heat of the air; $(e_s - e_a)$ represents the vapour pressure deficit of the air; ρ a is the mean air density at constant pressure; γ is the psychrometric constant; Rn is the net radiation; Δ represents the slope of the saturation vapour pressure temperature relationship; and r_s and r_a are the (bulk) surface and aerodynamic resistances.

The Penman-Monteith approach includes all parameters that govern energy exchange and corresponding heat energy flux from unit areas of vegetation. Many of the parameters are measured or is calculated from meteorological data. Equation (1) is used for the direct calculation of any crop evapotranspiration because the surface and aerodynamic resistances are crop specific.

2.1.3 FAO considerations

To obviate the necessity to outline distinctive *ET* parameters for every crop and stage of growth, the ideaof a reference surface was introduced. *ET* rates of the varied crops are associated with the *ET* rate from the reference surface *(ET$_o$)* by crop coefficients (Doorenbos and Pruitt, 1977) (Allen *et al.*, 1998a).

First, the open water surface has been suggested as a reference surface. However, the variations in vegetation management, aerodynamic circumstances, and radiation characteristics pose a challenge in relating *ET* to measurements of free water evaporation. Relating *ET$_0$* to a selected crop has the advantage of incorporating the biological and physical processes concerned in *ET* from cropped surfaces (Doorenbos and Pruitt, 1977) (Allen *et al.*, 1998a).

Grass is a well-studied crop concerning its aerodynamic and surface characteristics and is accepted worldwide as a reference surface. As a result of the resistance to diffusion of vapour powerfully depends on crop height, ground cover, *LAI* and soil wetness conditions, the characteristics of the reference crop ought to be outlined. Changes in crop height led to variations in roughness and *LAI*. Consequently, the associated canopy resistances can vary appreciably with time. Moreover, water stress and (also the) degree of ground cover have a control on the resistances and also on the albedo (Doorenbos and Pruitt, 1977). Allen *et al.* (1998a) accepted the following unambiguous definition for the reference surface as shown in Figure 3.

"A hypothetical reference crop with an assumed crop height of 0.12 m, a fixed surface resistance of 70 s m^{-1} and an albedo of 0.23."

The FAO Penman-Monteith method became a standard, because the evapotranspiration of this reference surface *(ET$_o$)* may be unambiguously determined, and this method provides consistent *ET$_0$* values over various regions and climates.
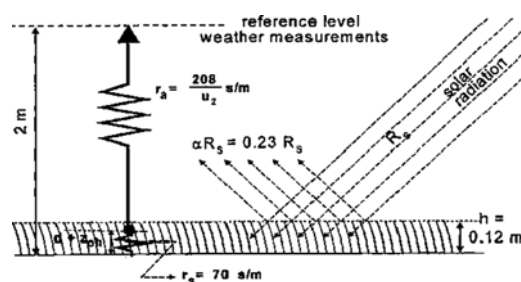
Figure 3. Characteristics of the hypothetical reference crop (Allen *et al.*, 1998a)

2.1.4 ET computed from meteorological data.

Due to the difficulty of getting correct field measurements, *ET* is often computed from weather data. A large variety of empirical or semi-empirical equations are developed for assessing crop or reference crop evapotranspiration from meteorological data. Several of them are solely valid beneath specific climatic and agronomical conditions and cannot be applied under conditions different from the ones they were originally developed.

The FAO Penman-Monteith equation is recommended since it is the most often used approach for defining and computing the ET.This method needs air temperature, radiation, wind speed data and Humidity. From the initial Penman-Monteith equation (Eq. 1), FAO will be derived: (Allen *et al.*, 1998a).

$$ETo = \frac{0.408.D.(R_n - G) + 900.\gamma.U_2.(e_s - e_a)/(T + 273)}{D + \gamma.(1 + 0.34U_2)} \qquad (2)$$

Where: ET_o: Reference evapotranspiration (mm.day^{-1}).

G: Soil heat flux density (MJ.m^{-2}.day^{-1}).

$U2$: Wind speed at 2 m height (m.s-1)

ea: Actual vapor pressure (kPa).

T: Mean daily air temperature at 2 m height (°C).

γ: Psychrometric constant (kPa. °C^{-1}).

Rn: Net radiation at the crop surface (MJ.m-2.day-1).

es: Saturation vapor pressure (kPa).

D: Slope vapour pressure curve (kPa. °C^{-1}).

No weather-based evapotranspiration equation will be expected to predict evapotranspiration underneath each climatically scenario because of simplification in formulation and errors in data measurements.

2.1.5 Crop Evapotranspiration ET$_c$

This is the evapotranspiration from disease free, well-fertilized crops, grownup in big fields, underneath optimum soil water conditions and achieving full production under the given weather conditions (Allen *et al.*, 1998a). The ET_c differs from the ET_o according to the crop characteristics. Principally, the aerodynamic resistances of the crops are different from that of

the grass used as a reference (Allen *et al.*, 1998a). Such distinction of characteristics between crops and grass are mirrored by the crop constant or coefficient, that may be single (K_c) or dual: basal crop coefficient (K_{cb}) + soil evaporation coefficient (K_e).

The single crop coefficient approach is principally used for producing the irrigation schedule, and water management purposes whereas the twin crop constant approach is usually applicable simulating the irrigation schedule or in real time irrigation programming wherever elaborate evaporation knowledge are required. Crop evapotranspiration ET is calculated by multiplying ET_o by the crop constant K_c:

$$ET_c = K_c \times ET_o \qquad\qquad (3)$$

2.1.6 Crop Coefficients K_c

According to (Allen *et al.*, 1998a), the various crop development stages are:

- Initial stage: it starts from planting date to around 10% ground cover.

- Development stage: it runs from 10% ground cover to effective full cover. Effective full cover for several crops happens at the initiation of flowering.

- Mid-season stage: it runs from effective full cowl to the beginning of maturity. the beginning of maturity is commonly indicated by the start of the ageing, yellowing or senescence of leaves, leaf drop, or the browning of fruit to the degree that the crop evapotranspiration is reduced relative to the ET_o.

- Late season stage: it runs from the beginning of maturity to harvest or full senescence.

The Penman-Monteith equation illustrate the physical and physiological factors governing the evapotranspiration. The crop coefficients can be calculated by dividing the crop evapotranspiration (ET_c) with the calculated ET_o, i.e., $K_c = ET_c/ET_o$.

the crop coefficient differs from one crop to the other according to the plant morphology and the age of the plant, which leads to a difference in the evapotranspiration between the crops. Typical trends in kc throughout the growing period are diagrammatic within the crop coefficient curve (Figure 4).

24
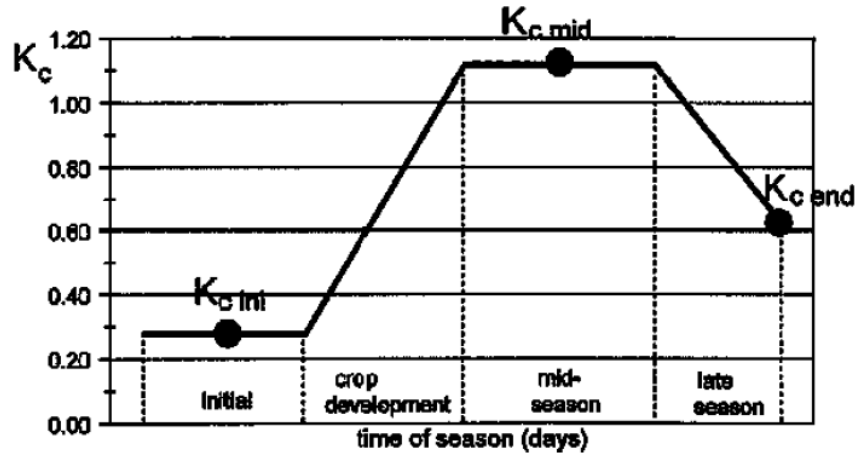
Figure 4. Crop coefficient curve (Allen *et al.*, 1998a)

2.3 Remote sensing-based ET estimation methods

Remote sensing data acquired by sensors on satellites or airplanes are thought to be useful for providing spatial evapotranspiration information. However, one of the limitations of this technique is the scarcity of information with sufficiently high temporal resolution and precision. Numerous models that simulate crop growth and hydrological cycle have been developed over the last ten years. These models provide strategies for managing the usage and distribution of water as well as improving in our understanding of the process of plant development. The primary factor in the water balance is evapotranspiration, which uses the majority of irrigation water and rainfall in agricultural regions.

2.3.1 Energy balance approaches

Remote sensing surface energy balance methods calculate surface energy fluxes to define the energy that is used for evaporating water. For this, data from several sources are required. A part of them, which describes the state of the surface, is derived from remote sensing. The other part, which describes mostly the state of the atmosphere and the incoming energy is derived from in situ observations. Actual evapotranspiration is proportional to the latent heat flux, so it is calculated as the residual of the energy balance equation (Moran *et al.*, 1994), (Equation 4).

$$\lambda ET_a = \text{Rn} - G - H \tag{4}$$

where: λ indicates the latent heat of the vaporization of water ($W.m^2$), ET_a is the actual evapotranspiration, Rn is the net radiation flux ($W.m^2$), G is the soil heat flux ($W.m^2$), and H is the sensible heat flux ($W.m^2$),.

the hemispherical surface reflectance is an important factor in determining net radiation and radiometric surface temperature (LST) obtained from thermal band images. as all these processes are done to obtain sensible heat flux.

 LST and T0 are linked, although there are distinctions between the two aspects. (Norman, Kustas and Humes, 1995),

Since each of them depends on several components, their interaction is quite complex. where T0 depends on surface aerodynamic roughness, wind speed, soil, and canopy cover as parts of the atmosphere while LST depends on the temperature of many elements that used the radiometer view. (Roerink *et al.*, 1997).

2.3.1.1 Surface Energy Balance Algorithm for Land

Remote sensing provides great and unlimited possibilities for the assessment of land cover. The surface energy balance algorithm for land (SEBAL) is the one of the single source SEB models for estimating evapotranspiration from the remote sensing. It calculates the evapotranspiration from the energy balance pixel by pixel (Bastiaanssen W.G.M. *et al.*, 1998).

The latent heat flux is computed directly from the surface energy balance at satellite over-pass, on a pixel-by-pixel basis.

The SEBAL model uses remote sensing to estimate the parameters related to the surface, such as temperature, normalized vegetation index and then associates these elements with information from meteorological and agricultural stations such as wind speed and crop height to calculate instantaneous net radiation and soil heat flux. The model depends on the estimation of the difference between land surface temperature and air temperature (dT (K)), and the aerodynamic resistance (r_a (s.m^{-1})) of the atmosphere for the calculation of sensible heat flux H. Two extreme points need to be selected within the processed image. One is the 'cold point,' where sensible heat flux is approaching 0 and the other is the 'hot point', where the potential heat flux is approaching 0. Based on these two points, a linear relationship between land surface temperature and dT is established. Then the energy balance equation is applied to calculate the instantaneous *ET* for the satellite overpass.

2.3.1.2 Surface Energy Balance System

Surface Energy Balance System (SEBS) model developed by Su (2002) to estimate evapotranspiration, needs two types of data: the first group includes land surface albedo, emissivity, temperature, fractional vegetation coverage and leaf area index, and the height of

the vegetation (or roughness height); these data can be retrieved from the satellite images. The second group comprises air pressure, temperature, humidity, and wind speed at a reference height, downward solar radiation, and downward longwave radiation these parameters can be determined from meteorological data directly or by using a model. This data can be used to estimate roughness length for heat transfer and evaporative fraction, The SEBS model is another physically based energy balance model that does not require any a priori knowledge of the actual turbulent heat fluxes. The model uses energy balance at wet and dry limiting conditions to compute instantaneous relative evaporation etc.

SEBS model is based on the energy balance equation illustrated by equation (5).

$$R_n = \lambda ET_a + G_0 + H \tag{5}$$

Where: R_n is the net radiation, λE is the turbulent latent heat flux (λ is the latent heat of vaporization and ET_a is the actual evapotranspiration), G_0 is the soil heat flux (W. m^{-2}) and H is the turbulent sensible heat flux (W. m^{-2}).

The calculation of net radiation flux on land surface, R_n (W. m^{-2}), is given by equation (6).

$$R_n = (1 - \alpha).R_{swd} + \mathcal{E}.R_{lwd} \atop - \mathcal{E}.\sigma.\text{LST} \tag{6}$$

Where: α is the albedo, R_{swd} is the downward solar radiation, ε is the emissivity of the surface, R_{lwd} is the downward longwave radiation, σ is the Stefan-Bolzmann constant, and LST is the surface temperature.

The soil heat flux depends on land surface characteristics, soil water content, and other factors. The calculation of soil heat flux by SEBS model is given equation (7).

$$G_0 = R_n.(\Gamma_c + (1 - f_c).(\Gamma_s - \Gamma_c)) \tag{7}$$

in which it is assumed that the ratio of soil heat flux to net radiation $\Gamma_c = 0.05$ for full vegetation canopy and $\Gamma_s = 0.315$ for bare soil. An interpolation is then performed between these limiting cases using the fractional canopy coverage, f_c.

The calculation of sensible heat flux is calculated using equation (8).

$$H = \left((R_n - G_0) - \frac{\rho C_p}{r_{ew}} \cdot \frac{e_s - e}{\gamma} \right) / 1 + \frac{\varDelta}{\gamma} \tag{8}$$

We will use SEBS to estimate evaporation fraction by makes energy balance at limiting cases at dry limit and the wet limit as shown in equation (9).

$$\Lambda_r = 1 - \frac{H - H_{wet}}{H_{dry} - H_{wet}} \tag{9}$$

Where: the H_{wet} is sensible heat flux at the wet limit and H_{dry} sensible heat flux at the dry limit.

Since the ET ration $\varLambda$ is a constant during a day, the daily ET_{24} (mm) can be estimated using the equations (10, 11).

$$\Lambda = \frac{\lambda E}{R_n - G_0} = \frac{\Lambda_r - \lambda \, E_{wet}}{R_n - G} \tag{10}$$

$$E_{daily} = \Lambda_0^{24} \times 8.64 \times 10^7 \times \frac{R_N - G_0}{\lambda \rho w} \tag{11}$$

Where: Λ_r is relative evaporation, Λ_0^{24} daily evaporative fraction, ρw density of water measured in kilograms per cubic meter. and λ is the latent heat of vaporization.

2.3.2 Land surface temperature downscaling

Many scientists have been studying land surface temperature (LST) because of its significant importance in water management science due to its direct effect on the hydrological water cycle. This effect is one of the most prominent factors affecting evapotranspiration (Zakšek and Oštir, 2012; Zhan *et al.*, 2013; Pan *et al.*, 2018; Li *et al.*, 2019). deriving land surface temperature from thermal remote sensing is one of the most promising means of achieving the mission, whether at the regional or global scale (Zhang *et al.*, 2016). The emergence of thermal sensors with high spatial resolution has improved and raised the quality of calculating LST (Adi Nugraha, Gunawan and Kamal, 2019; Bartkowiak, Castelli and Notarnicola, 2019), as these

sensors have a spatial resolution of 60-100 meters. However, with this high spatial resolution, the challenge is the poor temporal resolution, where the revisit time for these sensors is around 16 days (Hutengs and Vohland, 2016). One of these sensors is the Landsat 8 OLI TIRS, which has two thermal bands with 100 m resolution (U.S. Geological Survey, 2016). On the other hand, several sensors with low spatial resolution produce high temporal resolution images with a repetition time varying from less than an hour to three days (Hutengs and Vohland, 2016; Yang *et al.*, 2017). The poor spatial resolution of the evapotranspiration retrieved from MODIS data is one of the most important reasons for its limited suitability for scheduling and planning irrigation (Bindhu, Narasimhan and Sudheer, 2013; Pu, 2021). In developing countries, the agricultural lands are partitioned into small fields of less than 1 square kilometre. Applying coarse-resolution thermal data to the small fields, one faces a problem called the thermal mixing effect, resulting from the differences in the thermal properties of the land cover classes within one pixel. Therefore, this problem needs to be addressed, e.g., by finding a relationship between the temporal and spatial resolutions of the thermal images (Mukherjee, Joshi and Garg, 2014).

The downscaling process is defined as increasing spatial resolution by finding values of the smaller pixels as a function of the original measurement with the coarse pixel size and some additional information or in a simplified way, it can be described as decreasing the pixel size (Atkinson, 2013; Sattari, Hashim and Pour, 2018). There are many different approaches that have been followed for the downscaling of LST (Mukherjee, Joshi and Garg, 2014), but the most popular approach is the disaggregation of LST based on a co-variable. The approach improves the resolution of LST, whether spatially or temporally, and makes it suitable for many applications, e.g., with all applications that include the surface energy balance (SEB) (Zhan *et al.*, 2013). Maybe the most famous of these approaches is DisTrad (disaggregation procedure of radiometric surface temperature). Its principle is to find a mathematical relationship between the radiometric surface temperature and the normalized difference vegetation index NDVI through the inverse relationship between the LST and the NDVI (Kustas *et al.*, 2003; Yang *et al.*, 2019). A further developed approach is TsHARP (Temperature Sharpening), which is a modulation of the DisTrad, based on a linear relationship between the vegetation fractional cover (FC) and LST (Agam *et al.*, 2007).

To parameterise the regression equation between the vegetation index and the surface temperature, Kustas has developed a process of aggregating the NDVI map and then calculating the coefficient of variation (CV) of the native NDVI values within each pixel in the aggregated map, using 25% of the aggregated pixels with the lowest coefficients of variation for defining

the coefficients of the regression equation (Kustas *et al.*, 2003). This approach was successfully tested on homogenous areas, but when used on heterogenous areas, the problem of representativity occurs. Accordingly, the approach needs to be improved for heterogeneous areas (Mukherjee, Joshi and Garg, 2014; Ebrahimy and Azadbakht, 2019). This work aims to improve the DisTrad approach for downscaling LST for heterogeneous areas and improve the temporal and spatial distribution of the calculated high-resolution evapotranspiration maps.

2.5 Irrigation demand and efficiency

Water management for agricultural purposes is a complex task because it depends on several factors: social, environmental, and political factors such as population growth rate, change in water use patterns, climate changes, change in hydraulic systems of rivers and the development of water resources in riparian countries. it is performance still far below its potential especially in drought-prone areas, which has made the level of agricultural production and irrigation economically inefficient(Caldwell *et al.*, 1999). Effective irrigation systems are inevitable in providing adequate food to the world. Agriculture consumes about 60 to 70 % of the world's freshwater resources in the irrigation process, and the irrigation systems have efficiency ranging from 30 to 60 %. Although the available resources are mostly renewable, they have a higher limit for regeneration that cannot be exceeded (Darshana *et al.*, 2012). With the global population explosion, there is an excessive pressure on the freshwater resources. Irrigated agriculture is the most stressing sector, consuming a high percentage of fresh water, although it is highly competitive with other sectors such as the industry and the domestic sector. With the increase in population and the reduction in the amount of water available for agricultural purposes, the agricultural sector is facing a major challenge as it must increase food production using less water, i.e., to increase the crop water productivity (Zwart and Bastiaanssen, 2004a). Methods for assessing the performance of irrigation using data from satellites are being developed since the second half of the 1980s. There is a consensus that it is difficult to gather reliable and continuous terrestrial information on it. Initially, the focus was on the relationship between quantifying of water use and cultivated area, but later attention was given to other aspects such as the crop water requirements, water productivity, water stress and salinity of water (Akdim *et al.*, 2014). Crop water productivity considered as one of important methods to evaluate the irrigation efficiency and its defined by (Zwart and Bastiaanssen, 2004a) is the marketing value of crop yield divided by actual evapotranspiration. The three major steps for mapping process in producing water productivity map are: Crop productivity maps (CPMs;

kg.m^{-2} or kg/pixel), Water use (actual ET) maps (WUMs; m3.m^{-2} or m3.pixel^{-1}) and Water productivity maps (WPMs; kg.m^{-3}) (Thenkabail, 2008).

Engineers and scientists must carefully clarify the efficiency keywords they use in irrigation research to minimize reader misunderstanding. More importantly, they should consider adopting terminology based on the physics of the water resource system and mass conservation to minimize public misconceptions. Authors must also avoid making assertions that are either false or misleading.

2.5.1 Water balance

In this cause the calculation is going to be based on a daily accounting of all ingoing and outgoing water in the root zone according to (Toureiro *et al.*, 2017)

$$\theta m_i = \theta m_{i-1} + P_i + I_i + CR_i - RO_i - DP_i - ETca_i \qquad (12)$$

Where:

i= day in the calculation procedure

θm = water content within the soil root depth

P = total rainfall

I = the effective depth of water applied with irrigation

CR = capillary rise from deep (free) water table

RO= run off

DP= deep percolation

ETca= Actual crop evapotranspiration, crop water consumption.

2.5.2 Irrigation efficiency

When analysing the performance of an irrigated unit, the water balance component is commonly expressed as a ratio relative to the gross water supply provided to the study area. The primary ratio is often known as irrigation efficiency (Ei). It denotes the amount of irrigation water delivered to the target region that has evaporated or been used. Typically, this proportion is represented as a percentage as shown in equation (13).

$$E_i = \frac{ET_i}{W_g - P_e}$$

$$\qquad (13)$$

where ETi is the portion of irrigation water provided that was used by E and T, W_g is the gross supply, and Pe is the effective precipitation or precipitation that decreases the quantity of irrigation water required.

The other term refers to ratio of irrigation water given to water balance components that are not used, i.e., that stay in liquid form someplace in the system, are stored, or drain from the system as shown in equation (14).

$$(1 - E_i) = \frac{\Delta s + R_s + D}{W_g - P_e}$$

(14)

And because the amount of water changes in the root zone is small the ΔS can be ignored and then the equation (15) will in this format.

$$(1 - E_i) = \frac{R_s + D}{W_g - P_e}$$

(15)

2.6 Crop water stress

Crop classifications, harvest management, crop yield forecasting, disease detection and management, crop wellness evaluation, and crop water stress detection are all examples of remote sensing uses in farming. Crop water stress must be detected in different growing seasons in order to estimate plant conditions and manage irrigation schedule. Various approaches have been studied to differentiate crop water stress. These approaches are based on measurements of soil water, plant responses, and remote sensing (Virnodkar *et al.*, 2020).

In situ measurements of soil water content, plant characteristics, or climatic factors to estimate the quantity of water lost from the plant-soil system over a specific period are traditional approaches for monitoring agricultural water stress. These approaches are time consuming and yield point data that provides inadequate indicators of the general state of the field in consideration (González-Dugo *et al.*, 2006), Evapotranspiration models, on the other hand, assume a freely transpiring reference crop with uniform cover and soil type within a field. These approaches are time consuming and yield point data that provides poor indicators of the general state of the field. Other techniques of detecting plant water status include soil water balance calculations, direct and indirect detection of plant water status via stomatal conductance and leaf water potential, and so on. Due to soil and crop canopy heterogeneity, these procedures,

while reliable, are labour expensive, damaging, and unsuited for automation(Ihuoma and Madramootoo, 2017).

To boost water savings and improve agricultural sustainability, optimal irrigation scheduling methods must be implemented, as well as early identification of water stress in crops before it causes permanent damage and yield loss. Recent research has concentrated on the use of remotely sensed data as an alternative to standard field measurements of plant stress indices, as this gives information regarding crop spatial and temporal distribution (Zhao *et al.*, 2015).

2.7 Crop water stress indicators

Water is an important factor in determining the quality and quantity of developed harvests (Virnodkar *et al.*, 2020). Crop water stress is a lack of water availability, which can be recognized by a decrease in soil water content or by the physiological reactions of the plant to a water deficit. To satisfy their evapotranspiration demands, plants consume root zone soil water, which depletes soil accessible water. Under restricted soil moisture circumstances, chemical and hydraulic signals are sent to the plant leaf via xylem pathways, resulting in physiological responses such as stomatal closure and photosynthetic rate decreases.

Water stressed crops exhibit lower evapotranspiration and other signs such as leaf wilting, stunted development, and decreased leaf area. Furthermore, water stress has a negative impact on crop physiological and nutritional development, resulting in decreased biomass, yield, and crop quality(Ihuoma and Madramootoo, 2017).

Water shortage is another major issue in arid and semi-arid regions. Proper water management is thus required in such areas where irrigation is a critical component in achieving the target agricultural output, crop quality, and water usage. To regulate irrigation management and scheduling, one must first identify the quantity and time of the water supply, which may be done by a good spatial evaluation of plant water stress. Table 1 provides a comparison of traditional and current crop water stress evaluation methodologies, which are briefly explained below.

Table 1. A description of the methods for measuring plant water stress(Ihuoma and Madramootoo, 2017).

Methods	Description	Advantages	Disadvantages
1. Soil water measurement			

(a) Gravimetric method	Sampling of soil, which is weighed, oven-dried and reweighed to estimate the amount of water lost from the plant-soil system	It is reliable and serves as a guide on the amount of water to apply during irrigation	The method is labour intensive, destructive, and time consuming
(b) Soil moisture sensors			
(I) Neutron probe	Based on the emission of high energy neutrons by a radioactive source into the soil	Fast, non-destructive, and repetitive	Requires adequate operator training, storage, licencing, and inspection, due to its radioactive source
(II) TDR and FDR	Based on the difference between the dielectric constant of water and soil	Precise and easy to apply in practice. Estimates soil water levels at different depths along the soil profile. Readings can be logged automatically	Several sensors are required for an entire field. Prohibitive cost of installation of sensors
(III) Tensiometers	Measures soil water Potential	Easy to use for irrigation scheduling	Useful in coarse textured soils or in high frequency irrigation only. Used for a narrow range of available soil water
2. Soil water balance approach	Indirect estimate of soil moisture status	Good indicator of the amount of	Not perfectly accurate and requires calibration with

			actual soil measurements. Requires estimate of evaporation, rainfall, and irrigation events
	based on soil water balance calculations	irrigation water and easy to apply	
3. Plant-based approaches			
(a) Stomatal conductance	Indirect indicator of plant water stress by measuring the stomata opening	Good measure of plant water status. Used as benchmark for most research Studies	Labour intensive and unsuitable for automation and commercial application. Not exactly accurate for an isohydric crops
(b) Leaf water potential	Direct measurement of leaf water content	Widely accepted reference technique	Slow, destructive, and unsuitable for isohydric crops
(c) Relative water content	Direct measurement of leaf water status	Good indicator plant water status, requiring less sophisticated equipment	Destructive and time consuming
(d) Sap flow measurement	Measures the rate of transpiration through heat pulse	Sensitive to stomatal closure and water deficits. Adapted for automated recording and control of irrigation systems	Needs calibration for each tree and is difficult to replicate. Requires complex instrumentation and expertise
(e) Stem and fruit diameter	Measures fluctuation in stem and fruit diameters in	Sensitive measure of plant water stress	Not useful for the control of high frequency irrigation systems

	response to changes in water content		
4. Remote sensing methods			
(a) Infrared thermometry	Measures canopy temperature, which increases as a result of water stress	Reliable and non-destructive	Based on only a few point measurements. Does not account for soil and crop heterogeneity
(I) CWSI	Uses the difference between canopy and air temperatures to quantify crop water stress	Sensitive to stomatal closure and crop water deficit	Influenced by cloud cover, requires different baselines for different crops
(II) DANS, DACT, and Tc ratio	Measure single canopy temperature for quantifying water stress	Require less data than CWSI for detecting water stress. Tc ratio gives quantitative water stress coefficient (Ks) for calculating crop ET	Difficult to scale up to large cropped fields.
(b) Spectral vegetation indices			
(i) Structural indices	Measures reflectance indices within the VIS and NIR	Non-destructive with high temporal and spectral resolution	Requisite image analysis is still a
	spectral range (NDVI, RDVI, OSAVI, TCARI) to		challenging task. Precision reduces from leaf scale to canopy scale

			indicate canopy changes due to water stress
(ii) Xanthophyll indices	Measures PRI and PRInorm, which are sensitive to the epoxidation state of the xanthophyll cycle pigments	Account for physiological changes in photosynthetic pigment changes due to water stress	More work is needed to convert raw imagery to user-friendly irrigation application
(iii) Water indices	Measures the reflectance trough in the near-infrared region (WI, SRWI, and NDWI) used to represent canopy moisture content	Rapid and non-destructive measure of leaf water content	Problem of scaling up to canopy level

2.7.1 Field observation- based indicators

Measurement of the soil water

In situ observations of soil water content, plant characteristics, or climatic factors are used to estimate the quantity of water lost from the plant-soil system during a specific period in traditional agricultural water stress monitoring methods. These approaches are time-consuming and yield point data that provides poor indications of the field's general state(González-Dugo *et al.*, 2006). Information about the soil moisture it is a key role for agronomic, hydrological, and meteorological processes. It can also be a good indicator for detecting water stress and managing irrigation(Sharma *et al.*, 2018).

Plant responses

Plant-based indicators are commonly used to monitor water stress and plan irrigation. Measures of soil water or atmospheric demand are equally important for irrigation scheduling, but the benefit of plant-based measurements is that the plant acts as a biosensor, integrating soil and atmospheric water status as well as the plant's physiological reaction to available water. For the goal of scheduling irrigation, many approaches based on the measurement of plant factors have been devised. The most commonly used methods are either traditional, non-automated methods

for measuring leaf or stem water status, stomatal conductance, or photosynthesis, or methods in which records are taken continuously and automatically, based on measurements of sap flow, trunk diameter, and leaf turgor pressure(Fernández, 2017).

2.7.2 Remote sensing methods

Evapotranspiration based method

Evapotranspiration can be described as indicator of water lost to the atmosphere through the evaporation from the soil and transpiration from the plants. Which effect on hydrological water cycle, plants water status and agricultural planning(H . L. P e n m a n, 1947). For model simulations or empirical equations, ET estimation requires meteorological data. However, because to the diversity of land cover and temporal changes in the environment, these methodologies are not practical for estimating ET at a regional scale. The Penman–Monteith equation is now the most often used technique for determining ET. Because of the point-based approach, this strategy is confined to the local scale and hence unsuitable for large diverse areas. The RS approach has to be introduced to analyse ET at the local and regional levels. RS allows for large area coverage with high-resolution images in an immediate perspective, and the data may be used to obtain metrics such as radiometric surface temperature, VI, and albedo, therefore, Data are more suited for estimating ET using energy balance approaches. Most remote sensing methods used to determine ET employ the energy balance concept and net radiation as the primary factors (Virnodkar *et al.*, 2020).

Spectral indices

Remote sensing has created the opportunity to cover a vast field using non-invasive and productive approaches for detecting geographical variations in plant water status with high temporal resolution. Because they are non-destructive and labour- and time-intensive, remote sensing technologies based on spectral vegetation indices and infrared thermometry are commonly utilized for agricultural water stress detection. In vegetation studies that employ spectral reflectance of crops, the remote sensing approach is widely used. The wavelength of electromagnetic radiation gathered from things on Earth is measured by spectral reflectance. Plant biochemical and biophysical parameters, such as biomass, crop evapotranspiration, and canopy water content, are linked to the spectral qualities required to calculate spectral reflectance. Spectral indices are mathematical combinations of two or more spectral bands that are used to assess water stress in crops. The water index is one of many spectral water and vegetation indexes (WI)(Zarco-Tejada *et al.*, 2013).

Land surface temperature-based technique

Although using the derived LST from satellite data in the Idso technique for calculating CWSI simplifies the process, it is still essential to measure Ta in the field and do some preliminary calculations to determine dT, dTl, and dTu. To overcome these challenges, (Veysi *et al.*, 2017) present a novel method for calculating CWSI that is entirely based on satellite data and does not use any simplified calculations. The CWSI was calculated by replacing dTl (for non-transpiring crops) and dTu (for well-watered crops) with extracted values of TCold and THot from satellite images, respectively as Eq (16).

$$CWSI = \frac{T_S - T_{Cold}}{T_{Hot} - T_{Cold}} \tag{16}$$

Where T_S is LST over the crop, T_{Cold} is temperature for the well-watered plants, T_{Cold} is the temperature for the pixels with maximum amount of water stress. The approach for picking the cold pixel is almost identical to (Bastiaanssen W.G.M. *et al.*, 1998) suggested method for estimating evapotranspiration using the surface energy balance algorithm for land (SEBAL). The strategy used in this approach for choosing the hot pixel differs from that proposed by (Bastiaanssen W.G.M. *et al.*, 1998). The hot pixel in SEBAL must be chosen from the bare soil region, however, in this approach, the hot pixel should be a pixel covered by a plant with the highest level of water stress, as suggested by the CWSI. As a result, a threshold of NDVI > 0.2 was applied to pictures to assess the area covered by vegetation before selecting the Hot pixel. Then, 10% of pixels with the greatest temperature were chosen, and the hot pixel was chosen from among them (Veysi *et al.*, 2017).

3. RESEARCH METHOD

3.1 Study area

The construction of the Aswan High Dam caused the inundation of the old town of Wadi Halfa by Lake Nasser. The New Halfa Agricultural Scheme was initiated in response, as Sudan's largest resettlement project at the time. The New Halfa Agricultural Scheme is a 185,000 ha

agricultural settlement scheme on the western side of Kassala State, roughly 400 km east of Khartoum (Laxén, 2007). The project is located on the Butana plain, along the Atbara River. At the time of its construction, the New Halfa Scheme was Sudan's second-largest irrigation project after the Gezira Scheme, which is still the world's largest irrigation scheme. Sudan's irrigation agency manages the water through the Khasm el Girba dam on the Atbara river (Wallin, 2014). Climatology the area lies in the dry climatic zone, with annual rainfall varying from 200- 300 mm concentrated mainly in July and August, the highest mean daily maximum temperature is 42 C in May, and the lowest mean daily minimum temperature is 14 C in January. Humidity is low most of the year and solar radiation is very high (Adam, 2002). The irrigation system is gravity-fed, with the main canal transporting water to the project area via a network of subsidiary canals and by motorized pumps in the small scheme areas. The irrigation system includes main canals, branch canals, minor canals, quaternary canals, and tertiary farm ditches. Field irrigation is done using the traditional flooding (Angaya) approach. There are significant water losses in the system, reducing the available freshwater supplies, like evaporation, conveyance losses due to infiltration, etc. (Wallin, 2014). The dam was initially intended to store 1.3 billion cubic meters of water. However, by 1976, the reservoir's storage capacity had been decreased to 0.8 billion cubic meters due to significant siltation originated from the upstream catchment of the river Atbara in Ethiopia's highlands (Laxén, 2007). The reservoir's capacity is now about 0.6 billion m^3. During the growing season, water in the smaller canals typically flows permanently. Farmers, however, have complained that some regions receive less water than others. Since the reservoir's capacity is dwindling, the irrigated area is shrinking too. Each agricultural settler was given a 15-feddan hawasha (6.3 ha tenancy) to cultivate cotton, wheat, or sorghum, as well as groundnuts. Mostly cotton was chosen since it is the most important cash crop for the government to provide hard currency and profit for the tenants. Groundnuts are the scheme's second most significant cash crop, and wheat and sorghum were grown as food security crops (Wallin, 2014).
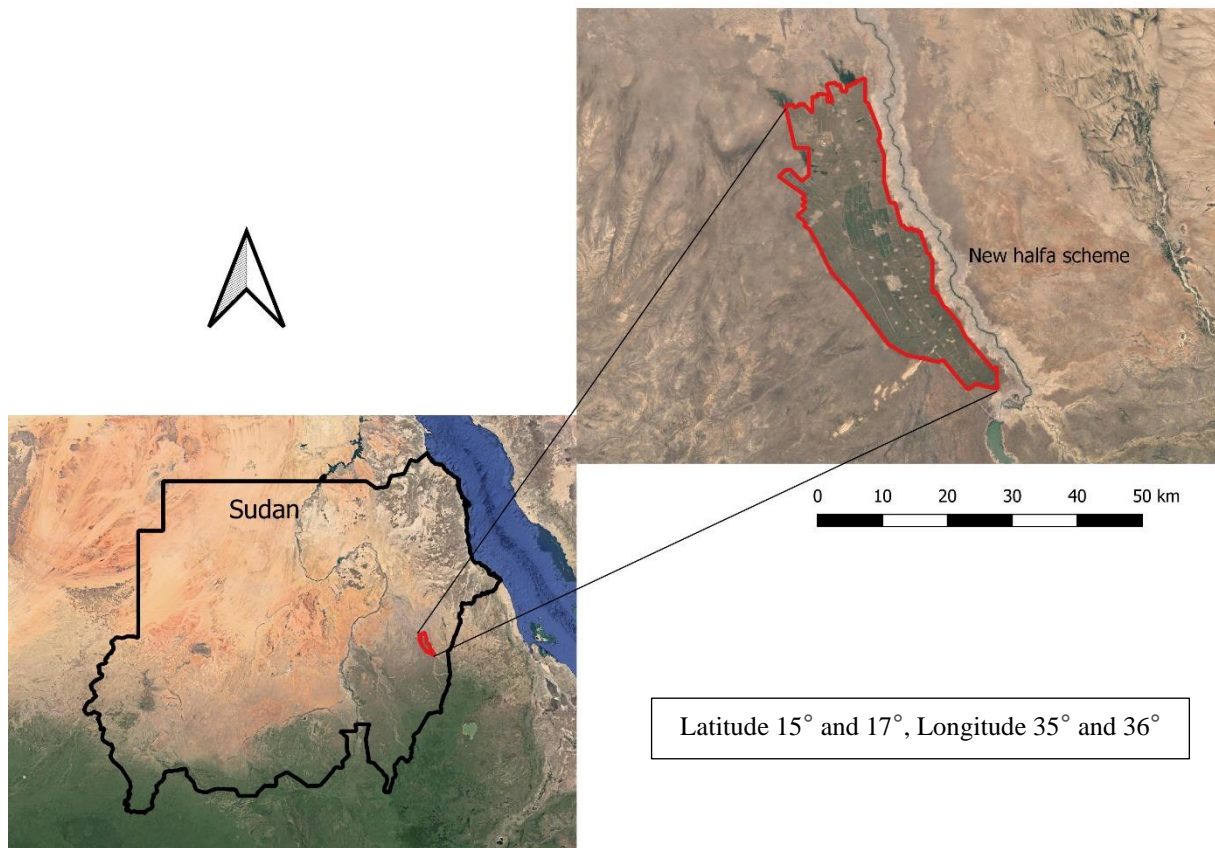
Figure 5. location map describes the study area.

3.2 The framework of the research

This research study is based on the calculation of crop water productivity, irrigation performance assessment and scheduling irrigation for the wheat crop in the New Halfa project. This study is based on several types of data and information such as evapotranspiration, water balance of soil, water requirement for wheat crop and methods of irrigation performance assessment as shown in Figure 6:
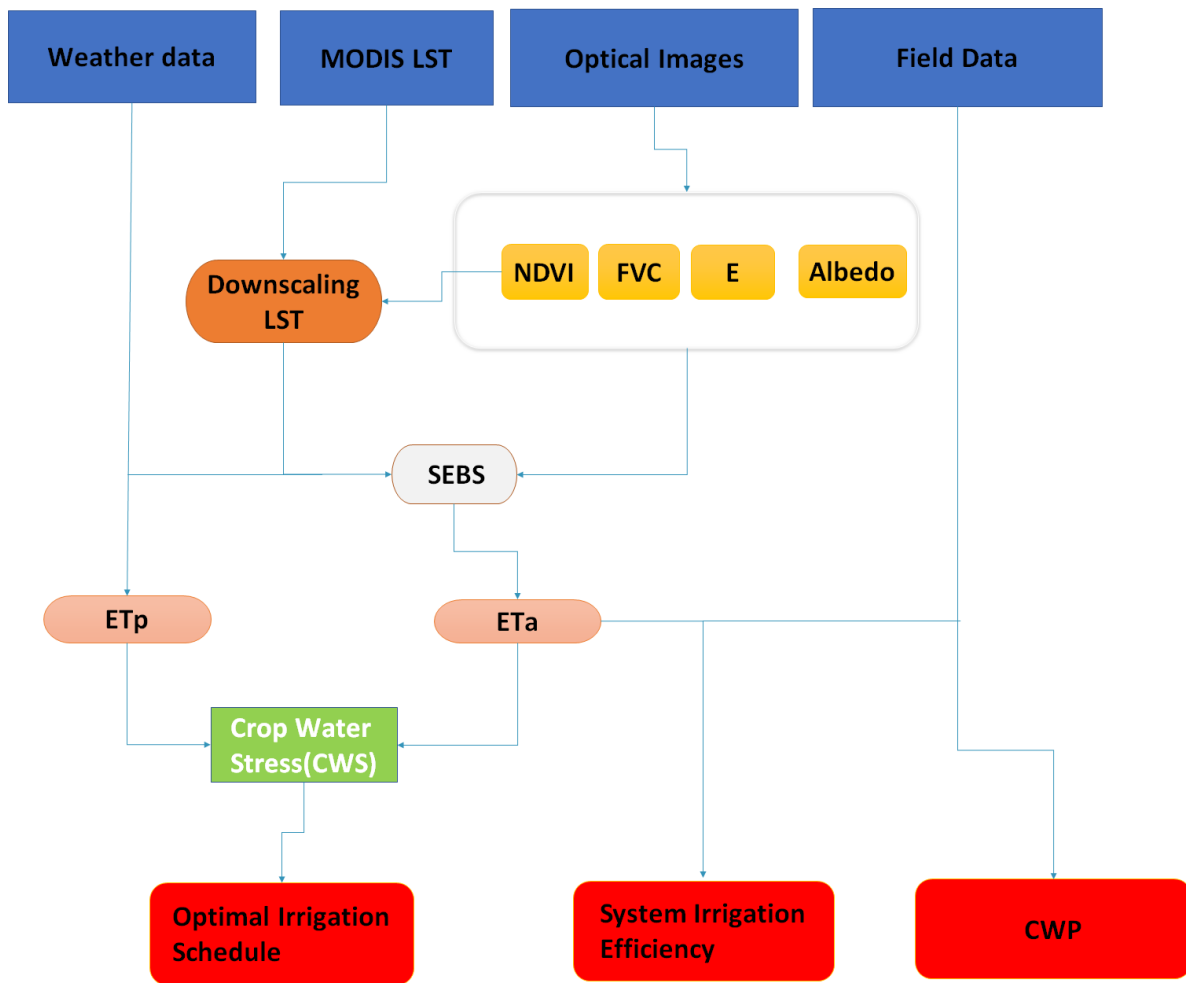
Figure 6. Flow chart of the research

3.3 Land surface temperature downscaling

3.3.1 The DisTrad downscaling procedure for radiometric surface temperature

For finding a mathematical relationship between the radiometric surface temperature and the normalized difference vegetation index, Kustas et al. (Kustas *et al.*, 2003) suggested aggregating the fine-resolution NDVI map to the same coarse-resolution as of the LST map and then to define the regression coefficients of Equation (17) with a least square fitting using a second order polynomial.

$$LST^*_{CR} = a + b\,NDVI_{CR} + c\,NDVI^2_{CR} \tag{17}$$

Where:

LST_{CR}^* : Land surface temperature at the coarser resolution (°C).

$NDVI_{CR}$: Aggregated normalized difference vegetation index at the coarser resolution (-).

The LST is influenced not only by the vegetation cover but also by other factors, such as soil moisture (Srivastava *et al.*, 2013). When these factors are overlooked during the downscaling process, the results are affected by the spatial variation of the factor values. To overcome this problem (Kustas *et al.*, 2003) used the difference of the aggregated downscaled LST and the original one (Equation (35)) for each pixel, to estimate the error that represented the influence of other factors, such as soil moisture, and then used it for correction by Equation (18).

$$\Delta\hat{T}_{CR} = LST_{CR} - \widehat{LST}_{CR} \qquad (18)$$

Where:

$\Delta\hat{T}_{CR}$: residual of the land surface temperature (°C).

LST_{CR}: land surface temperature defined from the satellite measurement (°C).

$\widehat{LST}_{CR}$: aggregated downscaled land surface temperature (°C).

$$LST_{FR} = LST_{FR}^* + \Delta\hat{T}_{CR} \qquad (19)$$

Where:

LST_{FR}: Corrected, downscaled land surface temperature at the fine resolution (°C).

LST_{FR}^*: Land surface temperature calculated by Equation (34) from the original fine-resolution NDVI (°C).

In practice, for defining the NDVI-LST relationship, the coarse-resolution NDVI map was divided into three NDVI classes and the coefficient of variation of the fine-resolution NDVI values within each coarse-resolution pixel was calculated. For avoiding the influence of heterogeneity, this map was divided into three classes: NDVI < 0.2 for the bare soil, 0.2 < NDVI < 0.5 for the partial vegetation, and NDVI > 0.5 for the full vegetation. Finally,

25% of the pixels, with the lowest coefficient of variation, were selected from each group to obtain the correlation (Kustas *et al.*, 2003).

3.3.2 DisTrad modification

The study area may be classified as a mixed landscape with a variety of distinct land cover types (dense vegetation, medium dense vegetation, low-density vegetation, bare soil, urban areas, and water). The DisTrad approach is based on the correlation between the LST and NDVI. The original approach uses a second-order polynomial regression, assuming a non-linear relationship between the two variables. However, in certain cases, outliers at the edges of the value range may strongly affect the second-order polynomial. To circumvent this issue, we tested whether a linear regression would improve the robustness of the regression equation.

Furthermore, the original DisTrad technique recommends using 25% of the aggregated pixels with the lowest coefficients of variation for parameterising the regression equation. Nonetheless, in the case of a heterogonous area (e.g., due to small agricultural fields relative to the coarse pixel size), where the CV of the original NDVI values within most of the coarse-resolution pixels is relatively high, we tested the effect of using only 10% of the aggregated pixels with the lowest coefficients of variation in defining the parameters of the regression equation.

3.4 Evapotranspiration estimation

Evapotranspiration is one of the largest fluxes in the water balance of arid and semi-arid regions. Due to the large temporal and spatial variation of ETa, there will be a need for a high spatial resolution for all the inputs for measuring the ETa by using earth observation, which is not available for the LST. Therefore, there is a need to downscale the available low spatial resolution data, like MODIS.

For the period December–March 2017/2018, 67 MODIS images and 7 Landsat images were collected that were relatively cloud-free and relevant to the research region. The images were spatially registered to each other and to the Universal Transverse Mercator map projection (UTM zone 36N - EPSG:29636).

In this study, the Surface Energy Balance System (SEBS) (Su, 2002) have been applied to map wheat ETa. The remote sensing data of Landsat-8 and Sentinel-2 have been used. The SEBS model also requires the meteorological data, such as wind speed and air temperature as input. The meteorological data obtained from the Meteorological Bureau of New Halfa.

The SEBS model combines the remote sensing data and the meteorological data to calculate the instantaneous net radiation Rn, soil heat flux G and sensible heat flux. Then the energy balance equation is applied to calculate the instantaneous ET when the satellite passes over the study area. The daily evapotranspiration is calculated from the instantaneous ET using the assumption of constant evaporation fraction over the day, we will use Penman-Monteith method to calculate ET when the satellite images are not available. The calculation of the main parameters by the SEBS model is given as follows Su (2002).

3.4.2 Preparation of the input data for SEBS

To estimate actual evapotranspiration in SEBS the following data need to be prepared.

Normalized different vegetation index (NDVI) for Lnadsat-8

The NDVI was derived from Landsat 8 using Equations (20).

$$NDVI = \frac{\rho_5 - \rho_4}{\rho_5 + \rho_4}$$

(20)

Where: ρ_5 is the reflectance in band 5, and ρ_4 is the reflectance in band 4.

Normalized different vegetation index (NDVI) for Sentinel-2

The NDVI was derived from Sentinel-2 by using Equations (21).

$$NDVI = \frac{\rho_8 - \rho_4}{\rho_8 + \rho_4}$$

(21)

Where: ρ_8 is the reflectance in band 8, and ρ_4 is the reflectance in band 4.

Figure 7 Spatial and temporal variation of the NDVI for the available Landsat-8 images during the winter season 2017-2018.
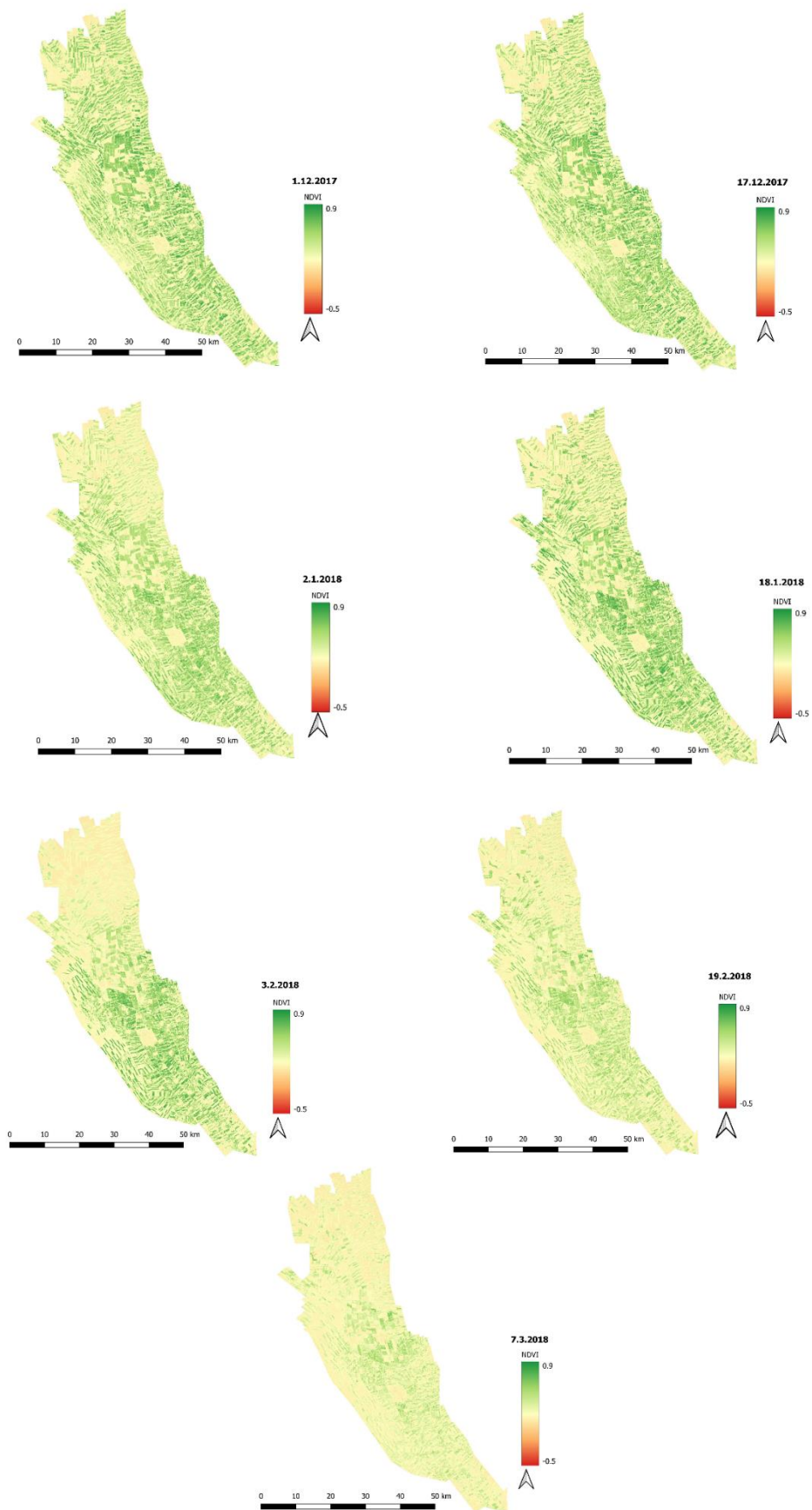
Figure 7. Spatial and temporal variation of the NDVI in the New Halfa scheme

Fraction of vegetation cover (FVC)

FVC can be derived from NDVI maps. In this study, FVC was estimated as proposed by (Jiménez-Muñoz *et al.*, 2009) for fully vegetated cover and bare soil, as presented in Equation (22).

$$FVC = \frac{NDVI - NDVI_s}{NDVI_v - NDVI_s}$$

(22)

where $NDVI_s$ represents the NDVI of bare soil, *NDVI* is the value of the actual pixel, and $NDVI_v$ corresponds to the NDVI value of the full vegetation canopy coverage.

Emissivity

The broad band land surface emissivity (ε) is calculated based on the FCV using Equation (23), which was introduced by Sobrino, Jiménez-Muñoz and Paolini (2004).

$$\varepsilon = 0.004 \times FVC + 0.986$$

(23)

Albedo

Albedo is the reflectance of a surface over a wide range of wavelengths. It indicates the reflected fraction of incoming radiation. Landsat 8 and Sentinel-2 are Earth observation satellite projects that provide useful data for a variety of purposes such as land monitoring, environmental assessment, agriculture, and urban planning. While their aims are similar, there are variances in their sensor properties and band arrangements. Despite this, attempts have been undertaken to achieve functional equivalence between the two satellite systems. A broad explanation of the substitution of comparable bands between Landsat 8 and Sentinel-2 follows:

Number of Bands:

Landsat 8: It has 11 spectral bands.

Sentinel-2: It has 13 spectral bands.

Spectral Range:

Landsat 8: Captures data in the visible, near infrared, and short-wave infrared regions.

Sentinel-2: Also captures data in the visible, near-infrared, and short-wave infrared regions, with an extended range into the coastal and the water-vapor bands.

47

Equivalent Bands:

To achieve functional equivalence and cross-compatibility between Landsat 8 and Sentinel-2 data, scientists and researchers have identified corresponding bands with similar spectral characteristics. the equivalent bands are as follows:

Red (Landsat 8 Band 4) ≈ Red (Sentinel-2 Band 4)

Green (Landsat 8 Band 3) ≈ Green (Sentinel-2 Band 3)

Blue (Landsat 8 Band 2) ≈ Blue (Sentinel-2 Band 2)

Near-Infrared (NIR) (Landsat 8 Band 5) ≈ Red-edge (Sentinel-2 Band 5)

Short-Wave Infrared (SWIR) (Landsat 8 Band 6) ≈ Vegetation Red-Edge (Sentinel-2 Band 5)

The broadband albedo was calculated using the Landsat 8 (OLI sensor) algorithm at the visible and NIR bands 2 to 7 in this study using Equation (24) and for Sentinel-2 as in the Equation (25) (Liang *et al.*, 2003).

$$\alpha_{OLI} = 0.362\rho_2 + 0.13\rho_4 + 0.373\rho_5 + 0.085\rho_6 + 0.072\rho_7 - 0.0018 \qquad (24)$$

Where: α_{OLI} is the shortwave albedo for Landsat, and ρ_i is the reflectance of bands i=2, 4, 5, 6 and 7.

$$\alpha_{Sentinel} = 0.362\rho_2 + 0.13\rho_4 + 0.373\rho_8 + 0.085\rho_{11} + 0.072\rho_{12} - 0.0018 \qquad (25)$$

Where: ρ_i is the reflectance of bands i=2, 4, 8, 11 and 12.

Meteorological data

ERA5 provides data on planetary boundary layer height, incoming shortwave radiation, specific humidity, and pressure, while the ERA interim data set provides data on sunlight hours.

The air temperature and wind speed inputs obtained from the New Halfa meteorological station. These data will be considered as representative of the study area.

3.4.3 Data and processing

Various data were downloaded from different open data sources as shown in Table 2.

Table 2. Data sources.

| Data	Source	Spatial Resolution	Temporal Resolution
Landsat 8	https://espa.cr.usgs.gov/ordering/new/	30 m	16 days
MODIS MOD11A1 V6	https://earthexplorer.usgs.gov/	1 km	Daily
NDVI	https://espa.cr.usgs.gov/ordering/new/	30 m	16 days
Sunshine Duration	https://apps.ecmwf.int/datasets/data/ interim-full-daily/levtype=sfc/	80 km	Daily
SRTM DEM	https://earthexplorer.usgs.gov/	30 m	-
Other climatic Data	https://www.ecmwf.int/en/forecasts/ datasets/reanalysis-datasets/era5	9 km	Daily
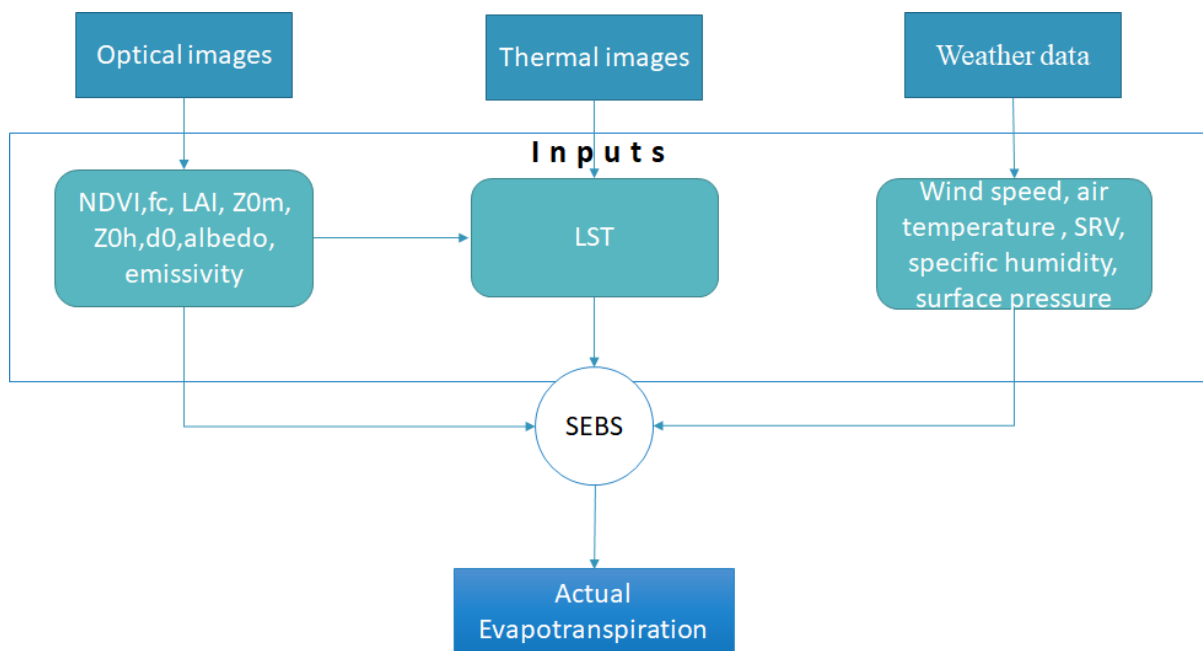
Figure 8 . Flow chart for SEBS.

3.4.4 Retrieval of actual evapotranspiration in SEBS

Using the SEBS extension in the ILWIS software, daily evapotranspiration was calculated from the MODIS Terra images. For all days of coinciding with the MODIS overpass, FVC, NDVI, emissivity, and albedo were calculated from Landsat 8 and Sentinel-2 images. Maps of

49

evaporative fraction, daily evapotranspiration, and relative evapotranspiration were produced. A total of sixty-seven maps were created, for the days when LST MODIS data was available.

3.4.5 Validation of evapotranspiration

SEBS-derived daily evapotranspiration was verified for the research region.

Since in situ ET data were not available in the irrigated fields, the SEBS estimate was validated by comparing it to potential evapotranspiration estimated using crop coefficient and reference ET. This was based on the assumption that under irrigated conditions the crop's actual ET is approximately equal to the crop's potential evapotranspiration. Potential evapotranspiration (ET_p) was estimated in the New Halfa scheme as a product of reference evapotranspiration (ET_0) using the Penman-Monteith method and k_c values.

The coefficient of determination (R^2), mean absolute error (MAE), and root mean square error (RMSE) are statistical measures of accuracy used to evaluate the performance of SEBS estimations (Equations 26, 27 and 28).

$$R^2 = 1 - \frac{\sum(X_{m,i} - X_{o,i})^2}{\sum(X_{m,i} - X)^2} \qquad (26)$$

$$RMSE = \sqrt{\frac{\sum_{i=1}^{n}(X_{m,i} - X_{o,i})^2}{2}} \qquad (27)$$

$$MAE = \frac{\sum_{i=1}^{n}[abs(X_{m,i} - X_{o,i})]}{n} \qquad (28)$$

Where: ET_{crop} is the actual ET for the crop under irrigation, K_c is the crop coefficient for the particular crop, $X_{m,i}$ is the modelled variable, $X_{o,i}$ is the observed variable, and n is the number of observations.

3.4.6 Sensitivity assessment of the SEBS-derived ET_a

SEBS is sensitive to all input parameters (Van Der Kwast *et al.*, 2009), but only the meteorological variables were subjected to sensitivity analysis, since the meteorological variables were acquired as point measurements. The sensitivity analysis sought to examine the uncertainty that is generated by spatial variations in the meteorological variables.

To perform a sensitivity assessment, SEBS was initially run under normal conditions at the time of satellite overpass for Julian day number 45, which corresponds to January 26thto calculate

the daily evapotranspiration. The input was then changed at 10-percent intervals between -20 and 20%. The following equation was used to calculate the sensitivity of SEBS generated ET.

$$S = \frac{\pm X - X_0}{X_0} \cdot 100$$ (29)

Where S is the sensitivity %, $\pm X$ is ET_a after modifying the variables, X_0 is ET_a under the normal conditions.

3.5 Crop coefficient estimation

Farbrother (1973) used GRS to undertake a series of tests to determine the crop factor of several crops, including wheat. The evaluation was based on soil moisture depletion (gravimetrically) and Penman's (1948) model for estimating evaporation from exposed water surfaces. Due to climate change and adoption of improvements in the field of crop husbandry and varieties, the historical Farbrother's k_c should be updated for the estimate of an adequate crop water requirement (CWR) for wheat required by the decision maker. The following equation (30) can also be used to calculate the kc:

$$Kc = \frac{ET_a}{ET_0}$$ (30)

Where ET_a is actual evapotranspiration estimated by SEBS and ET_0 is reference evapotranspiration derived by Penman-Monteith formula.

3.6 Irrigation performance

In this study two irrigation performance indicators were used to assess the irrigation performance in the New Halfa scheme.

3.6.1 Classical irrigation efficiency

This concept was used to assess the irrigation system performance as shown in equation (31).

$$E_i = \frac{ET_i}{W_g - P_e}$$ (31)

where ET_i is the water that was used by E and T, W_g is the gross supply which represents the water delivered by the canals, and Pe is the effective precipitation or precipitation that decreases the quantity of irrigation water required. Since the value of the effective precipitation during winter season is approximately zero that means the equation will be as Equation (32).

$$E_i = \frac{ET_i}{W_g}$$

(32)

3.6.2 Water productivity

Water productivity has been proposed as a metric for analysing water consumption and evaluating irrigation efficacy. WP (grain yield per unit of actual ET) was calculated in this study using Molden's indicator (Molden, 1997), Equation (33).

$$WP = \frac{Y}{ET_{cs}}$$

(33)

Where WP is water productivity, Y is the wheat seasonal crop yield in $Kg.ha^{-1}$ and ET_{cs} is actual seasonal evapotranspiration for wheat crop in $m^3.ha^{-1}$.

3.7 Scheduling irrigation for wheat crop

3.7.1 Crop water stress

For scheduling irrigation, the crop water stress index has been used as indicator for the crop water status which has a key role for applying the irrigation events. The evapotranspiration have been used to estimate the Crop water stress index (CWSI) where we can define the CWSI as the ratio between actual and potential evapotranspiration. which the crop with adequate water will transpire in the same rate as the potential evapotranspiration but when the water becomes limiting the actual evapotranspiration will fall below the potential evapotranspiration this ratio range from 0 to 1 where 0 it means that there is no stress and 1 is high rate of the stress.

Several writers have hypothesized that loss of turgor and stomatal closure is caused by both a lack of soil water and a high evaporative demand. This is based on the idea that high evaporative demand necessitates a high rate of water intake and transport, resulting in a larger energy loss between the water in the soil and the stomates. Because evaporative demand varies diurnally and from day to day, methods for estimating evapotranspiration on a daily basis with high accuracy are required.

The SEBS model was used to calculate the daily actual evapotranspiration. The potential evapotranspiration was calculated by multiplying ET_0 and the crop coefficient k_c

$$ET_c = k_c \times ET_o$$

(34)

Finally, the CWSI can be calculated as equation (35).

$$\text{CWSI} = 1 - \frac{ET_a}{ET_c} \tag{35}$$

The CWSI of the wheat crop for the growing season 2017-2018 was calculated in three different sites of the scheme for all the available days.

3.7.2 Scheduling irrigation

The calculation of the scheduling of irrigation is based on a daily accounting of all ingoing and outgoing water in the root zone according to Toureiro *et al.* (2017) In our case, the crop water requirement was considered to be equal to the actual evapotranspiration because the soil type in this area is vertosol where there is no infiltration more than one meter, and the fields in this scheme designed to be without considering drainage canal and that to encourage the farmers to use the water efficiently.

$$\theta m_i = \theta m_{i-1} + P_i + I_i + CR_i - RO_i - DP_i - ETca_i \tag{36}$$

Where:

i= day in the calculation procedure

θm = water content within the soil root depth

P = total rainfall

I = the effective depth of water applied with irrigation

CR = capillary rise from deep (free) water table

RO= run off

DP= deep percolation

ETca= Actual crop evapotranspiration, crop water consumption.

4. RESULTS AND DISCUSSION

4.1 Landsat-8 LST downscaling process

4.1.1 Relationship between land surface temperature and the vegetation cover

The DisTrad method recommended the use of 25% of aggregated pixels with the lowest coefficient of variation for defining the regression equation. Still, in the case of a heterogonous area, like the small fields in the study region, the coefficient of determination can be low due to the high number of mixed pixels. To overcome these problems, 10% of the aggregated pixels with the lowest coefficient of variation were used to fit the correlation. To investigate the reliability of using 10% of the aggregate pixels to establish the regression relation, we examined the correlation between NDVI and LST at 1km resolution by using 10% and 25%.

The results show that using 10% of the data with the lowest coefficient of variation gave a higher correlation than using 25% of the data with the lowest coefficient of variation, which R2 was 0.75 and 0.80 for LST25% and 10%, respectively, as shown in (Figure 10). LST is inversely linked to NDVI (Figure 10), as was shown by, among others, Karnieli *et al.* (2006) and Jeganathan *et al.* (2011).

(a)   (b)
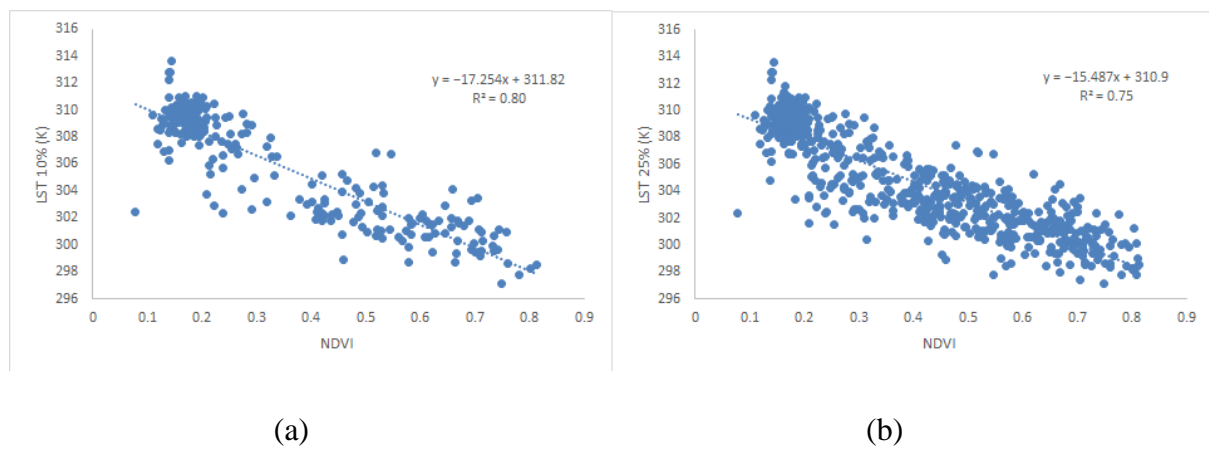
Figure 9 . (a), (b) correlation between the NDVI and LST for 25% and 10% methods, respectively.

The relationship between the vegetation cover and land surface temperature (Landsat-8 LST resampled to 30m, downscaled LST10%, and downscaled LST25%) have been investigated at 30 m resolution. (Figure. 11) shows the result of the correlation (R^2) between the NDVI and LST. (R^2) indicates that there is a strong correlation between LST and NDVI, with values ranging from 0.86 to 0.84, all statistically significant. As shown in (Figure 11), the results show an agreement when using 10% or 25% of the aggregated pixels for the downscaling process. Using 10% of the pixels gives a good result where R^2 values of both methods, 10%, and 25% were (0.84, 0.86). However, it was higher than R2 between LST and NDVI for the native LST

(Landsat-8 LST 100m resampled to 30m) R^2 (0.69). (Figure 11) shows that using 10% and 25% of the pixels with the lowest coefficient of variance enhances the correlation between land surface temperature and NDVI. We attribute that to the fact that LST is from the native Landsat image. It has a spatial resolution of 100 m and is resampled to 30 m resolution. As a result, the fields in the downscaled LST maps are more detailed as shown in figure 12.
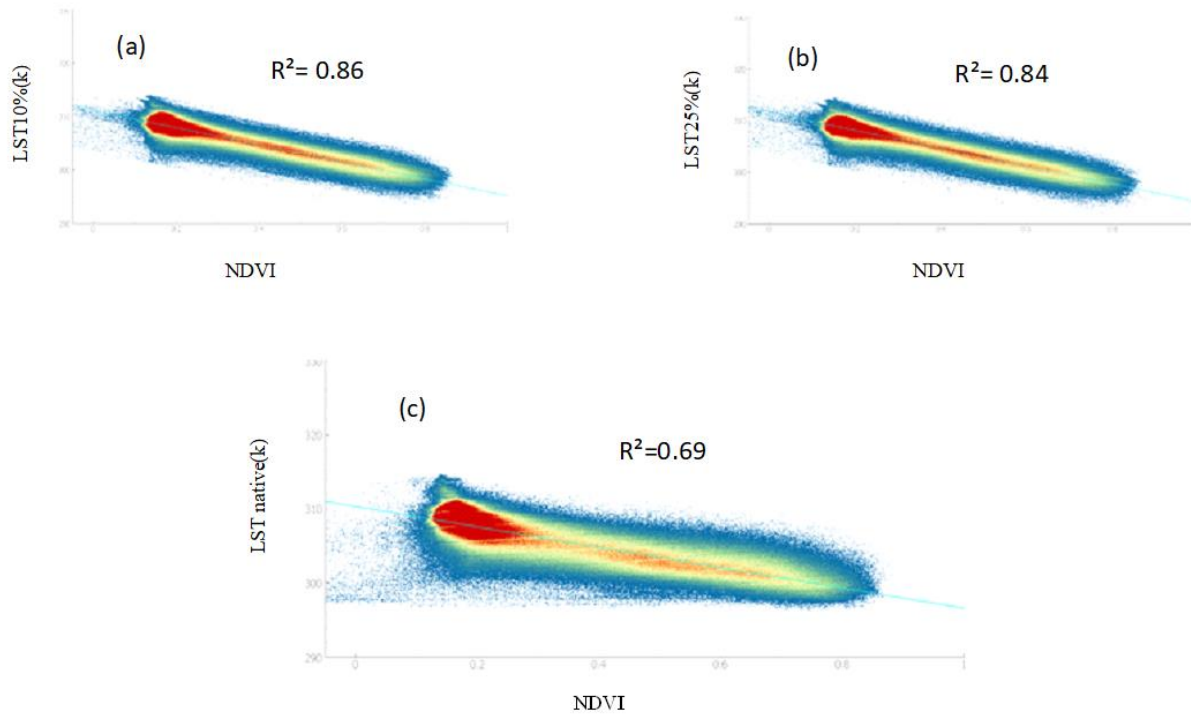
Figure 10. (a), (b), (c) scatter plot for the relation between NDVI and LST 10%, LST 25%, and LST native, respectively.

4.1.2 Effects of LST downscaling of the Landsat 8 image

Figures 12 show native LST (LSTnative) and downscaled LST (LSTdown) images of a subset of the study area with a target resolution of 30 m. Lower temperatures are associated with dense vegetation (and water surfaces), whereas higher temperatures are associated with urban and bare soil regions distant from cultivated land and dry sandy riverbanks. The mixed land cover zones have a moderate temperature. These downscaled LST patterns are identical to the original in contrast, tone, and saturation Figures 12.
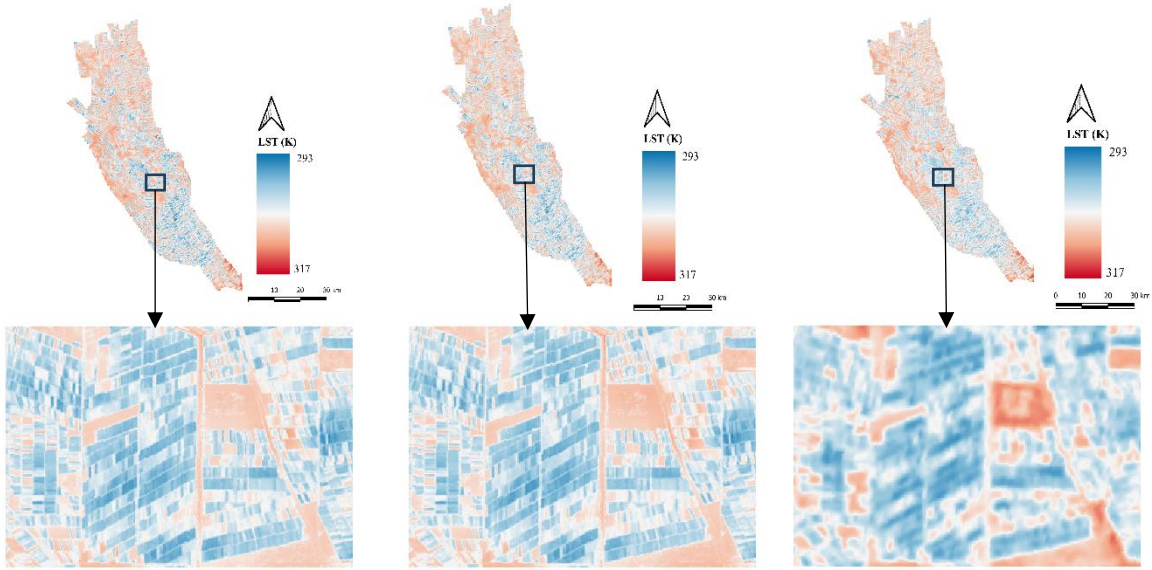
Figure 11. (a) LST Landsat10%, (b) LST Landsat 25%, and (c) LST Landsat native.

However, the simulated LST is unable to determine the temperature of the water bodies, because of the difficulty of downscaling LST in such a class due to the sharp NDVI contrast between the water body and surrounding land. Which is why LST10% and LST25% are greater than LSTnative with a difference of 2K. Since the DisTrad method is based on the relation between the vegetation cover and LST, from the visual interpretation we found that the error percentage is greater in the water body. These results agree with the results found by Mukherjee, Joshi and Garg (2014). Similarly, urban landscapes show higher error rates. A minimum error was found in the cultivated area. According to Agam *et al.* (2007) and Jeganathan *et al.* (2011), homogenous vegetated areas have a lower value of downscaling error due to the accurate fitting of regression models over such regions. Table 3 shows Mean Absolute Error MAE, the minimum and maximum MAE and Root Mean Square Error RMSE, calculated from the difference between LSTdown and LSTnative. The minimum and maximum temperature values of LSTdown surfaces also agree with the LSTnative.

Table 3. Statistical analysis for the relation between native LST, LST25%, and LST10%.

Method	Max MAE	Min MAE	MAE	RMSE
LST 25%	9.37	-5.12	-0.011	0.89
LST 10%	10.16	-5.63	-0.012	0.98

Figure 13. shows the correlation between LSTnative (x axis) and LST10% and LST 25% (y axis) for the linear regarrison. The coefficient of determination (R2) is 0.72, 0.74 respectively, while it was 0.61 for the polynomial regression. This result indicates that using linear regression for the downscaling process gives better result than using the polynomial regression, where the 25% polynomial results in several extreme values. The same result was observed by (Agam *et al.*, 2007). This is because of the increasing degree of subpixel variability. Based on this statistical analysis, this modification yields superior results since the other scientists were attempting to achieve coarser resolution than the goal of this research (30m).
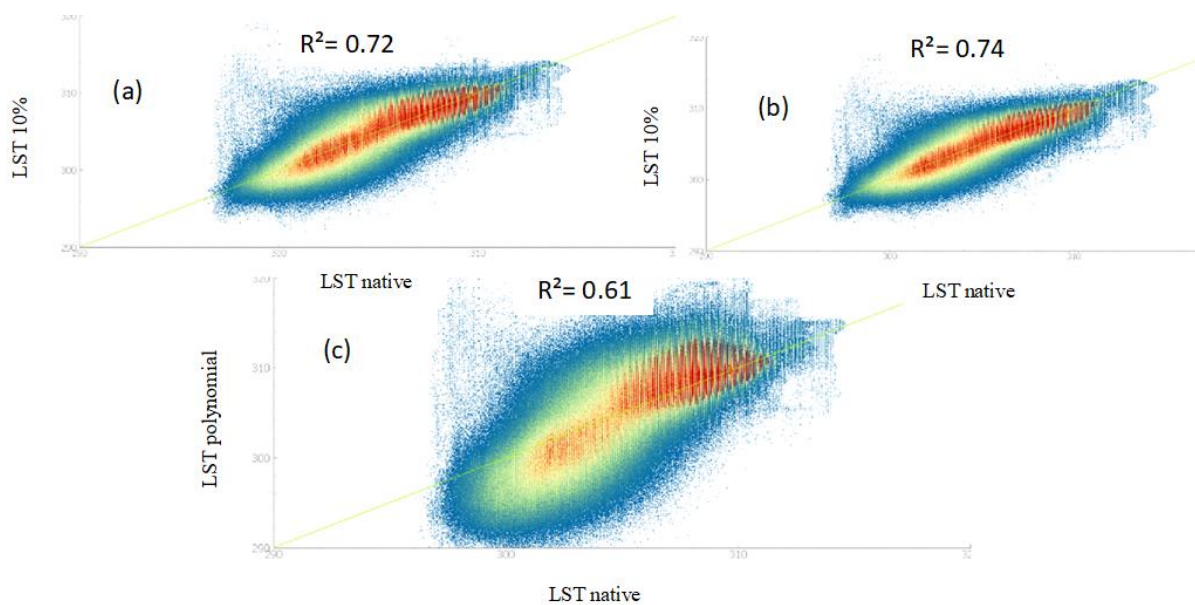
Figure 12. (a), (b), (c) scatter plot between native LST with LST10%, LST 25%, and LST25% polynomial, respectively.

4.1.3 Effects of downscaling LST on ET_a estimation

The Surface Energy Balance System utilized the downscaled land surface temperature to estimate the actual evapotranspiration with high spatial resolution as described in (section 3.4).

Concerning the effect of downscaling the land surface temperature on the evapotranspiration estimation, we found that the downscaling using only 10% of the pixels results in a good correlation between the ET_a calculated from the LSTnative and ETa calculated from LST10% and LST25%, due to the high degree of convergence between the results from these two methods and the native Land Surface Temperature. Where the coefficient of determination for both methods 10% and 25% were R^2= (84.5 and 84.1) as shown in (Figure 15), yielded an average RMSE (0.3 and 0.28 mm/day, respectively). The evapotranspiration maps produced

using downscaled land surface temperature had a higher spatial resolution than those produced using native land surface temperature, as the details and boundaries of small fields are more accurate on these maps than on the maps produced using native land surface temperature, as shown in Figures 14 and 15. Bindhu, Narasimhan and Sudheer (2013) produced RMSE in the similar range of 0.16 with TsHARP = 0.55 mm/day using the non-linear disaggregation approach (NL-DisTrad).
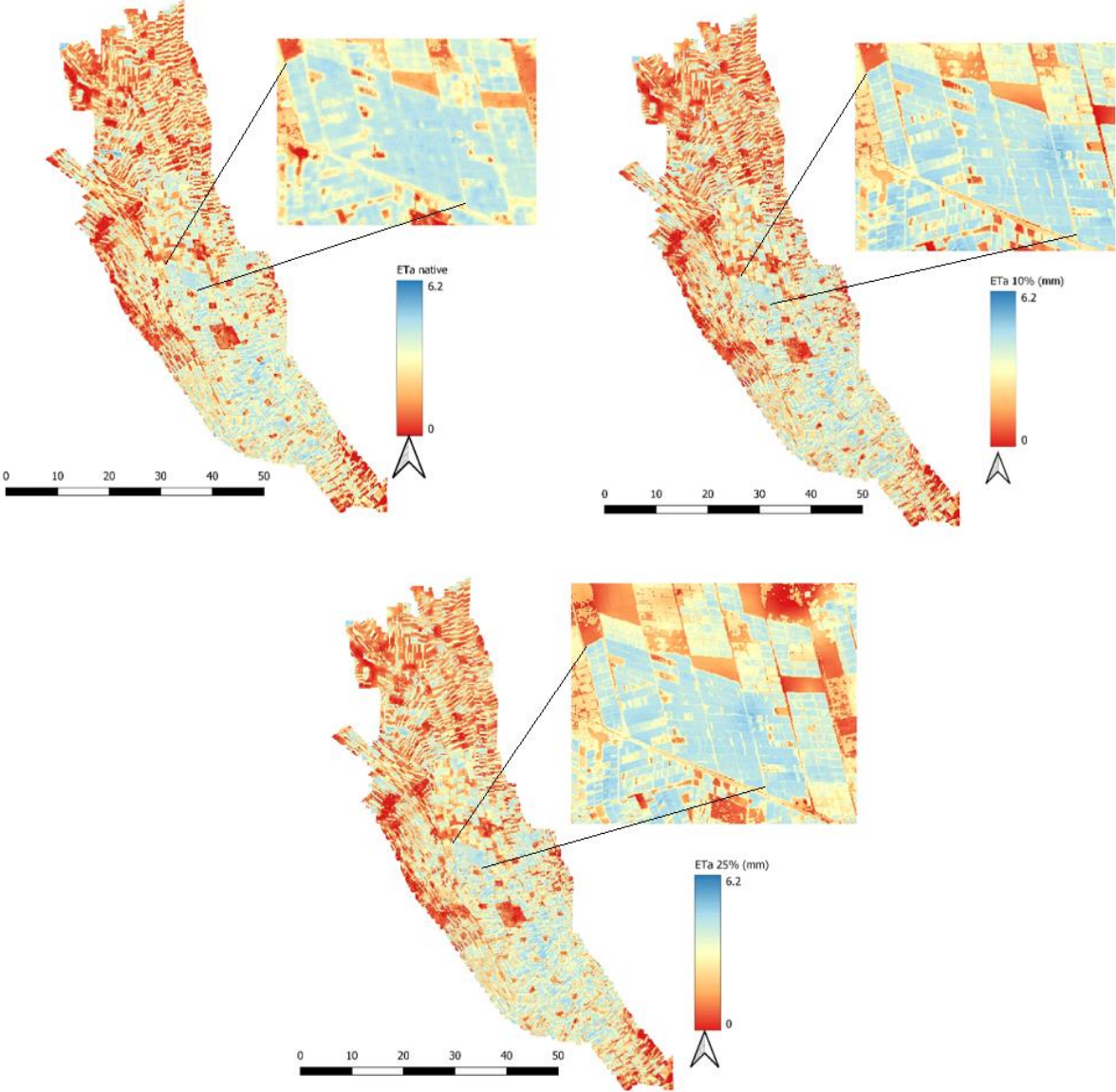
Figure 13. (a), (b), and (c): ET_a for native LST, LST 10% and LST 25% respectively.
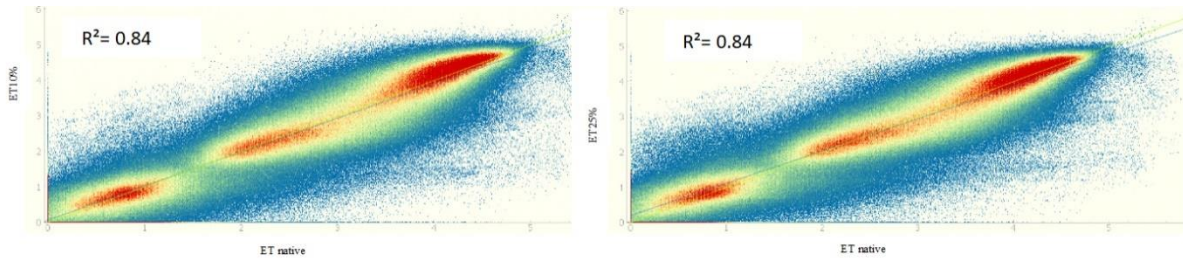
Figure 14. (a) and (b) scatter plots for the correlation between ETa (LST native) and ETa (LST10%), (LST25%) respectively.

4.2 Application of the downscaling model on MODIS data

After applying the downscaling model with both methods on the Landsat8 image, the downscaled surface temperature gives reasonable results at a resolution of 30 m as shown in (section 4.1.3). MODIS data at 1000 m spatial resolution is available with a temporal resolution of one day. The optical data of 250 m and 500 m are also available with temporal resolution every day, but the obstacle to using optical data from MODIS is that the results obtained from these sensors are not suitable for use in water management for small fields due to their poor spatial resolution. Therefore, it is preferable to use optical data from Landsat and Sentinel2 because they have a high spatial resolution of 30 m and 10m. We find that the NDVI from a single Landsat8 and Sentinel2 images is suitable for the downscaling model of more than one MODIS image, where it is assumed that the NDVI does not change significantly during this period. Therefore, the NDVI produced by Landsat8 and Sentinel2 was used to model the land surface temperature with MODIS products. By visual interpretation of the maps resulting from the downscaling process, we find that the downscaling process gives the same effect that appeared when the model was used on the thermal image of Landsat8, where the downscaling led to the clarification of the small fields and the indication of their boundaries. We also find that the land surface temperature pattern follows the NDVI pattern in terms of intensity. The low temperatures are in the fields with high NDVI values, while the hot temperatures appear in the fields with low NDVI intensities i.e., in the bare soil and urban areas. This method was followed due to the lack of land surface temperature data for the surface on these days to be taken as a reference. As several scientists indicated, we needed data taken on the same day to be considered a reference and used to validate these results (Njuki, 2016; Kyalo, 2017). Some scientists pointed out that the difference in the sensors could also affect the results (Mukherjee, Joshi and Garg, 2014). On the other hand, when comparing the modifications applied to the Kustas method, the parameterization improves the correlation between the vegetation cover and

LST, as shown in Figure 16 (a) NDVI and LST25% correlation, (b) NDVI and LST10% correlation and Figure 17 ET_a (a) derived from MODIS LST resampled and (b) downscaled, respectively. MODIS LST (c) resampled and (d) downscaled. However, when we tested the MODIS land surface temperature using Landsat 8 data, the findings revealed an average RMSE of 1.3 K.

LST-NDVI 10% 18-12-2017

y = -11.518x + 315.79
R² = 0.58

LST-NDVI 25% 18-12-2017

y = -8.5486x + 314.75
R² = 0.40

LST-NDVI 10% 21-12-2017

y = -11.21x + 313.76
R² = 0.55

LST-NDVI 25% 21-12-2017

y = -8.3733x + 312.68
R² = 0.37

LST-NDVI 10% 28-12-2017

y = -13.865x + 315.36
R² = 0.62

LST-NDVI 25% 28-12-2017

y = -10.791x + 314.19
R² = 0.48

LST-NDVI 10% 29-12-2017

y = -12.26x + 312.93
R² = 0.61

LST-NDVI 25% 29-12-2017

y = -9.3392x + 311.88
R² = 0.48

LST-NDVI 10% 30-12-2017

y = -16.155x + 315.41
R² = 0.69

LST-NDVI 25% 30-12-2017

y = -12.573x + 314.1
R² = 0.57

LST-NDVI 10% 31-12-2017

y = -9.486x + 308.29
R² = 0.51

LST-NDVI 25% 31-12-2017

y = -7.7772x + 307.6
R² = 0.42

LST-NDVI 10% 3-1-2018

y = -11.399x + 309.46
R² = 0.63

LST-NDVI 25% 3-1-2018

y = -8.4168x + 308.33
R² = 0.45

LST-NDVI 10% 4-1-2018

y = -14.707x + 311.36
R² = 0.61

LST-NDVI 25% 4-1-2018

y = -12.076x + 310.4
R² = 0.52

Figure 15 . Correlation between NDVI, LST25%, and LST10% respectively.
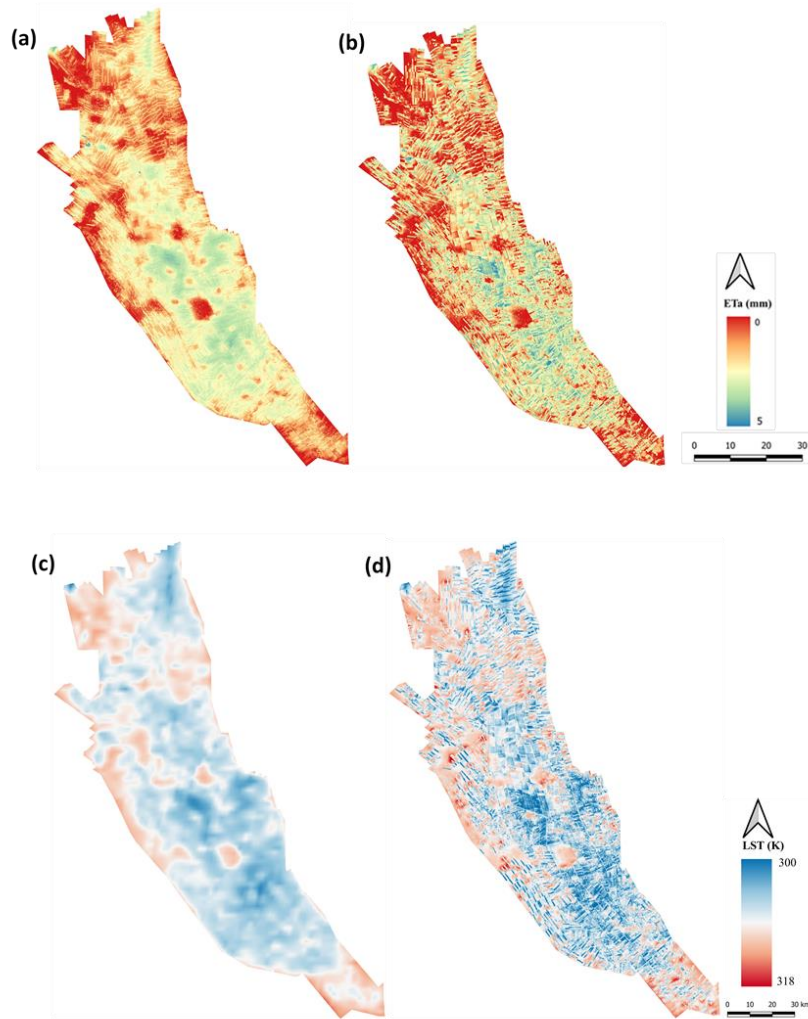
Figure 16. (a) and (b) ET$_a$ from MODIS LST resampled and downscaled, respectively. (c) and (d) MODIS LST resampled and downscaled, respectively.

4.3 A combination between different optical data for downscaling

The poor temporal resolution of the Landsat 8 images limits their use in estimating daily evapotranspiration for water management. This poor temporal resolution prevents the use of the Normalized Difference Vegetation Index produced by Landsat8 for the daily LST downscaling process. Cloud distortion can be another limiting factor that affects the Landsat images' usability for evapotranspiration estimation.

In order to fill the gap left by the Landsat images, images of Sentinel-2 with a higher spatial and temporal resolution were used (spatial resolution is 10-20 m and the temporal resolution is at least 5 days) for the days when Landsat images were not available. In this study, 6 images from Sentinel-2 were processed. We tested the correlation between the NDVI generated by the two sensors as shown in (figures 18, 19). The goal of this test was to check whether the Landsat

8 and Sentinel-2 images could be integrated into a consistent time series of NDVI maps with 30 m field resolution for the LST downscaling procedure.
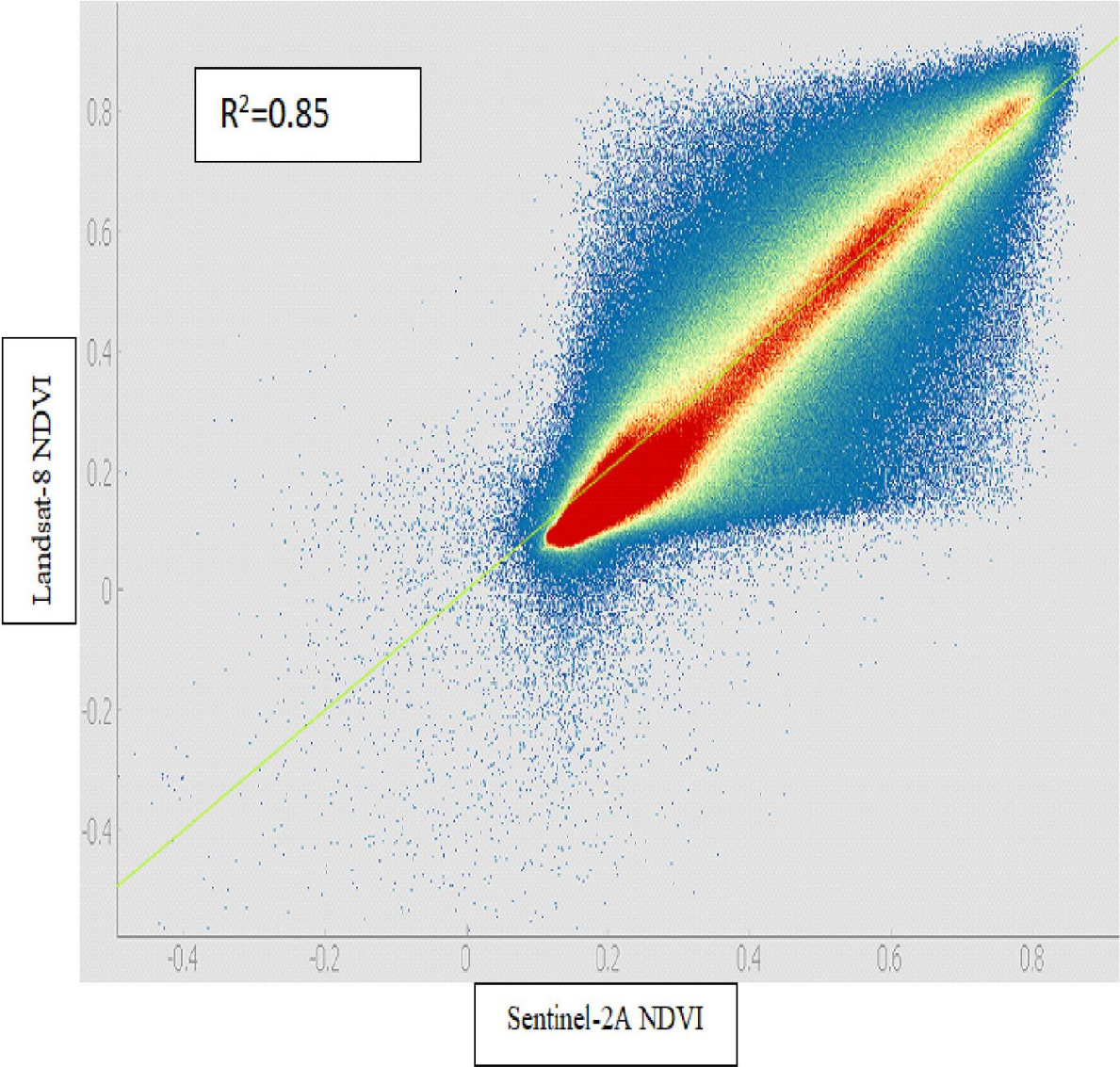
Figure 17. scatter plot for the correlation between Landsat-8 NDVI and Sentinel- 2A.
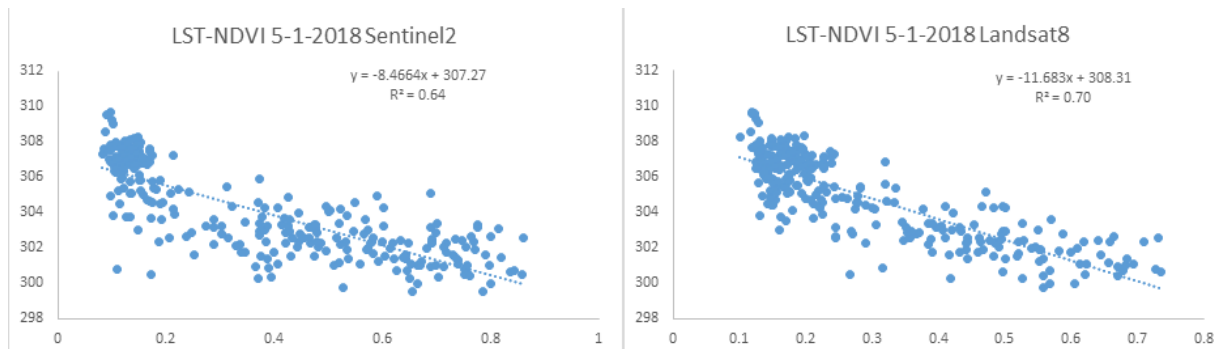
Figure 18. correlation between LST-NDVI 5.1.2018 for sentinel2 and Landsat8.

Vekerdy (2022) confirms the acceptability of the integration of the data from the two satellites by analysing an image taken on May 10, 2018. The NDVI maps were transferred to a common geometric basis. The scatterplot of the data (Figure 20 reveals a strong regression ($R^2 = 0.95$). This is in a good agreement with the results of Mandanici and Bitelli (2016) for an Iraqi area with similar coverage (lake, bare surface, and agricultural plants), based on a much larger data set ($R^2 = 0.98$). The discrepancy is in the same order as of the inaccuracy of the atmospheric correction techniques, which is 1.5 percent (Martins *et al.*, 2017). This inaccuracy varies slightly depending on the applied atmospheric correction method, however, for Sen2Cor (used in the processing of the Sentinel image) it is around 2% in the near-infrared range.
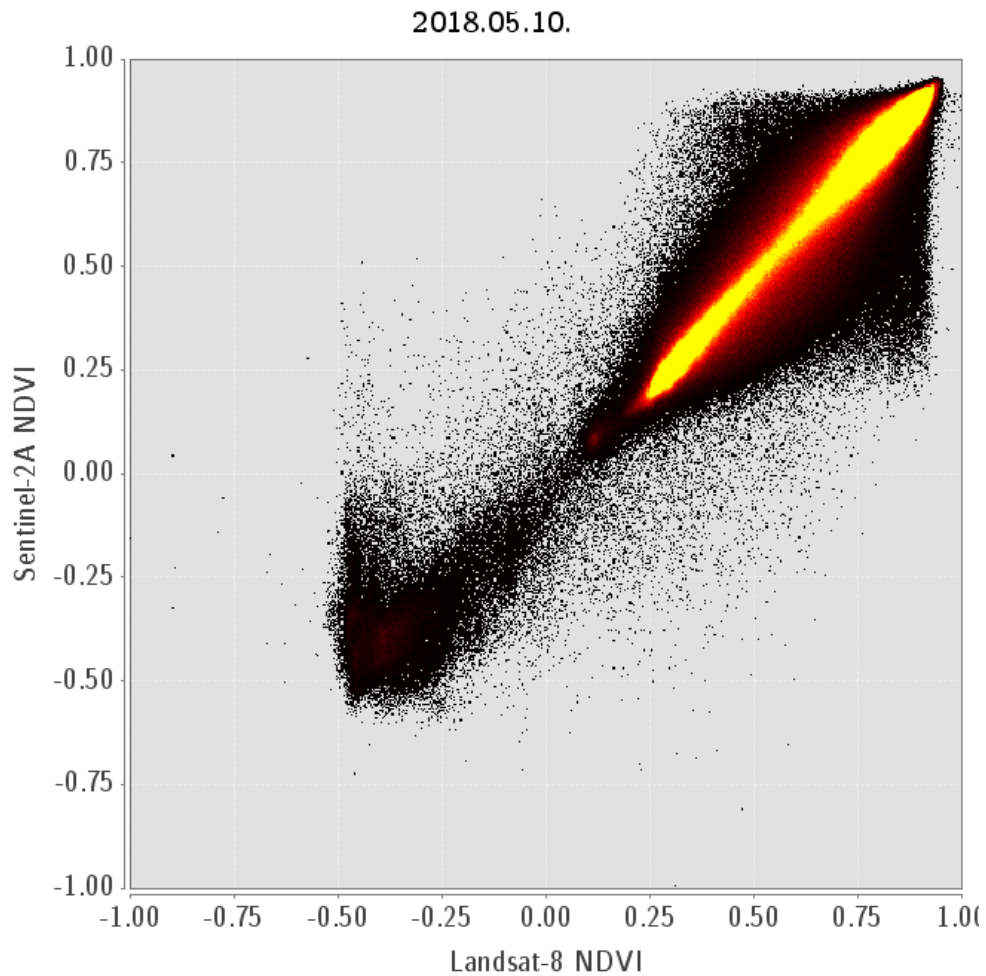
Figure 19. Scatter plot for the NDVI Sentinel2 and NDVI Landsat8(Zolt, *2022*).

Moreover, the acquisition of optical remote sensing cloud-free images is one of the biggest challenges for using remote sensing for monitoring agricultural lands. Using DisTrad for downscaling LST needs accurate fitting for the correlation curve between the aggregated Land surface temperature and the aggregated NDVI. Therefore, any distortion that may happen to the data will lead to unreliable results. (Figure 21) shows two NDVI images, Landsat-8 NDVI effected by distortion, where the area effected by the clouds identified in the red circle, and Sentinel-2A NDVI free of cloud cover. The two NDVI images has been used for fitting the correlation with the LST at coarse resolution (1000 km) for four MODIS LST as shown in (Figure 22). The results show how the cloud distortion effects the fitting of the correlation when using NDVI calculated from Landsat-8, which will affect the downscaling quality. Therefore Sentinel-2 data appear as a good alternative source, this is due to it is high spatial and temporal resolution.

67
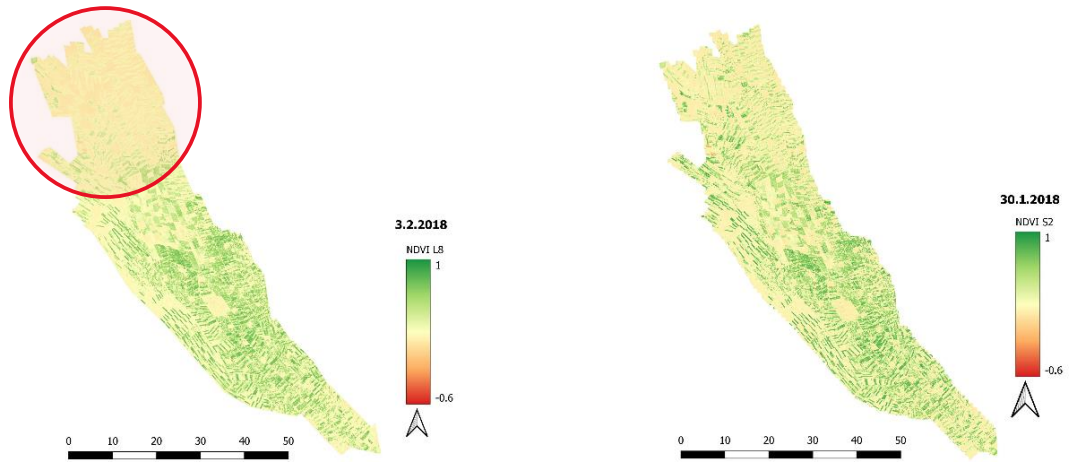
Figure 20 . NDVI Landsat-8 and NDVI sentinel-2A.
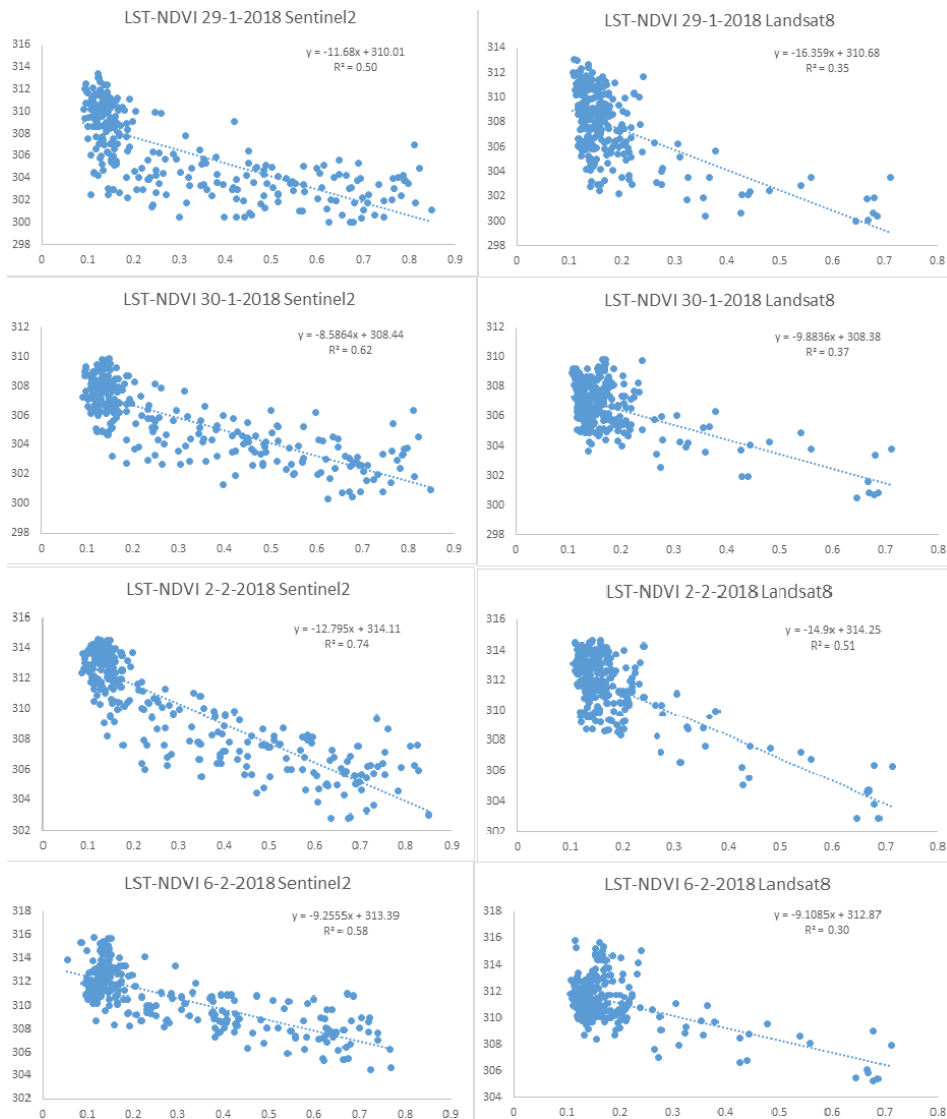
Figure 21. correlation between LST (MODIS1000 m) - NDVI Sentinel2 free of clouds and Landsat8 with cloud distortion.

The findings prove that the NDVI maps obtained from Sentinel-2 and Landsat 8 images can be combined into a uniform time series without alterations.

4.4 Evapotranspiration time series estimation and validation

Fifty-five downscaled land surface temperature maps were used to estimate the actual evapotranspiration of the wheat crops from December 2, 2017, to March 9, 2018. Eight pixels from eight different fields were chosen, and the mean calculated for these pixels was compared to potential evapotranspiration. Figure 23. shows the daily evapotranspiration (mm.day^{-1}) calculated using SEBS, ranging from 1.5 mm d^{-1} at the start of the season to 5.8 mm d^{-1} in the mid-season and 1.3 mm day^{-1} in the end of the season.
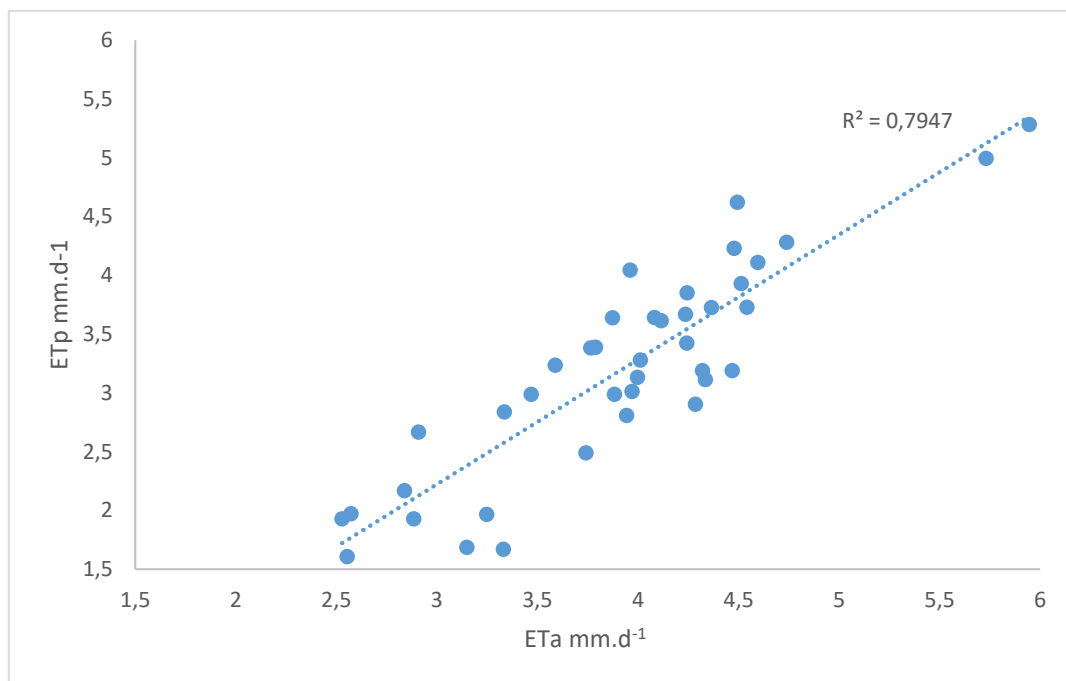
Figure 22 . correlation between the ET$_a$ and ET$_p$.

The result was compared to the potential evapotranspiration ET$_p$ estimated from the reference evapotranspiration, based on meteorological parameters and the crop coefficient, as illustrated in Figures 23 and 24. However, as shown in Figure 23 and 24, there was a strong correlation between the two products, with R^2 = 76. Figure 24, on the other hand, depicts realistic trends in the accuracy of ET$_a$ generated from SEBS. Figure 24.
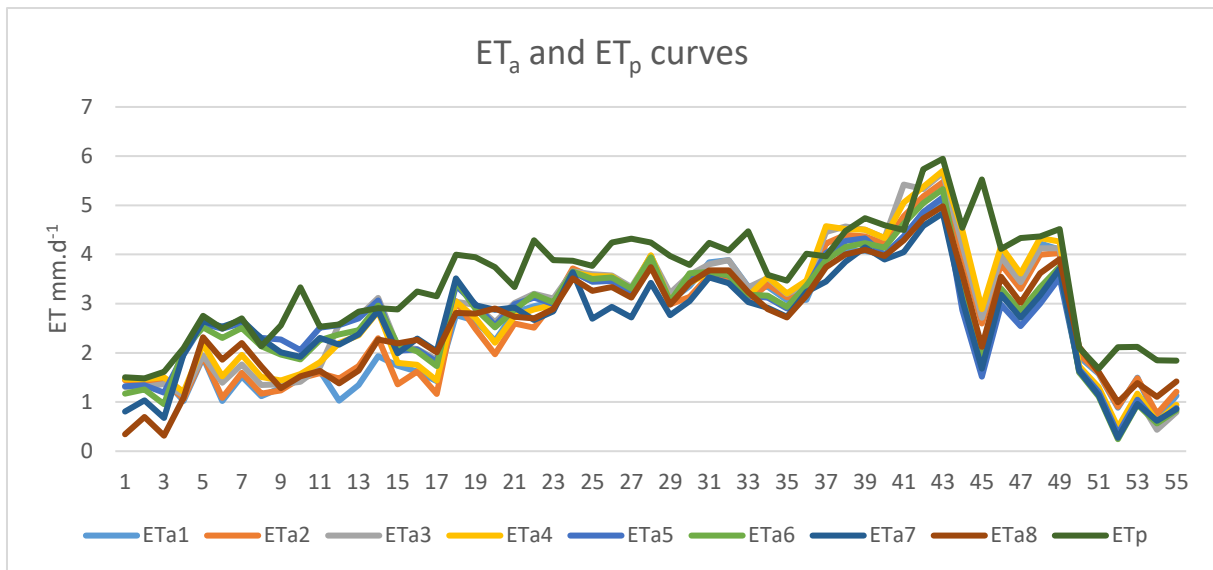
Figure 23. ETa and ETp curves for the winter season 2017-2018 ARC site.

likewise depicts steady trends in ETa over the course of the wheat growing season. From the above-mentioned results, we can indicate that the LST downscaling improves the temporal evapotranspiration resolution. The impacts of water stress might explain the disparities between the two results. Due to this fact, comparing such data to point-representative approaches are difficult. nonetheless, Figure 24 indicates realistic trends in the accuracy of ETa produced from the SEBS. In the temporal domain of the wheat growing season, Figure 24 likewise demonstrates continuous patterns in ETa. As the evapotranspiration gradually rises from the beginning of the season until it reaches its maximum level in the middle of the season, then it begins to gradually decrease again until the end of the season, when the crop reaches maturity.

The seasonal ETa for wheat cultivated in the New Halfa scheme was calculated. The average spatial ETs on a pixel basis derived by integrating daily ETa images from December 1st to March 9th (109 days) was around 350 mm. There are several limitations of using point measurement methods for calculating ETa at the regional scale, such as (a) it does not account for dynamic changes in vegetation; (b) it does not account for crop density and (c) it does not account for crop stress owing to water scarcity. The absence of field data in the New Halfa Scheme led to the impossibility of qualitative validation of the results. However, a quantitative analysis was performed by comparing the SEBS-calculated ETa with ETp obtained from meteorological data, where Figure24 demonstrated good agreement between SEBS and measured ETp patterns considering the influence of water stress, we also compared our results

with other researchers' results in similar areas to ours, where there was an agreement in the results.

4.4.1 Sensitivity assessment

The meteorological elements that contributed the most uncertainty to the SEBS-derived ET estimations were identified through sensitivity analysis of the ET estimates.

SEBS ET estimates demonstrate high sensitivity to air temperature and incoming shortwave radiation, with average sensitivity values of 176.5% and 80.3%, respectively. Average sensitivity had been calculated by adding the absolute sum of the four sensitivity values for each variable and dividing it by four (Table 4). Additionally, it was shown that the estimations were, on average, quite sensitive to the pressure (36%), and wind speed (28.2%). On the other hand, it was observed that the estimations were less influenced by changes in the height of the planetary boundary layer and the specific humidity.

Table 4. sensitivity assessment result for meteorological data.

Change in variable (%)	20	10	-10	-20	Average Sensitivity (%)
PBL Sensitivity (%)	-2.78	0	0	0	0.7
Radiation Sensitivity (%)	146	82.2	-35	-58	80.3
Pressure Sensitivity (%)	-25	-15	34	70	36
Air Temperature Sensitivity (%)	370	186	-63	-87	176.5
Sp. Humidity Sensitivity (%)	0.8	0.4	-0.3	-0.6	0.5
Sunshine Sensitivity (%)	8.0	4.2	-4.0	-8.0	6.0
Wind Speed Sensitivity (%)	-26	-14	25	48	28.2

The sensitivity analysis results in Figure 25 generally correspond with the findings of van der Kwast et al (2009) since it was observed to be less sensitive to the majority of the factors tested (sensitivity 10%). It was also in accordance with the findings of Z. Su (2002), who stated that it is particularly sensitive to air temperature fluctuations and advised that the temperature be accurate to within 2 K, as illustrated in Figure 25.
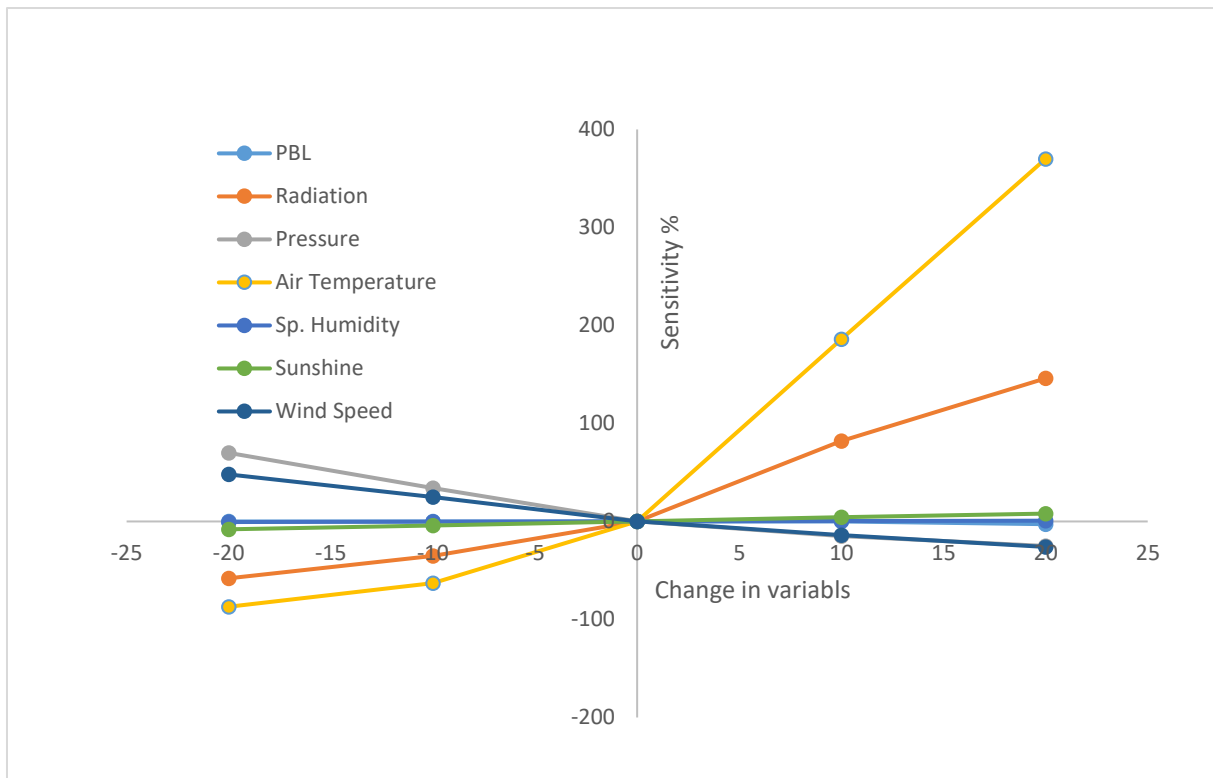
24. Graph showing the sensitivity of SEBS model to the meteorological variables.

The evapotranspiration retrieval in SEBS assumed a constant value of air temperature. Given that SEBS is particularly sensitive to air temperature, this can cause large inaccuracies in predicted evapotranspiration. But in the case of the New Halfa Scheme, there is no big variation in the air temperature where this scheme is located in a flat area with a gentle slope to the north, as the elevation is considered one of the main determinants of the variation in air temperature.

4.5 land use land cover change

The New Halfa scheme is an agricultural scheme with a rich tapestry of land cover, showcasing the intricate interplay between human activities and natural elements. With its mixed land cover, this area presents an enchanting blend of agriculture, urbanization, bare soil, water bodies, and rocky formations as described in Figure 26.
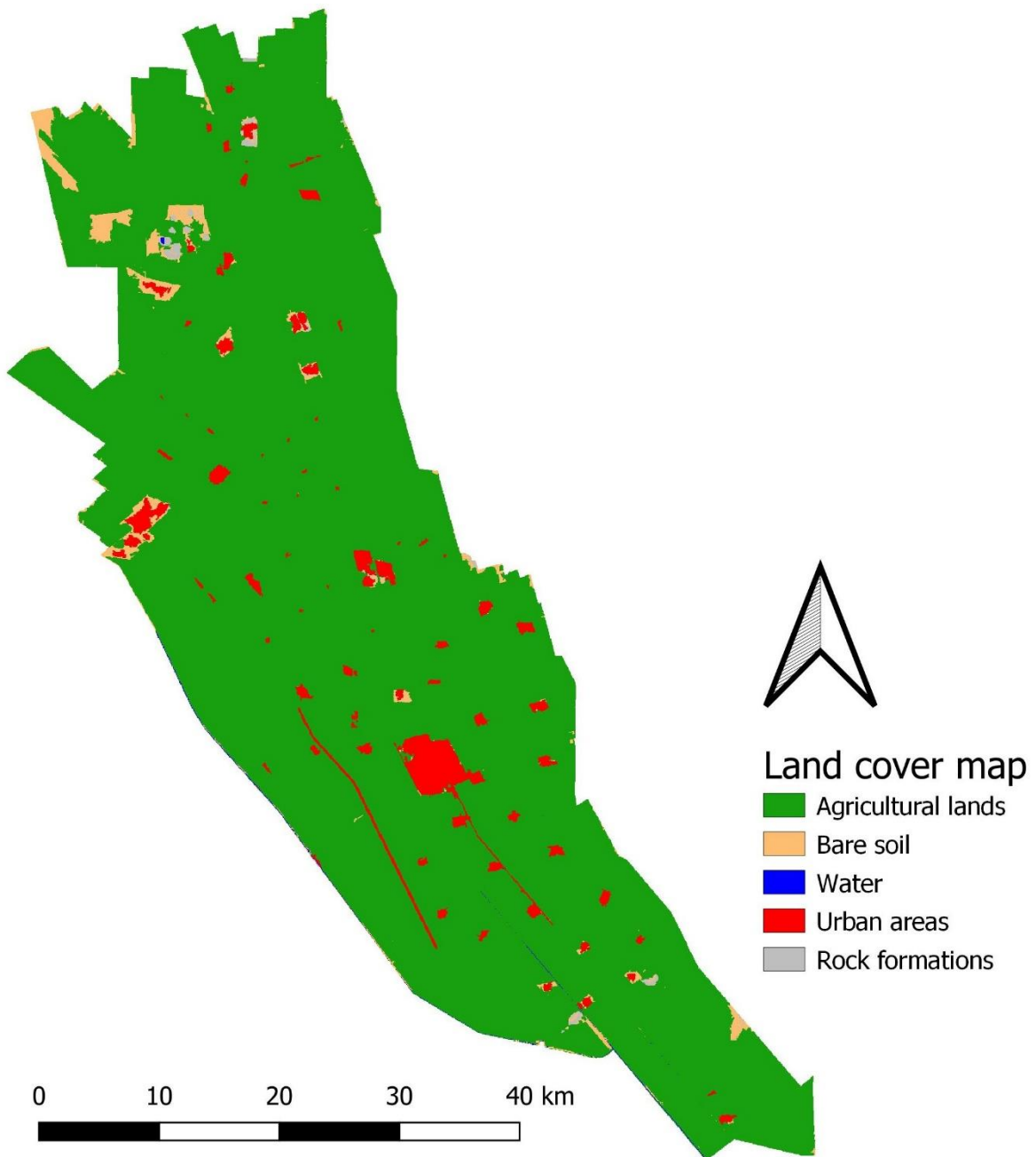
Figure 25. Land cover 2020

The agricultural land in the New Halfa scheme is divided into two parts, one part is managed by the New Halfa Agricultural Authority, where based on the crop rotation there are two season summer season and winter season the main crops in the summer season are cotton, groundnut, and sorghum, and the main crop in winter season is wheat. The other part is managed by the Sudanese Sugar Company. this part is for sugar cane cultivation, as it is considered a perennial crop. Figure 27 shows the crop distribution for the winter season over the new Halfa Scheme.
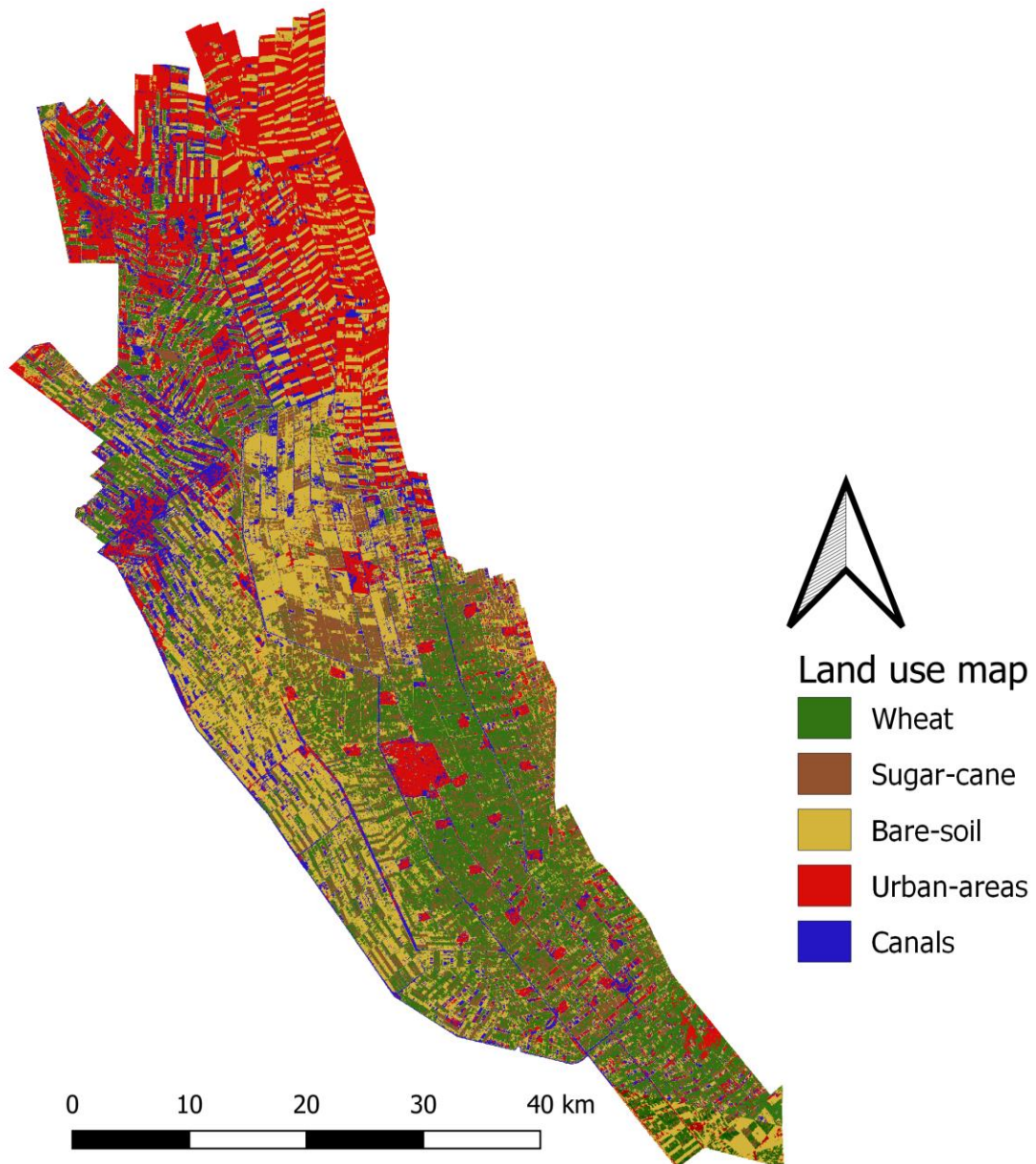
Figure 26. Land use map (crops map) winter season 2017- 2018.

4.5.1 Effects of the land cover changes on evapotranspiration.

Mixed land cover refers to an area where different types of land uses, such as urban areas, forests, agricultural fields, grasslands, and water bodies, coexist within a relatively small geographical area. The spatial arrangement and distribution of these land cover types significantly impact the local evapotranspiration (ET) patterns, which is the combined process of evaporation from the Earth's surface (such as soil, water bodies, and vegetation) and transpiration from plants.

Factors affecting the ET in the mixed land cover area.

Surface properties and albedo: Different land cover types have varying surface properties, including albedo (reflectivity). For example, urban areas typically have low albedo due to the prevalence of concrete and asphalt surfaces, while agricultural fields have higher albedo due to vegetation cover. Areas with low albedo tend to absorb more solar radiation, leading to increased heating and higher evaporation rates.

Vegetation density and type: Vegetation significantly influences evapotranspiration. Forested areas typically have higher ET rates compared to bare soil or water bodies because of the large number of trees transpiring water through their leaves. In mixed land cover regions, areas with dense vegetation will contribute more to evapotranspiration than areas with sparse or no vegetation.

Soil moisture and land management: The moisture content in the soil affects evaporation rates. Different land uses have different soil moisture retention capacities. For instance, agricultural lands with irrigation may have higher soil moisture levels, promoting higher evaporation rates. In contrast, urban areas with impermeable surfaces may lead to less water infiltration and lower soil moisture.

Temperature variation: Different land cover types can influence the local temperature patterns due to variations in heat absorption and release. Urban areas tend to be warmer than vegetated areas, which can lead to differences in evapotranspiration rates.

Water bodies: Presence of water bodies in mixed land cover areas can lead to increased evaporation from their surfaces. Additionally, nearby vegetation and land use can influence the humidity and wind patterns around water bodies, affecting their evaporation rates.

Understanding the effect of mixed land cover on Evapotranspiration distribution is crucial for various reasons, including managing water resources and studying the local climate. Satellite data, remote sensing, and help scientists and policymakers analyse and predict the impacts of land cover changes on the water cycle and regional climate. Proper land use planning and sustainable management practices can help mitigate adverse effects on local ET distribution and maintain environmental balance.

4.6 Water application efficiency

Water application efficiency is defined as the ratio of the water delivered to the farm with respect to the amounts of water preserved by irrigation in the soil root zone and ultimately consumed (via transpiration, evaporation, or both). In this study, Water Application Efficiency (WAE) was calculated using SEBS-estimated ETa after converting it to volume and water delivered to canals that measured in the field as the first attempt to analyse water application efficiency spatially in Sudan's NEW Halfa Scheme, for the period from December 2nd to February 11th, 2018. It was computed every ten days and represents the time interval between two irrigations, which were distributed as shown in (Table 5). The average values of WAE were shown in (Table 5) and (Figure 28). Obviously, in this research WAE was extremely low compared to the surface irrigation standard rate of 75%. The main reasons for the low WAE based on the information received from the management of the New Halfa Scheme can be attributed to the proliferation of parasitic weeds in the irrigation system in this scheme, which affects the distribution and flow of water in the branch channels and into the fields. Second, silting removal is done in an unstudied way, which increases the depth of the channels, obstructing the water distribution process since the water in these channels flows by gravity without the need for pumps to lift the water. This makes it lose through the surface runoff from the channels at the end of the scheme. The third reason is that the water management process in this scheme is done by estimating the evapotranspiration of a point measurement and using it to represent the entire project, and irrigation operations are performed on a fixed schedule without taking into account plant status or surrounding climatic conditions.

Table 5. Water application efficiency (WAE) 01.12.2017- 11-02-2018.

Irrigation events	ET_a volume m^3	Water delivered m^3	WAE
10-12-2017	37548.8	63850	59%
20-12-2017	36962.12	63900	58%
30-12-2017	24713.86	61975	40%
10-01-2018	40631.37	66675	60%
20-01-2018	31610.862	51400	61%
31-01-2018	54217.62	68505	79%
11-02-2018	36483.72	59800	61%
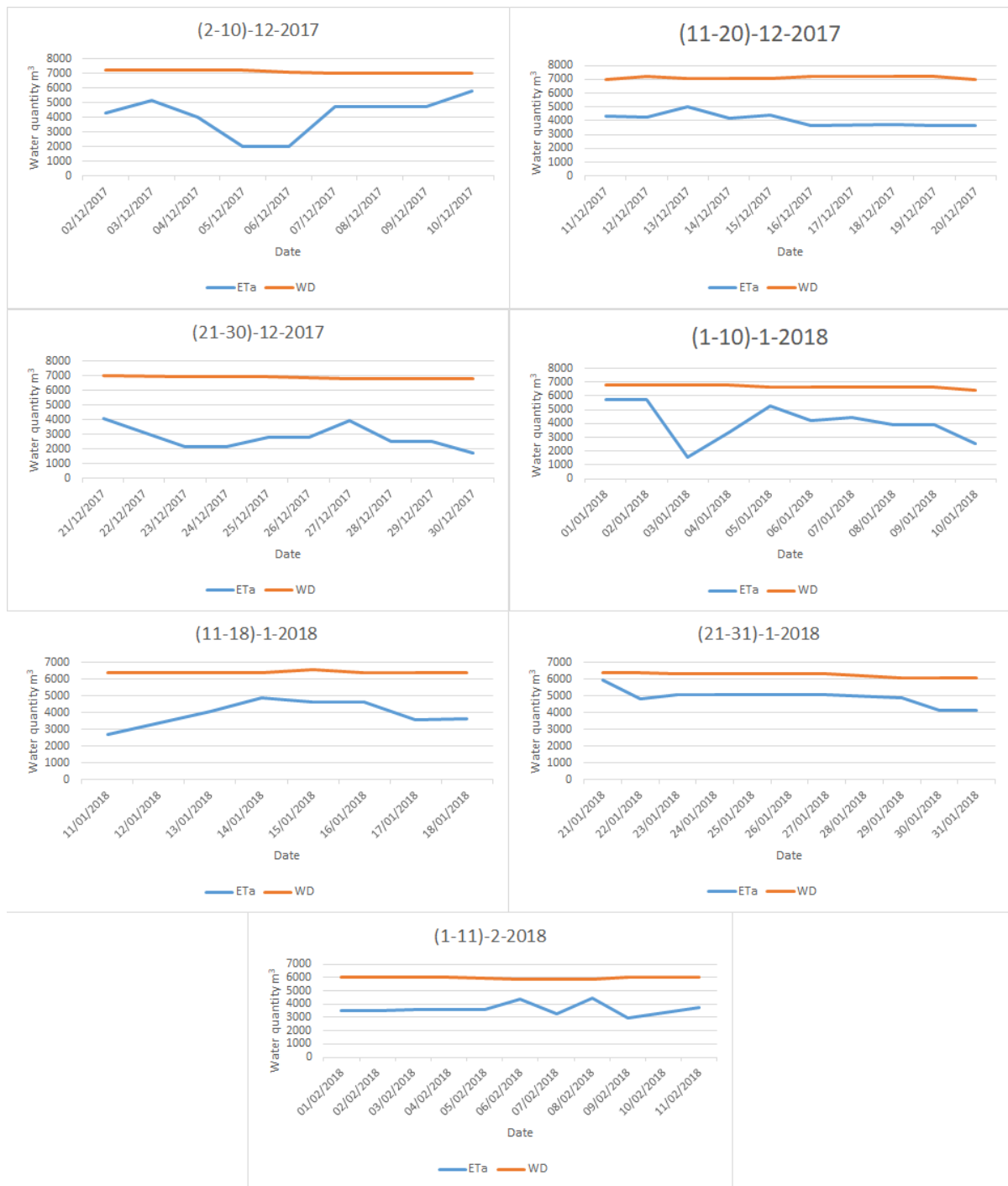
Figure 27. Relation between the water delivered to the system (WD) and ET_a.

Regarding solutions to improve the water application efficiency, there are two aspects:

- The scientific aspect is concerned with using remote sensing techniques to determine the spatial and temporal distribution of the crop water requirement. Remote sensing is a tool for estimating evapotranspiration with its spatial and temporal distribution. This is the basis of estimating crop water requirements, where the actual need of the crop can

be estimated based on the condition of the plants in the field as well as the weather conditions.

- The other aspect is practical where we can propose that the first step is to eliminate these parasitic weeds and prevent their spread. Physical control with machinery or chemical control with herbicides is two options for control. Furthermore, in terms of silt removal, the procedure must be carried out under the supervision of experts, with the proper depths taken into consideration to facilitate the water flow process.

4.7 Crop water productivity

In this work, WP was computed using predicted ETa from SEBS and crop production data based on in situ data in an effort to analyse WP regionally for the first time in Sudan's New Halfa scheme.

The WP over the research region is displayed in Table 7. WP for the New Halfa Irrigation Scheme was 0.69 kg.m^{-3} on average. Evidently, the wheat water productivity in this investigation was quite low compared to the 1.7 kg.m^{-3} range provided by Zwart and Bastiaanssen (2004b). The main causes of poor WP may be attributed to the low yields of wheat produced under semi-arid conditions as a result of high temperatures. Liu *et al.* (2007) simulated the worldwide wheat production and WP using the Environmental Policy Integrated Climate (GEPIC) model, which is based on geographic information systems. According to the authors, Sudan's simulated WP is 0.67 kg.m^{-3} as opposed to 0.32 kg.m^{-3} as defined by Adeeb (2006), who, on the other hand, used point measurements to investigate the water potential of important food crops in the Gezira scheme. He found that wheat had a WP that varied between 0.07 and 0.27 kg.m^{-3} and attributed the lower WP to poor management and low input levels rather than water wastage. However, in recent years, increasing tenant engagement in water governance, training on water management, and better levels of funding have all contributed to an improvement in land and water production.

Therefore, a good yield of wheat is not always guaranteed by adding extra water. According to (Farah *et al.*, 1997), sorghum generated a nonsignificant rise when two additional irrigations were added, but grain production tended to drop when three supplemental irrigations were added.

In the New Halfa Scheme, increasing water consumption efficiency during the winter is crucial and urgent since, according to Adam (2005), a 10% reduction equates to two million m^3 per day. It may also be stated that a water savings of between 21 and 53 percent in the Gezira plan,

which has many similar characteristics with the New Halfa scheme, can result in a daily quantity of 4 to 10 million m^3. The irrigation of sugarcane and various pump systems along the river Nile will benefit greatly from this winter's water conservation efforts. The wheat variety cultivated in New Halfa Scheme is Bohain, which it considered one of the fast-ripening varieties, in order to adapt to the short winter period in arid and semi-arid regions. Table 6 shows the field information for Bohain wheat cultivated in agricultural research corporation field.

Table 6. field information for Bohain wheat variety for the winter season 2017/2018.

Variety	Bio t/ha	HI	No.sp/m^2	No.s/sp	1000sw(g)	PH(m)	D H	DM
Bohain	9080.75	22	310	27.25	45.5	60.5	47.25	77.75

Where:

Bio t/ha: Biomass yield, **HI**: harvest index, **No.sp/m^2:** number of spike/m^2, **No.s/sp:** number of seed/spike, **1000sw(g):** seed weight, **PH:** plant height, **DH:** day to heading, **DM:** day to maturity.

Table 7. Monthly ETa, ETa/ha, Yield/ha and CWP season 2017/2018.

Month	ET_a mm	ET_a/ha mm.ha^{-1}	Yield T.ha^{-1}	CWP Kg.m^{-3}
December	13984.1			
January	22186.17			
February	27160.12			
March	2413.9			
SUM	65744.29	2776.364	1.938	
				0.69

4.8 Crop water stress

Crop evapotranspiration under arid and semi-arid conditions must be quantified to manage irrigation scheduling to reduce crop water stress and achieve optimal water productivity. A stress coefficient is commonly used to quantify the effect of soil water shortage on crop evapotranspiration. Estimating ET_a is necessary to accomplish target crop water use and keep soil water levels within a range that reduces stress and enables the generation of acceptable yields. Although plant measures such as leaf water potential, stomatal resistance, or canopy temperature can be used to monitor current plant stress levels, ET_a must be approximated to regulate irrigation within ranges that minimize water use without causing undue stress and yield loss. The CWSI (Equation 35) is used to assess the decline in ET_a caused by water stress.

The CWSI of wheat crop for the growing season of 2017-2018 was calculated in three different sites of the scheme (A, (B and C see appendix 5)) for all the available days as shown in (Figure 29), including the site (A) of the Research Farm of the Agricultural Research Corporation (ARC).
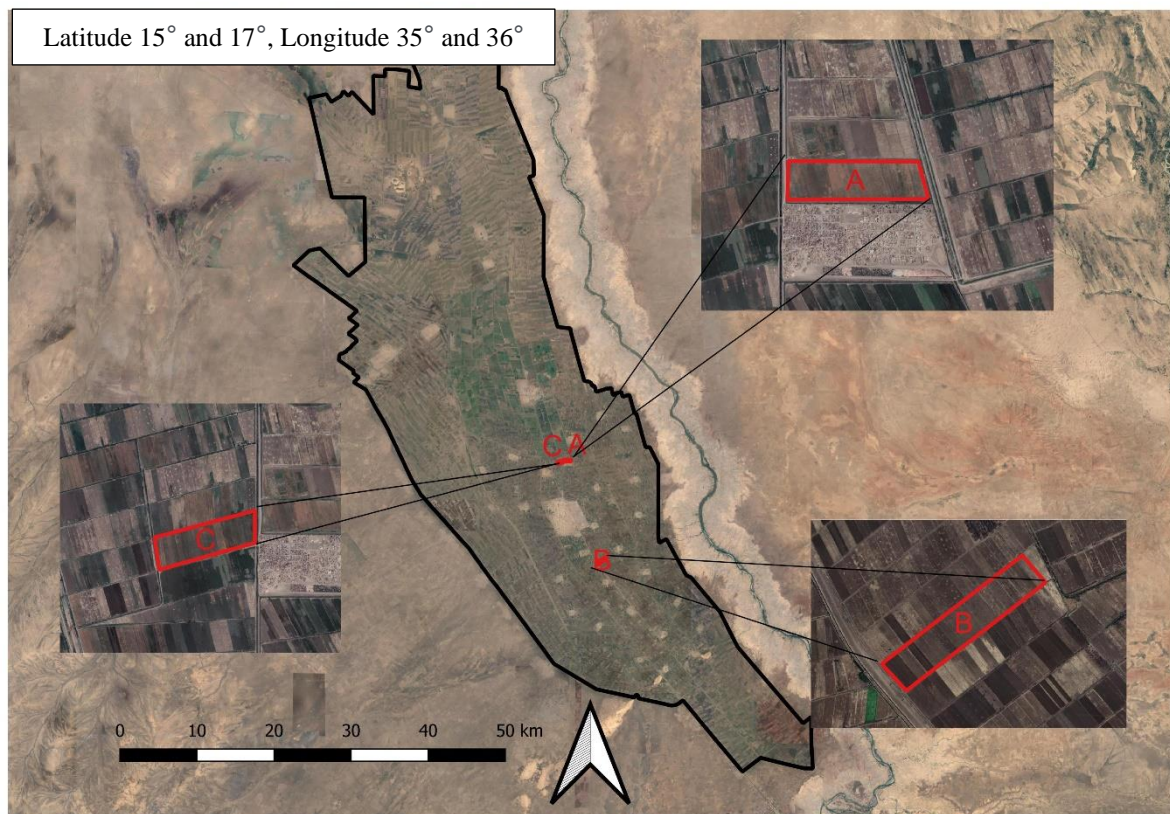

Figure 28. CWS Sites A, B and C.

81

The CWSI is estimated as the ratio between the actual and potential evapotranspiration. The actual ET was calculated using the SEBS model which mean it is under the normal condition of the field while the potential ET estimated using the Penman-Monteith equation multiplied by the crop coefficient, assuming that the plant is under standard conditions where there is no stress. The value of the CWSI ranges from 0 to 1 where 0 means that there is no stress and 1 means that the stress reached the highest value. The growing season has been divided into three phases: initial and development stage, mid-season, and late season.

4.8.1 Initial and development stage

The initial and development stage of the season starts from the date of the first irrigation to effective full cover. The water loss in this stage through the evaporation is more than transpiration because the irrigation process is through surface irrigation. Where the field is flooded with water and because the crop is in the stage of establishment, a large part of the field is not covered with vegetation and this area decreases with the development and growth of the crop.

Since the plants are at a young age and have an incomplete vegetative and root system, which affects the ability of plants to absorb water from the soil, the availability of water is the main influence on the differences in the percentage of water stress during the initial and development stage of the season, so the need for the irrigation is regular and at close intervals.

Figure 30 shows that, while there is a difference in the water stress between the fields, there is also an underestimation for the CWSI values in irrigated fields, as the areas in each site are divided into small fields that are irrigated sequentially, the colours in the upcoming figures are an indication of the state of the water stress, as the red colour indicates that there is no water stress going gradually to the red colour, which means that the region suffers from the highest state of stress compared to the neighbouring fields, which also described in the legend. This can be attributed to the fact that when calculating the potential evapotranspiration from the reference evapotranspiration and the single crop coefficient, the value of evaporation from the soil is ignored, making the actual evapotranspiration value higher than the potential evapotranspiration.
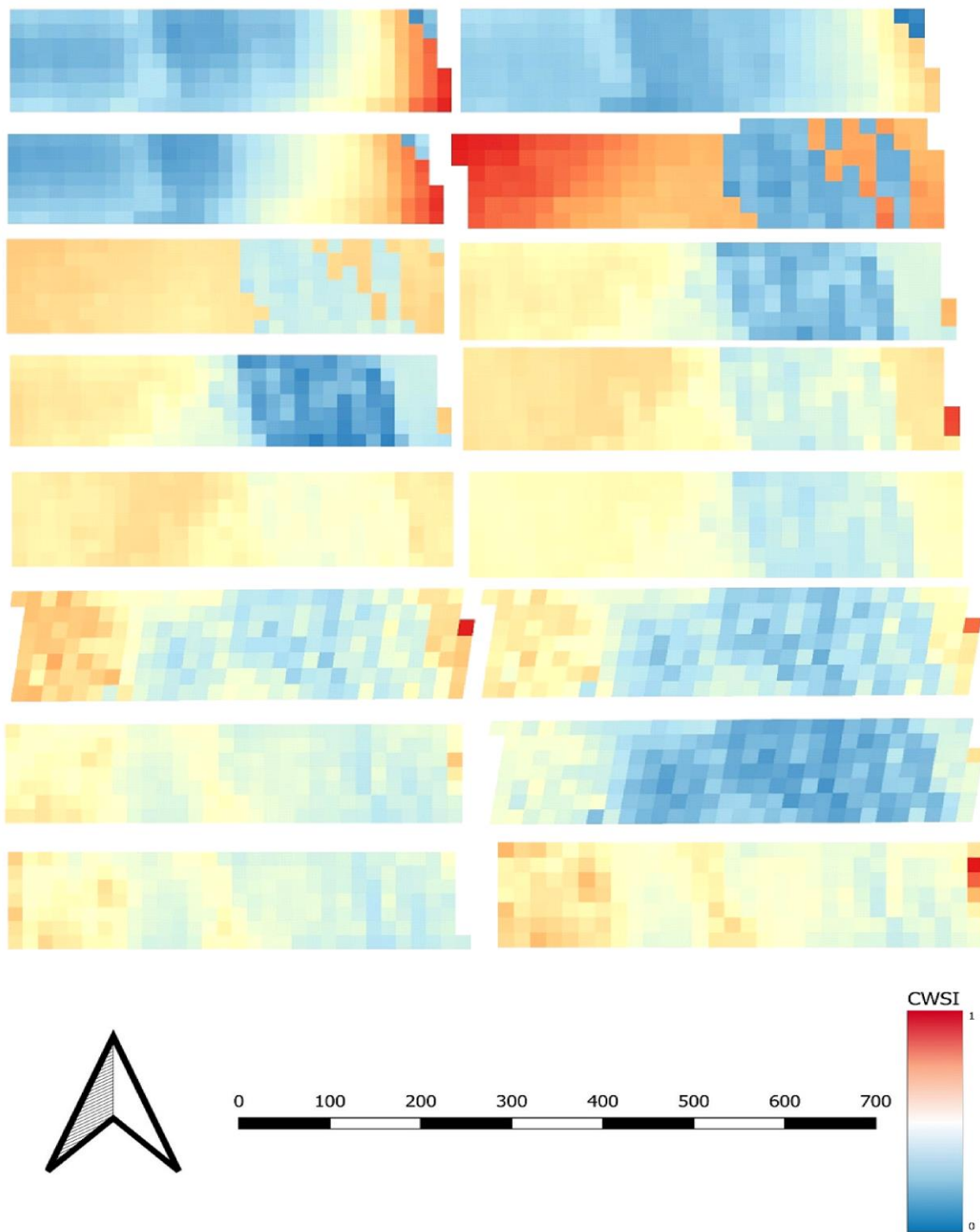
Figure 30. crop water stress maps for the available dates December 2017 site (A).

4.8.2 Mid-season stage

It extends from effective complete cowl until the start of maturity. The initiation of maturity for wheat is typically indicated by the commencement of aging, yellowing or senescence of leaves, and leaf drop, to the extent that crop evapotranspiration is lowered relative to ET0.

This stage is considered one of the most important stages when water must be available for the plants, because in this stage the flowering occurs so the lack of irrigation in it leads to the production of lean and poor-quality grains, which negatively affects the productivity. Figure 31 and 32 shows that there is a discrepancy in the water stress between the different sites, and also a difference within the same site. This discrepancy indicates poor water distribution, which negatively affects the regularity of the productivity.
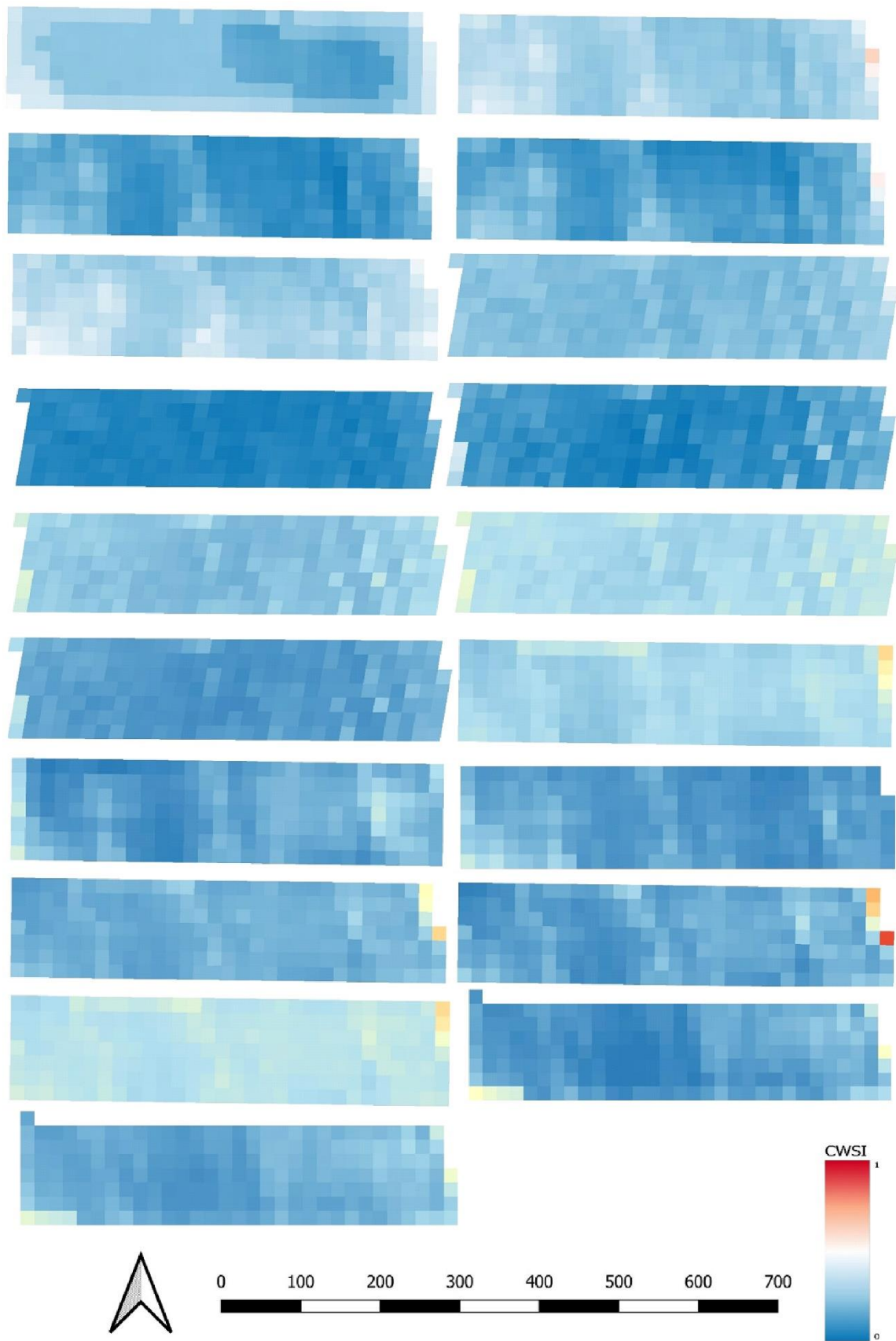
Figure *31*. Crop water stress maps for the available dates January 2018 site (A).
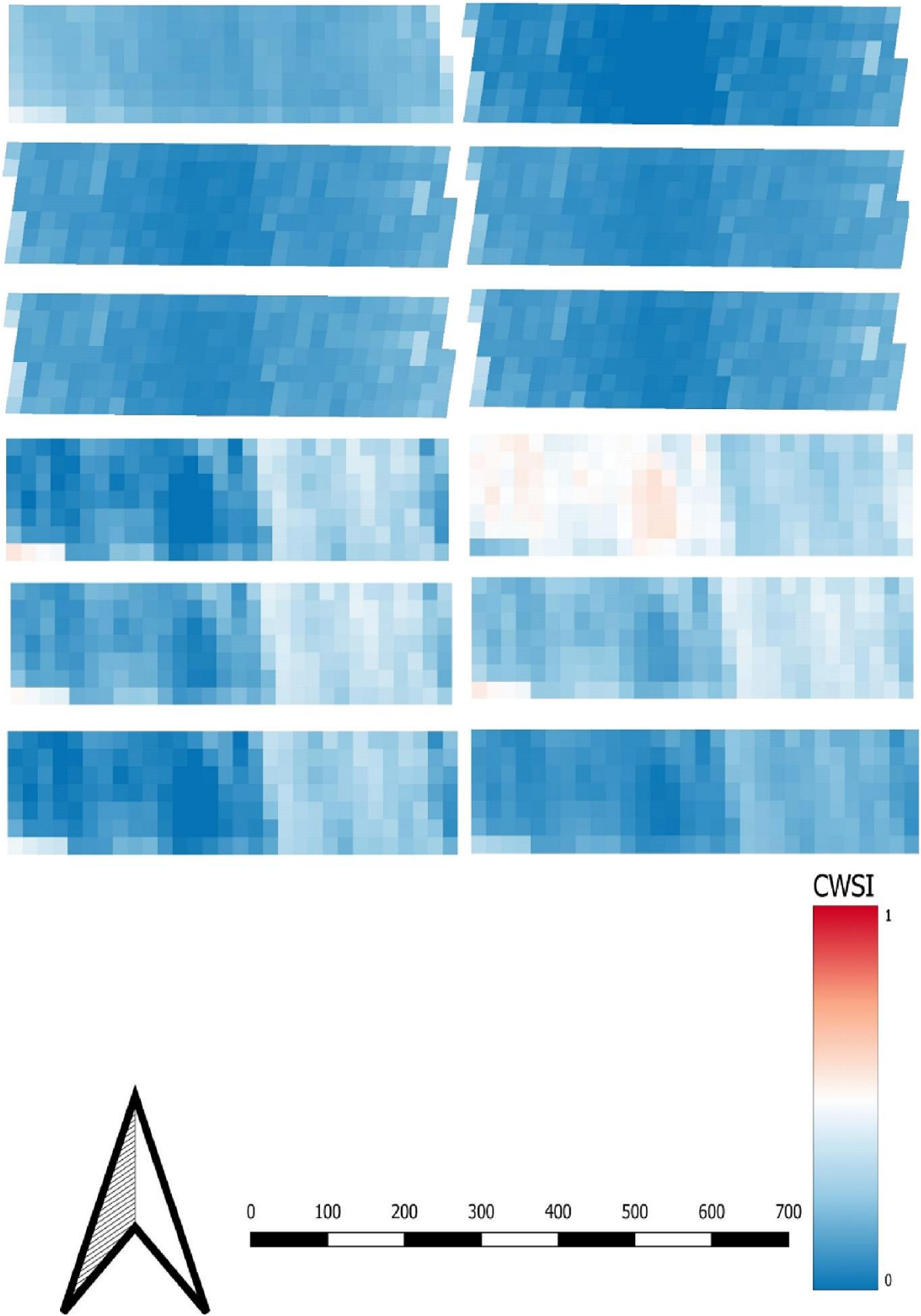
Figure 29. Crop water stress maps for the available dates February 2018 site (A).

Based on the results of monitoring crop water stress in the mid-season we can indicate that CWS maps can provide valuable information about the health and productivity of crops. The results show that crop water stress maps can estimate the difference between fields, this suggests that the maps can be a useful tool for farmers and agronomists to manage their crops more effectively.

By identifying areas of high and low water stress, farmers can adjust irrigation schedules or other management practices to optimize crop growth and yield. They can irrigate more frequently in areas with high water stress and reduce irrigation in areas with low water stress to avoid overwatering and wasting resources.

Overall, the ability to estimate the difference in crop water stress between fields using maps can be a valuable tool for improving crop management and productivity. By monitoring water stress in the mid-season, farmers, and agronomists can make informed decisions about irrigation and other management practices, leading to more efficient use of resources and better crop yields.

The mid-season monitoring of crop water stress can yield valuable insights into the health and productivity of crops. The findings indicating that crop water stress maps can accurately estimate variations between fields can be beneficial for farmers and agronomists in managing their crops more effectively.

4.8.3 Late season stage

It runs from the beginning of maturity to harvest or full senescence. During this stage, irrigation should be light so that it does not cause damage to the crop and difficulty to the harvest process, because any intensive irrigation operation at this stage is reducing the productivity of the crop. Figure 33 shows how water stress moves from lower to higher until reaching the end of the season. At this stage, the main purpose of monitoring water stress is to know if the crop has reached the stage of full maturity to start the harvest.
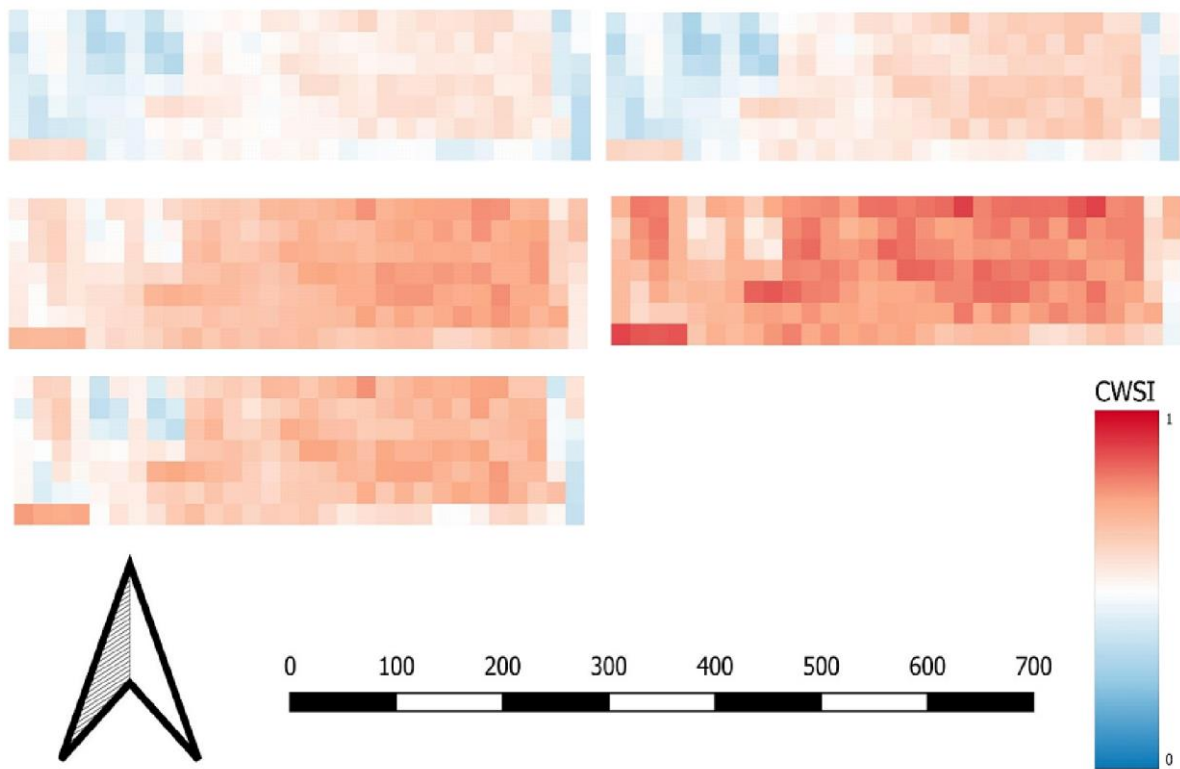
Figure 30. Crop water stress maps for the available dates March 2018 site (A).

Based on the discussion above, we can conclude that the methodology used in this study was successful in evaluating crop water status in the field, where irrigation is the main determinant factor for crop water stress, and where the time series can show the movement of the water stress pattern through the field following irrigation events. According to (Trout and DeJonge, 2021) crop water stress is an excellent indication for quantifying the impacts of insufficient water on crop evapotranspiration. They conducted a six-season experiment to drive the maize stress coefficient and discovered that crop evapotranspiration was regulated by the effect of soil water deficiency on water absorption and stomatal resistance, as well as prior water stress on plant development.

The CWSI was calculated by (Gerosa, no date) utilizing infrared thermometry, and the accuracy of the method for irrigation scheduling was tested using the established upper and lower CWSI baselines in the husk tomato crop. Due to the low canopy cover, they observed that it was not relevant during the early part of the growth season. They discovered that CWSI values close to zero were associated with treatments where there was no stress, and the irrigation depth was changed (between 100 and 120% of ET0 over the crop season). The CWSI value rose as water availability declined, peaking at 0.7 in the treatment with severe irrigation limitations (40% ET_0). (Marino *et al.*, 2019) used remote-sensing-based UAV systems to

explore the effects of varying irrigation levels on crop physiological responses and discovered that the seasonal reference evapotranspiration was 252.4 mm, whereas crop evapotranspiration was 194.3 mm. also (Bastiaanssen *et al.*, 2005) used SEBAL module to determine the CWS using remote sensing.

In conclusion, the ability to estimate differences in crop water stress between fields through maps is a valuable tool for improving crop management and productivity. By monitoring water stress, farmers and agronomists can make informed decisions regarding irrigation and other management practices, leading to more efficient resource utilization and improved crop yields.

5.CONCLUSIONS AND RECOMMENDATIONS

In this research, a remote sensing-based method was developed to support improving irrigation efficiency under in situ data scarcity conditions. To reach this goal, the following steps were developed:

1. For creating a time series of land surface temperature data with high spatial (30 m) and high temporal (1 day) resolution, the LST downscaling process DisTrad was re-parameterised. The study area has a variety of land cover types. These types include dense vegetation, medium vegetation, low vegetation, bare soil, urban areas, and water. They are in a strongly mosaicked pattern. All the fields are off a small area; therefore, it is difficult to find areas corresponding to the original LST pixels of 1 km resolution with a homogeneous land cover. This loads the definition of the regression parameters between the NDVI and the LST with a relatively high uncertainty. To decrease the number of course-resolution pixels with strongly mixed land cover pattern, we suggested to use a smaller number of pixels for the downscaling process in DisTrad. We also suggested to use linear regression instead of a second-order polynomial, since the linear regression is more robust at the edges of the value range. This method helps avoid the extreme values that can result from the second-order polynomial. The results proved that the proposed parameterisation improves downscaling process in regions with complex land cover, similar to the study area. The coefficient of determination of the linear regression for the downscaled LST was $R^2 = 0.74$ using 25% of the pixels and $R^2 = 0.72$ and using 10% of the pixels in comparison to the $R^2 = 0.61$ of the polynomial regression. This demonstrates that the use of the modified parameters of the DisTrad method resulted in an improvement of the downscaling.

2. The downscaled land surface temperature (LST) with reductions of 10% and 25%, characterized by the lowest coefficient of variation (CV), was employed within the Surface Energy Balance System to estimate actual evapotranspiration at a high spatial resolution. The utilization of downscaled LST resulted in root mean square errors (RMSE) of 0.3 mm day-1 and 0.28 mm day-1 for the downscaling with reductions of 10% and 25% in coarse resolution pixels, respectively. In comparison with previous studies ((Bindhu, Narasimhan and Sudheer, 2013)and (Tan, Wu and Yan, 2019)), it is evident that our methodology has significantly improved both the temporal and spatial resolution of evapotranspiration estimation. Notably, the coefficient of determination

for both downscaling methods (10% and 25%) was found to be nearly identical, registering at 84.5 and 84.1, respectively.

3. The next step was to create a daily ET_a map time series by combining data from different optical sensors. We can conclude that combining data from Landsat 8 and Sentinel 2 is possible due to the strong correlation. This way a consistent daily ET_a map time series can be created with high spatial and temporal resolution. Even if distortion occurs in the images of one of the sensors, the data of the other sensor can be used as an alternative data source.

4. The crop water productivity in the New Halfa scheme was very low (0.69 kg.m^{-3}) compared to the average world crop water productivity of 1.7 kg.m^{-3}. This needs to be improved. The efficiency of the irrigation system performance was very low 60% compared to the average world irrigation efficiency of the surface irrigation systems (75%).

5. The last step was to evaluate the wheat crop water status by using the crop water stress index. Based on the results, we can conclude that the spatial distribution map of the crop water stress helps to plan the spatial and temporal distribution of irrigation, so it contributes to an improved water management.

Finally, we may extrapolate from the indicated findings that these changes enhanced and provide dependable ET_a maps for irrigation scheduling and agricultural planning.

The final recommendation is that earth observation is an optimal method for analysing irrigation performance under the condition of data scarcity, if the information about the water distribution is available, where it provides information about the water status in the field which is considered a key point in water management.

In conclusion, this thesis has sought to address critical questions within the scope of its defined parameters. However, it is imperative to acknowledge that our findings represent a snapshot of the ongoing pursuit of knowledge in this field. The complexity and multifaceted nature of the subject matter demand a sustained and rigorous commitment to further investigation. To this end, I recommend that future research endeavours focus on expanding the scope, employing larger sample sizes, employing more varied methodologies, and considering longitudinal approaches where applicable. Moreover, it is essential for subsequent studies to explore the nuanced intricacies that this thesis may have left unexamined due to its limitations such as incorporating the management practices specific to the crops being cultivated.

6. NEW SCIENTIFIC RESULTS

1. I have improved the downscaling of coarse spatial resolution LST by modifying the DisTrad method to make it more robust and reliable for areas with complex land cover. The modifications include the application of linear regression combined with the reduction of the number of sampled pixels.

2. I created a high spatial and temporal resolution daily actual evapotranspiration time series of the New Halfa irrigation scheme from the data of a single satellite to cover the cropping season.

3. I demonstrated that the integration of data from different optical sensors for calculating actual evapotranspiration can result in a homogeneous dataset, which helps to fill gaps in the time series, most frequently caused by cloud cover.

4. Based on the potential and the actual evapotranspiration data I defined the spatial and temporal distribution of water stress and calculated water efficiency in the New Halfa scheme for the 2017/2018 season.

5. I proposed a new approach for optimizing the irrigation schedule in New halfa region by using the crop water stress as indicator for the water status in the field under condition of in situ data scarcity.

SUMMARY

Water management for agriculture is a complex task influenced by various factors, including social, environmental, and political. Effective irrigation systems are crucial for providing adequate food to the world, but the available water resources have limits for regeneration. Monitoring soil and crop during the growing season is necessary to improve agricultural production, and methods for assessing irrigation performance using satellite data have been developed since the 1980s. With an increase in the global population and a decrease in the amount of available water, the agricultural sector must increase food production using less water, which can be achieved through improving water use efficiency and defining the net irrigation water requirement. Remote sensing images captured by sensors on satellites or airplanes can be used as tools to provide spatial information about evapotranspiration. In the past decade, various models have been developed to simulate plant growth and water balance, and several models have been developed to quantify actual evapotranspiration based on surface energy balance.

The New Halfa project in Sudan is experiencing water scarcity, which is affecting the productivity of crops such as winter wheat, cotton, sorghum, and groundnut. To ensure sustainable water usage, farmers need to match irrigation to crop water requirements, and accurate estimation of crop evapotranspiration is crucial for in-season irrigation management, water allocations, and long-term predictions of water supply and demand. Traditional irrigation methods like surface irrigation have low efficiency, and more effective methods like sprinkler and drip irrigation are limited by high costs and maintenance requirements. Lack of knowledge on evapotranspiration variation makes water management difficult, and there is a need for methods to improve water management under conditions of data scarcity. This study aimed to develop a remote sensing-based method that supports improving the efficiency of water use for irrigation. To achieve this goal, The DisTrad (Disaggregation of Radiometric Surface Temperature) method was used for the LST downscaling procedure, which is based on aggregating the NDVI map to the LST map resolution and then calculating the coefficient of variation of the native NDVI map within the aggregated pixel and classifying the aggregated map into three classes: NDVI less than 0.2 for the bare soil, NDVI between 0.2 to 0.5 for the partial vegetation, and NDVI more than 0.5 for the full vegetation. DisTrad uses 25% of the pixels with the lowest coefficient of variation from each class to calculate the regression coefficients. In this work, adjustments to the DisTrad method were implemented to enhance downscaling LST and to examine the impacts of that alteration on the evapotranspiration

estimation. The linear regression model was tested as an alternative to the original second-order polynomial. In using 10% of the pixels instead of the originally proposed 25% with the lowest coefficient of variation values, it is assumed that a group of pixels with a lower coefficient of variation represents a more homogeneous area, thus it gives more accurate values. Secondly, a high spatial and temporal resolution time series of actual evapotranspiration (ET) maps using remote sensing has been generated to define the spatial distribution of the actual ET that has been done by implanting downscaled land surface temperature in surface energy balance system SEBS model to estimate the actual ET. Thirdly, an optimal integration method of optical data has been followed to overcome the cloud cover problem, where the optical data from Landsat8 and Sentinel-2 optical sensors were combined to fill the gap when there is distortion resulting from the clouds for any of the sensors. Finally, a method to optimize the irrigation schedule for wheat has been proposed by considering the crop water stress index as an indicator for the crop water status which has a key role in applying the irrigation events. where three types of evapotranspiration have been used to estimate the Crop water stress index (CWSI) where we can define the CWSI measure of the potential evapotranspiration to the actual evapotranspiration which the crop with adequate water will transpire at the same rate as the potential but when the water becomes limiting the actual evapotranspiration will fall below the potential evapotranspiration this ratio range from 0 to 1 where 0 it means that there is no stress and 1 is a high rate of the stress.

The downscaled LST map retrieval was validated using Landsat 8 thermal maps (100 m). Applying the modified DisTrad approach to disaggregate Landsat LST to 30 m (NDVI resolution) yielded an R2 of 0.72 for the 10%, 0.74 for the 25% and 0.61 for the second-order polynomial lowest coefficient of variation compared to native LST Landsat, which means that 10% can be used as an alternative. Applying the downscaled LST map to estimate ETa yielded R2 0.84 in both cases, compared to ETa yielded from the native Landsat LST. These results prove that using the robust linear regression provided better results than using polynomial regression. With the downscaled Land Surface Temperature data, it was possible to create detailed ETa maps of the small agricultural fields in the test area.The Surface Energy Balance System uses downscaled land surface temperature to estimate actual evapotranspiration with high spatial resolution. When using only 10% of the pixels for downscaling, there is a good correlation between ETa calculated from the downscaled LST and the native LST, with a coefficient of determination of 84.5 and 84.1 for 10% and 25% downscaled methods, respectively, and an average RMSE of 0.3 and 0.28 mm/day, respectively. The downscaled LST

produces more accurate evapotranspiration maps with higher spatial resolution than those produced using native LST. A similar RMSE of 0.16 was achieved using a non-linear disaggregation approach.

The poor temporal resolution of Landsat 8 images limits their use in estimating daily evapotranspiration, and cloud distortion is another limiting factor. To fill this gap, higher spatial and temporal resolution Sentinel-2 images were used in this study for the days when Landsat images were not available. The correlation between the NDVI generated by the two sensors was tested, and the integration of data from the two satellites was found to be acceptable, with a strong regression (R2 = 0.95) shown in the scatterplot. This is consistent with previous results and the discrepancy is within the range of atmospheric correction technique inaccuracies, which is around 1.5-2%.

The study used downscaled land surface temperature maps to estimate the actual evapotranspiration of wheat crops in the New Halfa scheme. Daily evapotranspiration calculated using SEBS showed a strong correlation with potential evapotranspiration estimated from reference evapotranspiration. The LST downscaling improved the temporal evapotranspiration resolution. The average spatial ETs on a pixel basis from December 1st to March 9th was around 350 mm. The study acknowledges limitations in using point measurement methods for calculating ETa at the regional scale, and water stress was identified as a potential cause for disparities between SEBS ETa and ETp. Nonetheless, SEBS showed good agreement with the ETp pattern measured from meteorological data. The study discusses the use of crop water stress index (CWSI) maps to monitor crop water stress during different stages of growth. CWSI is estimated as the ratio between actual and potential evapotranspiration and ranges from 0 (no stress) to 1 (highest stress). The growing season is divided into three stages: initial and development, mid-season, and late season. The study described the water stress patterns and discrepancies observed during each stage and emphasizes the importance of regular irrigation during the mid-season stage to avoid poor-quality grains and optimize productivity. The study concluded that CWSI maps can provide valuable information to farmers and agronomists for managing crops more effectively, leading to better yields and efficient use of resources. The methodology used in the study was successful in evaluating crop water status in the field, and CWSI was found to be an excellent indication for quantifying the impacts of insufficient water on crop evapotranspiration.

In conclusion, this study aimed to enhance irrigation efficiency in arid and semi-arid regions with limited data availability by utilizing Earth observation techniques. Through several steps,

including downscaling LST data, estimating actual evapotranspiration, creating daily ETa maps, calculating crop water productivity, and evaluating irrigation system performance, the study demonstrated the potential of Earth observation in addressing these challenges. Specifically, the study recommends the new parameterisation of DisTrad for downscaling LST in areas with complex vegetation cover and the integration of data from Sentinel-2 and Landsat 8 sensors to overcome cloud cover issues in creating ETa time series. The study also advocates for the use of EO-based ETa maps to plan irrigation and water management, by defining crop water stress. Overall, this study provides valuable insights into the use of Earth observation for improving irrigation efficiency and water management in arid and semi-arid regions.

ACKNOWLEDGMENTS

I am profoundly grateful to everyone who has contributed to the completion of this dissertation. This research journey has been a remarkable and transformative experience, and I could not have reached this milestone without the support, guidance, and encouragement of many individuals and institutions.

First and foremost, I extend my deepest gratitude to my supervisor, [Dr. Zoltán Vekerdy, and Dr. István Waltner], for their unwavering commitment, insightful guidance, and invaluable mentorship throughout the research process. Their expertise, patience, and encouragement have been instrumental in shaping the direction and quality of this work.

I extend my appreciation to the faculty and staff of [MATE University] for providing a conducive academic environment and access to resources that have been crucial in conducting this research.

My heartfelt thanks go to my colleagues and friends who have provided me with invaluable insights, stimulating discussions, and emotional support. Your camaraderie has made the academic journey both enjoyable and meaningful.

I am indebted to my family for their unwavering love, encouragement, and belief in my abilities. Your constant support has been a source of strength and motivation, driving me to pursue excellence.

Last but not least, I express my gratitude to the research participants who generously shared their time and perspectives, making this study possible. Your contributions are deeply appreciated.

In conclusion, this dissertation represents the culmination of years of dedication and hard work, and I am profoundly thankful to all those who have been a part of this remarkable journey.

With sincere appreciation,

[Taha Ibrahim]

 [08, 2023]

REFERENCES

Adam, H. S. (2005) 'Agroclimatology, crop water requirement and water management', *Gezira University Publication Company. Wadmedani, Sudan.*

Adeeb, A. M. (2006) 'Water productivity of food crops in Gezira scheme, Sudan', *Proceedings of Environmentally Sound Technology in Water Resources Management*, pp. 11–13.

Adi Nugraha, A. S., Gunawan, T. and Kamal, M. (2019) 'Downscaling land surface temperature on multi-scale image for drought monitoring', (November 2019), p. 6. doi: 10.1117/12.2544550.

Agam, N. *et al.* (2007) 'A vegetation index based technique for spatial sharpening of thermal imagery', *Remote Sensing of Environment*, 107(4), pp. 545–558. doi: 10.1016/j.rse.2006.10.006.

Akdim, N. *et al.* (2014) *Monitoring of irrigation schemes by remote sensing: Phenology versus retrieval of biophysical variables*, *Remote Sensing*. doi: 10.3390/rs6065815.

Allen, R. G. *et al.* (1998a) 'Crop evapotranspiration - Guidelines for computing crop water requirements - FAO Irrigation and drainage paper 56 By', pp. 1–15.

Allen, R. G. *et al.* (1998b) 'Fao,1998', *Irrigation and Drainage Paper No. 56, FAO*, p. 300. doi: 10.1016/j.eja.2010.12.001.

Allen, R. G., Tasumi, M. and Trezza, R. (2007) 'Satellite-Based Energy Balance for Mapping Evapotranspiration with Internalized Calibration „ METRIC … — Model', (August), pp. 380–394.

Atkinson, P. M. (2013) 'Downscaling in remote sensing', *International Journal of Applied Earth Observation and Geoinformation*. Elsevier B.V., 22(1), pp. 106–114. doi: 10.1016/j.jag.2012.04.012.

Bartkowiak, P., Castelli, M. and Notarnicola, C. (2019) 'Downscaling land surface temperature from MODIS dataset with random forest approach over alpine vegetated areas', *Remote Sensing*, 11(11), pp. 1–19. doi: 10.3390/rs11111319.

Bastiaanssen, W. G. M. *et al.* (2001) 'Low cost satellite data for monthly irrigation performance monitoring: Benchmarks from Nilo Coelho, Brazil', *Irrigation and Drainage Systems*, 15(1), pp. 53–79. doi: 10.1023/A:1017967021198.

Bastiaanssen, W. G. M. *et al.* (2005) 'SEBAL Model with Remotely Sensed Data to Improve Water-Resources Management under Actual Field Conditions', *Journal of Irrigation and Drainage Engineering*, 131(1), pp. 85–93. doi: 10.1061/(asce)0733-9437(2005)131:1(85).

Bastiaanssen W.G.M. *et al.* (1998) 'A remote sensing surface energy balance algorithm for land (SEBAL): 1. Formulation', *Journal of Hydrology*, 212–213(1–4), pp. 198–212. doi: 10.1016/S0022-1694(98)00253-4.

Bindhu, V. M., Narasimhan, B. and Sudheer, K. P. (2013) 'Development and verification of a non-linear disaggregation method (NL-DisTrad) to downscale MODIS land surface temperature to the spatial scale of Landsat thermal data to estimate evapotranspiration', *Remote Sensing of Environment*. Elsevier Inc., 135, pp. 118–129. doi: 10.1016/j.rse.2013.03.023.

Bos, M. G. and Nugteren, J. (1990) 'On irrigation efficiencies. 4th edition', in. Wageningen: International Institute for Land Reclamation and Improvement.

Caldwell, T. *et al.* (1999) 'Multicriterion decision making in irrigation planning K.S', *Agricultural Water Management*. Wageningen: Elsevier B.V., 6(2), pp. 117–129. doi: 10.1016/S0378-3774(00)00118-9.

Calera, A. *et al.* (2017) 'Remote sensing for crop water management: From ET modelling to services for the end users', *Sensors (Switzerland)*, 17(5), pp. 1–25. doi: 10.3390/s17051104.

Darshana *et al.* (2012) 'Simulation and optimization for irrigation and crop planning', *Irrigation and Drainage*, 61(2), pp. 178–188. doi: 10.1002/ird.633.

Doorenboos, J. and Pruitt, W. O. (1977) 'Guidelines for predicting crop water requirements, Irrigation and Drainage Paper 24', *L. Water Dev. Div. FAO Rome*, p. 144.

Doorenbos, J. and Pruitt, W. O. (1977) 'Guidelines for predicting crop water requirements, Irrigation and Drainage Paper No. 24', *FAO, Rome, Italy*.

Ebrahimy, H. and Azadbakht, M. (2019) 'Downscaling MODIS land surface temperature over a heterogeneous area: An investigation of machine learning techniques, feature selection, and impacts of mixed pixels', *Computers and Geosciences*. Elsevier Ltd, 124(January), pp. 93–102. doi: 10.1016/j.cageo.2019.01.004.

Farah, S. M. *et al.* (1997) 'Grain sorghum response to supplementary irrigations under post-rainy season conditions', *Agricultural Water Management*, 33(1), pp. 31–41. doi: 10.1016/S0378-3774(96)01283-8.

Fernández, J. E. (2017) 'Plant-based methods for irrigation scheduling of woody crops', *Horticulturae*, 3(2). doi: 10.3390/horticulturae3020035.

Gerosa, G. (no date) *FROM MEASUREMENTS TO AGRICULTURAL AND ENVIRONMENTAL Edited by Giacomo Gerosa.*

González-Dugo, M. P. *et al.* (2006) 'Canopy temperature variability as an indicator of crop water stress severity', *Irrigation Science*, 24(4), pp. 233–240. doi: 10.1007/s00271-005-0022-8.

H . L. P e n m a n (1947) 'Natural evaporation from open water, bare soil and grass Physics', *Proceedings of the Royal Society of London*, pp. 2–4.

Hutengs, C. and Vohland, M. (2016) 'Downscaling land surface temperatures at regional scales with random forest regression', *Remote Sensing of Environment*. Elsevier Inc., 178, pp. 127–141. doi: 10.1016/j.rse.2016.03.006.

Ihuoma, S. O. and Madramootoo, C. A. (2017) 'Recent advances in crop water stress detection', *Computers and Electronics in Agriculture*, pp. 267–275. doi: 10.1016/j.compag.2017.07.026.

Jeganathan, C. *et al.* (2011) 'Evaluating a thermal image sharpening model over a mixed agricultural landscape in India', *International Journal of Applied Earth Observation and Geoinformation*. Elsevier B.V., 13(2), pp. 178–191. doi: 10.1016/j.jag.2010.11.001.

Jia, L. *et al.* (2009) 'Regional estimation of daily to annual regional evapotranspiration with MODIS data in the Yellow River Delta wetland', *Hydrology and Earth System Sciences*. Copernicus GmbH, 13(10), pp. 1775–1787.

Jiménez-Muñoz, J. C. *et al.* (2009) 'Comparison between fractional vegetation cover retrievals from vegetation indices and spectral mixture analysis: Case study of PROBA/CHRIS data over an agricultural area', *Sensors*, 9(2), pp. 768–793. doi: 10.3390/s90200768.

K. Raju, D. K. (1999) 'Multicriterion decision making in irrigation planning K.S', *Agricultural Systems*, 62(1999), pp. 117–129. doi: 10.1002/ird.197.

Karnieli, A. *et al.* (2006) 'Comments on the use of the Vegetation Health Index over Mongolia', *International Journal of Remote Sensing*, 27(10), pp. 2017–2024. doi: 10.1080/01431160500121727.

Kustas, W. P. *et al.* (2003) 'Estimating subpixel surface temperatures and energy fluxes from

the vegetation index-radiometric temperature relationship', *Remote Sensing of Environment*, 85(4), pp. 429–440. doi: 10.1016/S0034-4257(03)00036-1.

Van Der Kwast, J. *et al.* (2009) 'Evaluation of the Surface Energy Balance System (SEBS) applied to ASTER imagery with flux-measurements at the SPARC 2004 site (Barrax, Spain)', *Hydrology and Earth System Sciences*, 13(7), pp. 1337–1347. doi: 10.5194/hess-13-1337-2009.

Kyalo, D. K. (2017) 'Sentinel-2 and MODIS land surface temperature-based evapotranspiration for irrigation efficiency calculations', p. 50. Available at: http://www.itc.nl/library/papers_2017/msc/wrem/kyalo.pdf.

Laxén, J. (2007) ''Is prosopis a Curse or a Blessing?An ecological-economic analysis of an invasive alien tree species in Sudan .'', *Researchgate.Net*. Available at: http://www.researchgate.net/publication/237580507_Climate_change_and_African_drylands/file/3deec5202932943c4a.pdf.

Li, W. *et al.* (2019) 'Selection of Predictor Variables in Downscaling Land Surface Temperature using Random Forest Algorithm', *International Geoscience and Remote Sensing Symposium (IGARSS)*. IEEE, pp. 1817–1820. doi: 10.1109/IGARSS.2019.8899845.

Liang, S. *et al.* (2003) 'Narrowband to broadband conversions of land surface albedo: II. Validation', *Remote Sensing of Environment*, 84(1), pp. 25–41. doi: 10.1016/S0034-4257(02)00068-8.

Liu, J. *et al.* (2007) 'GEPIC - modelling wheat yield and crop water productivity with high resolution on a global scale', *Agricultural Systems*. doi: 10.1016/j.agsy.2006.11.019.

Lott, R. B. and Hunt, R. J. (2001) 'Estimating evapotranspiration in natural and constructed wetlands', *Wetlands*, 21(4), pp. 614–628. doi: 10.1672/0277-5212(2001)021[0614:EEINAC]2.0.CO;2.

Mandanici, E. and Bitelli, G. (2016) 'Preliminary comparison of sentinel-2 and landsat 8 imagery for a combined use', *Remote Sensing*, 8(12). doi: 10.3390/rs8121014.

Marino, S. *et al.* (2019) 'Evaluation of the effect of irrigation on biometric growth, physiological response, and essential oil of Mentha spicata (L.)', *Water (Switzerland)*, 11(11). doi: 10.3390/w11112264.

Martins, V. S. *et al.* (2017) 'Assessment of atmospheric correction methods for sentinel-2 MSI images applied to Amazon floodplain lakes', *Remote Sensing*, 9(4). doi: 10.3390/rs9040322.

Molden, D. (1997) 'Accounting for water use and productivity-SWIM Paper 1'. International Irrigation Management Institute: Colombo.

Moran, M. S. *et al.* (1994) 'Estimating crop water deficit using the relation between surface-air temperature and spectral vegetation index', *Remote Sensing of Environment*. doi: 10.1016/0034-4257(94)90020-5.

Mukherjee, S., Joshi, P. K. and Garg, R. D. (2014) 'A comparison of different regression models for downscaling Landsat and MODIS land surface temperature images over heterogeneous landscape', *Advances in Space Research*. COSPAR, 54(4), pp. 655–669. doi: 10.1016/j.asr.2014.04.013.

Njuki, S. M. (2016) 'Assessment of Irrigation Performance by Remote Sensing in the Naivasha Basin , Kenya', *ITC MSc Thesis*, p. 65.

Norman, J. M., Kustas, W. P. and Humes, K. S. (1995) 'Source approach for estimating soil and vegetation energy fluxes in observations of directional radiometric surface temperature', *Agricultural and Forest Meteorology*. doi: 10.1016/0168-1923(95)02265-Y.

Pan, X. *et al.* (2018) 'Applicability of Downscaling Land Surface Temperature by Using Normalized Difference Sand Index', *Scientific Reports*. Springer US, 8(1), pp. 1–14. doi: 10.1038/s41598-018-27905-0.

Pu, R. (2021) 'Assessing scaling effect in downscaling land surface temperature in a heterogenous urban environment', *International Journal of Applied Earth Observation and Geoinformation*. Elsevier B.V., 96(May 2020), p. 102256. doi: 10.1016/j.jag.2020.102256.

Roerink, G. J. *et al.* (1997) 'Relating Crop Water Consumption to Irrigation Water Supply by Remote Sensing', *Water Resources Management*, 11(6), pp. 445–465. doi: 10.1023/A:1007982411718.

Roerink, G. J., Su, Z. and Menenti, M. (2000) 'S-SEBI: A simple remote sensing algorithm to estimate the surface energy balance', *Physics and Chemistry of the Earth, Part B: Hydrology, Oceans and Atmosphere*, 25(2), pp. 147–157. doi: 10.1016/S1464-1909(99)00128-8.

Sattari, F., Hashim, M. and Pour, A. B. (2018) 'Thermal sharpening of land surface temperature maps based on the impervious surface index with the TsHARP method to ASTER satellite data: A case study from the metropolitan Kuala Lumpur, Malaysia', *Measurement: Journal of the International Measurement Confederation*. Elsevier, 125(December 2015), pp. 262–278. doi:

10.1016/j.measurement.2018.04.092.

Senatilleke, U. *et al.* (2022) 'Estimation of Potential Evapotranspiration across Sri Lanka Using a Distributed Dual-Source Evapotranspiration Model under Data Scarcity', *Advances in Meteorology*, 2022. doi: 10.1155/2022/6819539.

Senay, G. B. *et al.* (2013) 'OPERATIONAL EVAPOTRANSPIRATION MAPPING USING REMOTE SENSING AND WEATHER DATASETS : A NEW PARAMETERIZATION FOR THE SSEB APPROACH 1', *JOURNAL OF THE AMERICAN WATER RESOURCES ASSOCIATION*, 49(3). doi: 10.1111/jawr.12057.

Sharma, P. K. *et al.* (2018) 'Assessment of Different Methods for Soil Moisture Estimation : A Review', *Journal of Remote Sensing & GIS*, 9(1), pp. 57–73.

Sobrino, J. A., Jiménez-Muñoz, J. C. and Paolini, L. (2004) 'Land surface temperature retrieval from LANDSAT TM 5', *Remote Sensing of Environment*, 90(4), pp. 434–440. doi: 10.1016/j.rse.2004.02.003.

Srivastava, P. K. *et al.* (2013) 'Machine Learning Techniques for Downscaling SMOS Satellite Soil Moisture Using MODIS Land Surface Temperature for Hydrological Application', *Water Resources Management*, 27(8), pp. 3127–3144. doi: 10.1007/s11269-013-0337-9.

Su, Z. (2002) 'The Surface Energy Balance System (SEBS) for estimation of turbulent heat fluxes', *Hydrology and Earth System Sciences*, 6(1), pp. 85–100. doi: 10.5194/hess-6-85-2002.

Tabari, H. *et al.* (2012) 'Spatial distribution and temporal variation of reference evapotranspiration in arid and semi-arid regions of Iran', *Hydrological Processes*, 26(4), pp. 500–512. doi: 10.1002/hyp.8146.

Tan, S., Wu, B. and Yan, N. (2019) 'A method for downscaling daily evapotranspiration based on 30-m surface resistance', *Journal of Hydrology*. Elsevier, 577(July), p. 123882. doi: 10.1016/j.jhydrol.2019.06.054.

Thenkabail, P. S. (2008) 'Water productivity mapping methods using remote sensing', *Journal of Applied Remote Sensing*, 2(1), p. 023544. doi: 10.1117/1.3033753.

Toureiro, C. *et al.* (2017) 'Irrigation management with remote sensing: Evaluating irrigation requirement for maize under Mediterranean climate condition', *Agricultural Water Management*. Elsevier B.V., 184, pp. 211–220. doi: 10.1016/j.agwat.2016.02.010.

Trout, T. J. and DeJonge, K. C. (2021) 'Evapotranspiration and Water Stress Coefficient for Deficit-Irrigated Maize', *Journal of Irrigation and Drainage Engineering*, 147(10), pp. 1–17. doi: 10.1061/(asce)ir.1943-4774.0001600.

U.S. Geological Survey (2016) 'Landsat 8 Data Users Handbook', *Nasa*, 8(June), p. 97. Available at: https://landsat.usgs.gov/documents/Landsat8DataUsersHandbook.pdf.

Veysi, S. *et al.* (2017) 'A satellite based crop water stress index for irrigation scheduling in sugarcane fields', *Agricultural Water Management*. Elsevier B.V., 189, pp. 70–86. doi: 10.1016/j.agwat.2017.04.016.

Virnodkar, S. S. *et al.* (2020) *Remote sensing and machine learning for crop water stress determination in various crops: a critical review*, *Precision Agriculture*. Springer US. doi: 10.1007/s11119-020-09711-9.

Wallin, M. (2014) *Resettled for Development – The Case of New Halfa Agricultural Scheme, Sudan*, *Current African Issues*.

Wang, H. *et al.* (2001) 'Improving water use efficiency of irrigated crops in the North China Plain - Measurements and modelling', *Agricultural Water Management*. doi: 10.1016/S0378-3774(00)00118-9.

Wood, A. and van Halsema, G. E. (2008) *Scoping agriculture – wetland interactions*, *FAO Water Reports*. doi: 10.1016/j.biocon.2015.04.016.

Xu, C. Y. and Singh, V. P. (2001) 'Evaluation and generalization of temperature-based methods for calculating evaporation', *Hydrological Processes*, 15(2), pp. 305–319. doi: 10.1002/hyp.119.

Yang, C. *et al.* (2019) 'Downscaling Land Surface Temperature Using Multiscale Geographically Weighted Regression over Heterogeneous Landscapes in Wuhan, China', *IEEE Journal of Selected Topics in Applied Earth Observations and Remote Sensing*, 12(12), pp. 5213–5222. doi: 10.1109/JSTARS.2019.2955551.

Yang, Y. *et al.* (2017) 'Downscaling land surface temperature in complex regions by using multiple scale factors with adaptive thresholds', *Sensors (Switzerland)*, 17(4). doi: 10.3390/s17040744.

Zakšek, K. and Oštir, K. (2012) 'Downscaling land surface temperature for urban heat island diurnal cycle analysis', *Remote Sensing of Environment*, 117, pp. 114–124. doi:

10.1016/j.rse.2011.05.027.

Zarco-Tejada, P. J. *et al.* (2013) 'A PRI-based water stress index combining structural and chlorophyll effects: Assessment using diurnal narrow-band airborne imagery and the CWSI thermal index', *Remote Sensing of Environment*. Elsevier Inc., 138, pp. 38–50. doi: 10.1016/j.rse.2013.07.024.

Zhan, W. *et al.* (2013) 'Disaggregation of remotely sensed land surface temperature: Literature survey, taxonomy, issues, and caveats', *Remote Sensing of Environment*. Elsevier Inc., 131(19), pp. 119–139. doi: 10.1016/j.rse.2012.12.014.

Zhang, Z. *et al.* (2016) 'Validation of the generalized single-channel algorithm using Landsat 8 imagery and SURFRAD ground measurements', *Remote Sensing Letters*. Taylor & Francis, 7(8), pp. 810–816. doi: 10.1080/2150704X.2016.1190475.

Zhao, T. *et al.* (2015) 'A detailed field study of direct correlations between ground truth crop water stress and normalized difference vegetation index (NDVI) from small unmanned aerial system (sUAS)', *2015 International Conference on Unmanned Aircraft Systems, ICUAS 2015*. IEEE, pp. 520–525. doi: 10.1109/ICUAS.2015.7152331.

Zolt, V. (no date) 'Optikai és mikrohullámú földmegfigyelési adatok integrációja mezőgazdasági vízgazdálkodási alkalmazásokhoz'.

Zwart, S. J. and Bastiaanssen, W. G. M. (2004a) 'Review of measured crop water productivity values for irrigated wheat, rice, cotton and maize', *Agricultural Water Management*, 69(2), pp. 115–133. doi: 10.1016/j.agwat.2004.04.007.

Zwart, S. J. and Bastiaanssen, W. G. M. (2004b) 'Review of measured crop water productivity values for irrigated wheat, rice, cotton and maize', *Agricultural Water Management*. doi: 10.1016/j.agwat.2004.04.007.

Appendix

Appendix1. Potential and reference evapotranspiration
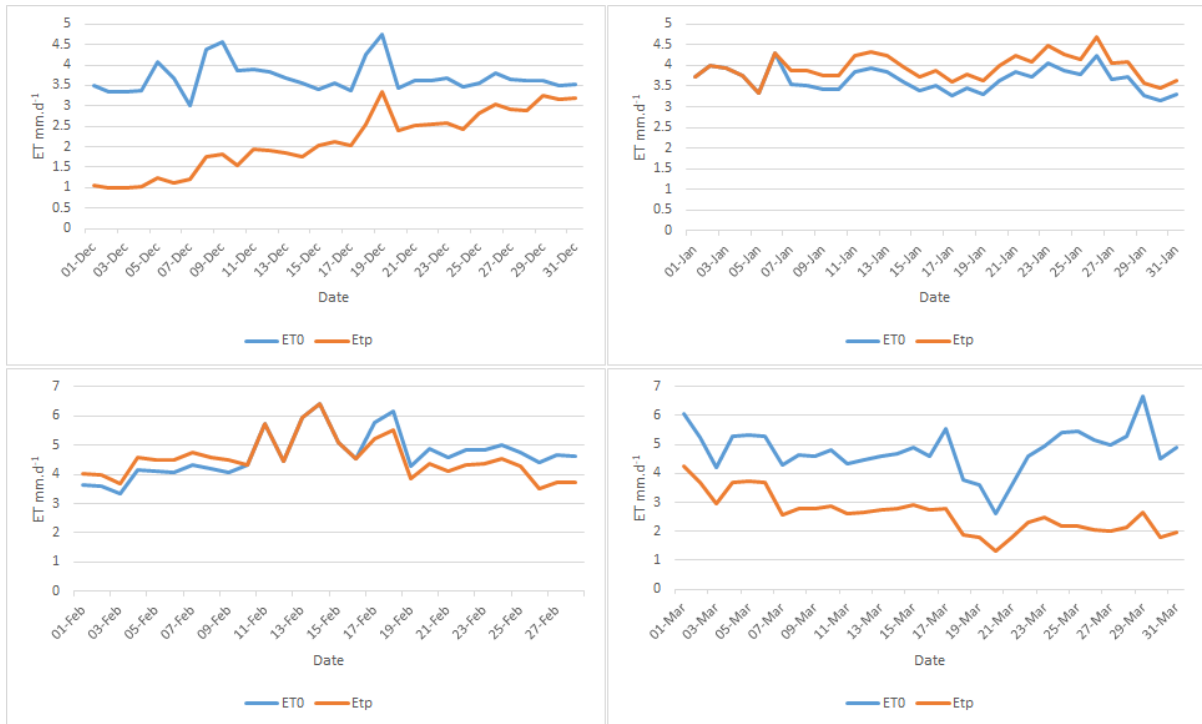
Appendix2. SEBS Climatic Data

date	Blh m	Msdwswrf W m⁻²	sp Pa	t2m K	SH kg kg⁻¹	Wind speed m s-1	Sunshine h day⁻¹
2.12.2017	750.19824	677.53064	96129	302.04678	0.0123134	2.1	6.25
3.12.2017	807.66815	677.562	96237.34	303.35336	0.0119255	2.1	6.25
4.12.2017	691.9695	682.5317	96127.76	300.65	0.0116131	2.1	6.25

5.12.2017	666.3584	690.0318	96037.27	300.35	0.0096419 7	2.6	6.25
6.12.2017	959.3868	687.5940 6	95922.41	305.0974 4	0.0085331 6	2.1	6.25
12.12.201 7	550.47	678.0315 6	96097.96	304.1527 7	0.0093419 4	2.1	6.25
13.12.201 7	556.5914	681.5625 6	96136.85	303.1596 4	0.0086431 6	2.1	6.25
14.12.201 7	612.8471	676.6557	96127.51	302.4907 5	0.0088609 8	2.1	6.25
15.12.201 7	794.72986	665.9999 4	96255.18	301.8524 2	0.0097518 1	2.1	6.25
16.12.201 7	816.8882	661.7496 3	96253.54	300.4739 7	0.0112339	2.1	6.25
18.12.201 7	540.38995	667.6869 5	96200.69 5	302.0655	0.0098095 9	2.6	6.25
19.12.201 7	669.62146 m	658.8124	96078.38	303.1027 8	0.0094753 6	3.1	6.25
20.12.201 7	706.94403	668.4062 5	96116.94 5	304.6482 5	0.0077218 5	2.1	6.25

21.12.2017	675.8566	666.06274	96176.71	300.17	0.00712937	2.1	6.25
22.12.2017	654.4319	678.87506	96020.086	299.55	0.00460768	2.1	6.25
28.12.2017	521.988	650.46875	96071.28	302.56607	0.00910441	2.1	6.25
29.12.2017	521.2797	649.68805	96170.73	304.47244	0.00864569	2.1	6.25
30.12.2017	768.0564	645.7503	96224.94	304.02518	0.00694878	2.1	6.25
31.12.2017	751.2227	640.2811	96176.38	302.48618	0.0107508	2.1	6.25
1.1.2018	878.1	638.8	96296.38	300.7	.008	3.1	6.25
3.1.2018	685.9	644.1	96310.78	297.2	.007	3.1	7.5
4.1.2018	746.8	641.3	96464.01	297.9	.006	3.1	7.3
5.1.2018	812.2	643.3	96431.945	297.5	0.008	2.6	7.3
6.1.2018	738.7	666.3	96359.43	296.8	0.006	3.1	7.4

7.1.2018	750.2	668.3	96409.05	294.65	0.008	2.1	7.5
14.1.2018	644.5	664.7	96148.88	298.75	0.008	2.1	7.5
15.1.2018	720	651.3	96322.53	298.4	0.011	2.1	7.5
16.1.2018	725.1	665.4	96352.914	298.1	0.01	2.1	7.5
17.1.2018	745.9	667.6	96153.85	298.9	0.009	2.1	7.5
19.1.2018	692	659.5	96284.445	298.5	0.01	2.1	7.5
20.1.2018	768	660.6	96364.79	298.5	0.01	2.6	7.5
21.1.2018	535.5	650.6	96206.26	299.1	0.01	2.6	7.5
22.1.2018	665.8	655.2	96159.32	301.9	0.008	2.6	7.5
23.1.2018	719.4	660.4	96140.89	23.75	0.005	2.6	7.5
29.1.2018	719.6	689.7	96270.35	296.1	0.006	2.1	7.5
30.1.2018	899.2	680.5	96270.45	295.8	0.007	2.1	7.5
31.1.2018	716.9	681	96270.71	295.3	0.008	2.1	7.5
1.2.2018	695.58185	674.56384	96270.35	297.6291	0.00959825	2.1	7.5

2.2.2018	776.6153	596.9677	96216.16	297.5798 3	0.0116699	2.1	7.5
4.2.2018	716.9193	686.2499	96185.44	300.9575 8	0.0115458	2.6	7.5
5.2.2018	640.7316	688.9988	96033.76	301.6556 7	0.0089564 6	2.6	7.5
6.2.2018	567.6793	692.6576	95983.32	302.686	0.0087925 7	2.6	7.5
7.2.2018	541.374	693.8125	95945.45	301.4170 5	0.0103294	2.1	7.5
8.2.2018	528.3842	699.5298 5	95804.62	301.5143 7	0.0094531 5	2.1	7.5
14.2.2018	590.3606	697.3441	95910.37 5	304.8359 4	0.01036	3.6	7.5
15.2.2018	625.21716	695.6546 6	95755.6	305.3823 2	0.0105581	3.1	7.5
16.2.2018	595.1248	692.6862	95807.01 6	303.8137	0.011	3.6	7.5
18.2.2018	850.5227	693.1253	96223.94	299.3	0.0113843	2.6	7.5
20.2.2018	586.4921	716.4369	95933.51 6	303.1933 3	0.0071780 6	2.1	7.5
21.2.2018	1170.7473	723.9996	95820.49	307.3137 8	0.0062640 2	2.1	7.5
22.2.2018	898.8577	721.4702	95695.2	308.5672 6	0.0077290 9	2.1	7.5
23.2.2018	757.884	718.7817 4	95652.30 5	307.4416 5	0.0099153 9	2.1	7.5

24.2.2018	2437.2712	726.9998	95560.42	311.07697	0.00633271	2.1	7.5
2.3.2018	918.49634	775.68646	96078.52	300.65	0.00713868	2.6	7.5
3.3.2018	665.00214	780.063	95992.35	299.15	0.00621182	2.1	7.5
4.3.2018	941.3625	761.31165	95964.055	304.26028	0.0081142	2.6	7.5
5.3.2018	1015.66077	769.74884	96058.66	304.3321	0.00951154	2.6	7.5
6.3.2018	945.429	763.1263	96062.42	305.57928	0.01085	2.6	7.5
8.3.2018	647.60254	773.4671	95971.03	307.5862	0.00888527	2.1	7.5
9.3.2018	669.302	790.4394	95842.15	307.78595	0.00673368	2.1	7.5
10.3.2018	717.3676	784.5018	95702.134	307.71414	0.00912688	2.1	7.5

Appendix3. Water Quantity

Date	Water applied m^3
01/01/2017	900
02/01/2017	900
03/01/2017	900
04/01/2017	900
05/01/2017	900

06/01/2017	7050
07/01/2017	7000
08/01/2017	7000
09/01/2017	7000
10/01/2017	7000
11/01/2017	7175
12/01/2017	7075
13/01/2017	7175
14/01/2017	7175
15/01/2017	7175
16/01/2017	7175
17/01/2017	7175
18/01/2017	7175
19/01/2017	7175
20/01/2017	6975
21/01/2017	6975
22/01/2017	6950
23/01/2017	6950
24/01/2017	6950
25/01/2017	6950
26/01/2017	6850
27/01/2017	6825
28/01/2017	6825

Date	Water applied m^3
29/01/2017	6825
30/01/2017	6825
31/01/2017	6825

Date	Water applied m^3
01/01/2018	6825
02/01/2018	6825
03/01/2018	6800
04/01/2018	6825
05/01/2018	6600
06/01/2018	6600
07/01/2018	6600
08/01/2018	6600
09/01/2018	6600
10/01/2018	6400
11/01/2018	6400
12/01/2018	6400
13/01/2018	6400
14/01/2018	6400
15/01/2018	6600
16/01/2018	6400
17/01/2018	6400
18/01/2018	6400

19/01/2018	6405
20/01/2018	6405
21/01/2018	6405
22/01/2018	6400
23/01/2018	6300
24/01/2018	6300
25/01/2018	6300
26/01/2018	6300
27/01/2018	6300
28/01/2018	6300
29/01/2018	6050
30/01/2018	6050
31/01/2018	6050

Date	Water applied m^3
01/02/2018	6050
02/02/2018	6050
03/02/2018	6050
04/02/2018	6050
05/02/2018	5950
06/02/2018	5850
07/02/2018	5850
08/02/2018	5850

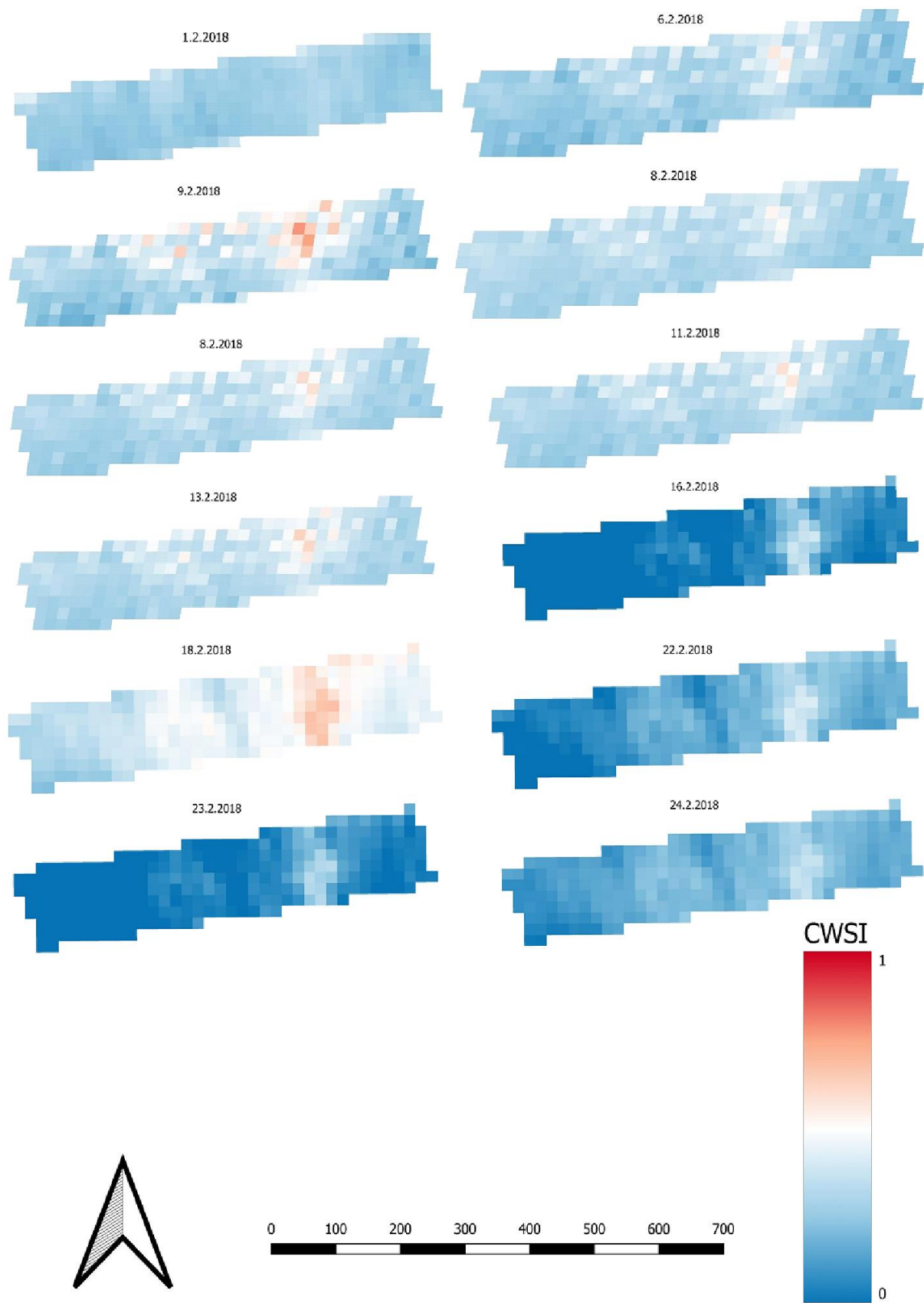|	
09/02/2018	6050
10/02/2018	6050
11/02/2018	6050
12/02/2018	6050
13/02/2018	6050
14/02/2018	6050
15/02/2018	6050

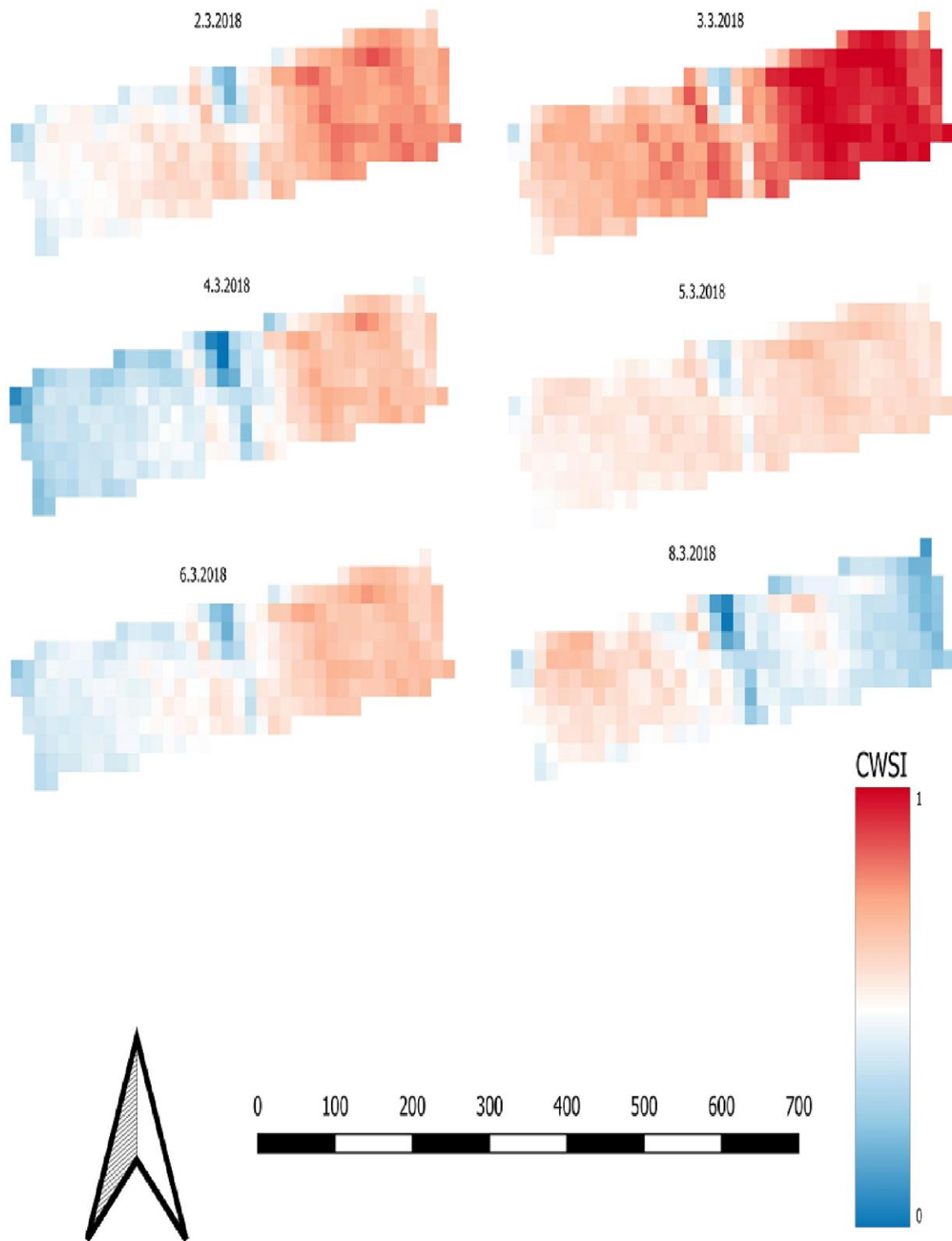Appendix 5: Crop water stress maps.
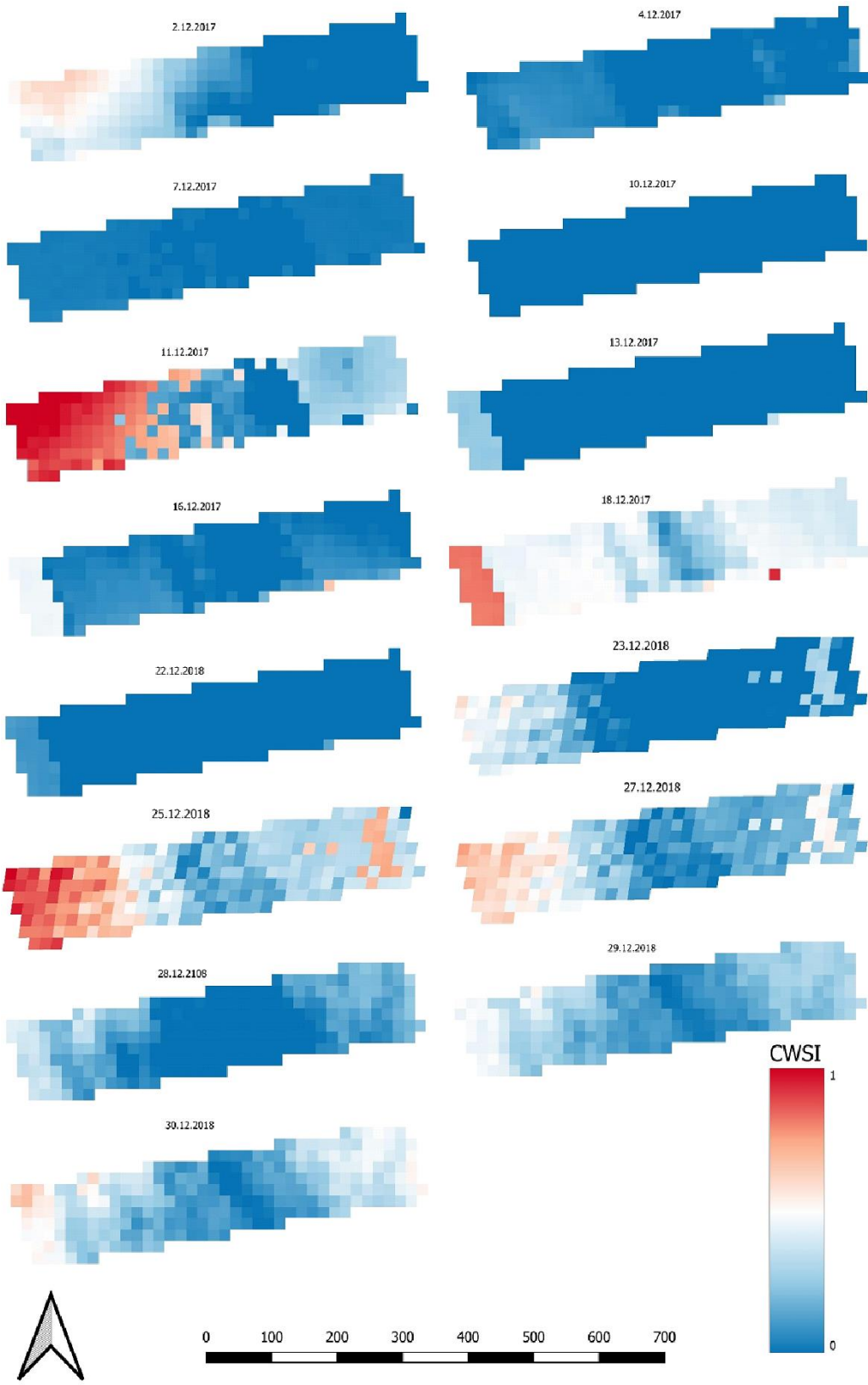
Crop water stress maps for the available dates December 2018 site (B).
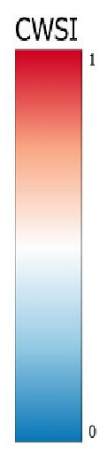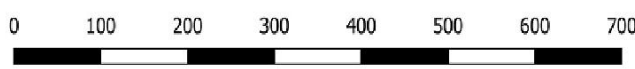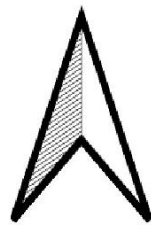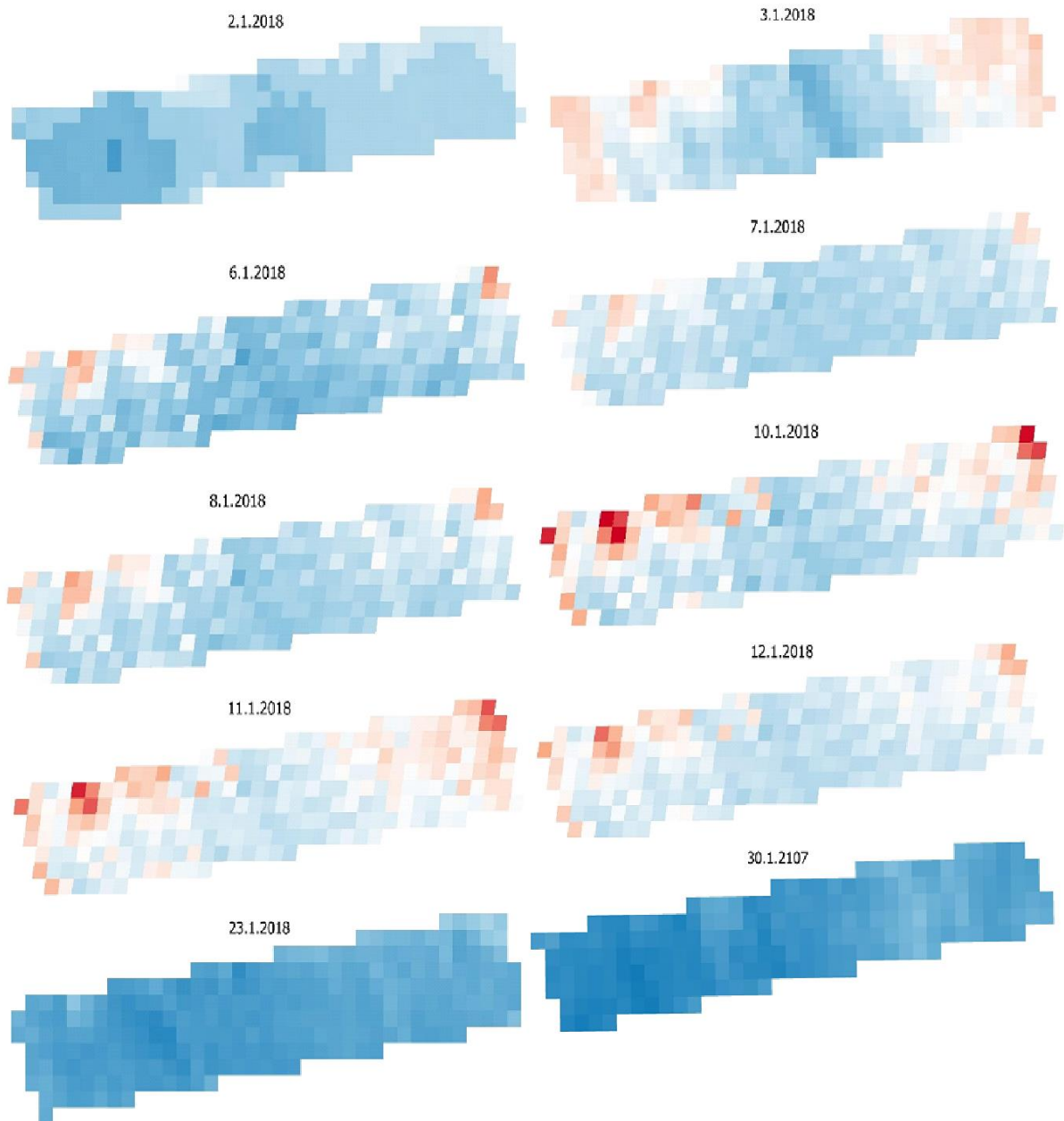
Crop water stress maps for the available dates January 2018 site (B).

117

Crop water stress maps for the available dates February 2018 site (B).

Crop water stress maps for the available dates March 2018 site (B).